THERMAL PERFORMANCE OF COMPUTER MICRO-PROCESSOR USING MICROCHANNEL HEAT SINK WITH NANOFLUIDS

TONY TAN HIN JOO

UNIVERSITI SAINS MALAYSIA

2016

THERMAL PERFORMANCE OF COMPUTER MICRO-PROCESSOR USING MICROCHANNEL HEAT SINK WITH NANOFLUIDS

by

TONY TAN HIN JOO

Thesis submitted in fulfilment of the
requirements for the degree of
Doctor of Philosophy

December 2016

ACKNOWLEDGEMENTS

Herein I would like to express my greatest appreciation to main my supervisor, Prof. Dr. Zulkifly bin Abdullah, who has given me the most valuable guidance and advices in guiding me to carry out my research work. With his wide professional experience in research work, I have most of the necessary knowledge and skill to be applied in my research systematically and successfully in terms of research methods. Besides this, I also very appreciate his helping effort / advice in necessary arrangement in terms of finance support and tool-equipments preparation that enable me to continuously implement my research professionally.

Herewith I also would like to express my greatest gratitude to my 2nd supervisor, Prof. Dr. Hazizan bin Md. Akil, for his guidance and supporting me in research, especially for the nanofluidic project. Under his guidance, I obtain a lot of knowledge about the nano-materials which is required in my research. Furthermore, the supply of necessary materials and technical advice on the usage of available facilities in laboratory of Material Engineering School are also given to ensure my research can go on smoothly. Besides my supervisors in guiding me in research, I also won't miss out my colleagues, Mr. Khor Chu Yee, Mr. Leong Wei Chiat, Mr. Lau Chun Sean, Mr. Dadan Ramdan, Mr. Muhammad and Khalil Abdullah @ Harun, who have supported and helped me in my research work. Furthermore, I would like to thank Institute of Postgraduate Student (Universiti Sains Malaysia) for financial support in the program of Fellowship along my research work.

Finally, I also won't forget the support and encouragement that have been given from all of my family members along the period of my research work, especially my father, mother and my wife Goh Min Li, and I am very appreciate them.

Tony Tan Hin Joo (December 2016)

TABLE OF CONTENTS

ACKNOWLEDGEMENTS		ii
TABLE OF CONTENTS		iii
LIST OF TABLES		vi
LIST OF FIGURES		vii
LIST OF SYMBOLS		xvi
LIST OF ABBREVIATIONS		xvii
ABSTRAK		xviii
ABSTRACT		xx
CHAPTER ONE: INTRODUCTION		
1.1	Introduction	1
1.2	Problem Statement	2
1.3	Objectives of the study	6
1.4	Scope of research work	6
1.5	Thesis outline	8
CHAPTER TWO: LITERATURE REVIEW		
2.1	Introduction	10
2.2	Study on the effect of fluid flow, various microchannel heat sink configurations and physical channel dimensions	10
2.3	Study on the effect of nanofluid in cooling performance of microchannel heat sink	24
2.4	Summary	34

CHAPTER THREE – METHODOLOGY

3.1	Introduction		37
3.2	Development of Model		38
	3.2.1	Equation solution for modelling	40
	3.2.2	Development of mesh modelling	42
	3.2.3	Boundary conditions	43
	3.2.4	Grid independency	44
3.3	Experiment setup		45
	3.3.1	Equipment setup	45
	3.3.2	Nanofluids preparation	51
3.4	Work flow of experimental and simulation analysis		53
3.5	Summary		58

CHAPTER FOUR – RESULT AND DISCUSSION

4.1	Introduction	59
4.2	Validation of simulation work through experimental work	60
4.3	Analysis of the effect of various geometrical configurations of microchannels on the heat sink performances	67
4.4	Analysis of performance of microchannel by considering the effect of nanofluid on the heat sink performances	76
4.5	Analysis of performance of microchannel by considering the effect of nanofluid concentrations	81
4.6	Analysis of performance of microchannel by considering the effect of nanofluid types	85
4.7	Analysis of the effect of vertical and horizontal fin-tip gaps for the various geometrical configurations of microchannels	91

4.8 Analysis of the effects of geometry and number of hollow on the performance of microchannel heat sinks 101

CHAPTER FIVE – CONCLUSION

5.1 Conclusion 110

5.2 The effects of various geometrical configurations of microchannel on heat sink performance 110

5.3 The effect of nanofluid on the performance of microchannel heat sink 111

5.4 The effect of nanoparticle concentration of nanofluid on the performance of microchannel heat sink 111

5.5 The effect of nanoparticles types of nanofluid on the performance of microchannel heat sink 112

5.6 The effect of vertical and horizontal fin tip gaps on the performance of microchannel heat sinks 112

5.7 The effect of geometry and number of hollow on the performance of microchannel heat sinks 113

5.8 Recommendation for future works 113

REFERENCES 115

LIST OF PUBLICATIONS

LIST OF TABLES

		Page
Table 1	Comparison of experimental result with simulation result at various grid sizes.	45

LIST OF FIGURES

		Page
Figure 1.1	Computer processor cooling by heat sink with the application of fan.	2
Figure 1.2	Heat pipe with fins for cooling.	2
Figure 1.3	Various configurations of heat sink fin geometry.	3
Figure 1.4	Heat sink using liquid medium for cooling in computer CPU.	4
Figure 1.5	Microchannel heat sink.	5
Figure 2.1	Geometric configurations of N-, S-, D-, U-, and V-type arrangement of inlet and outlet of microchannel heat sink.	11
Figure 2.2	Schematic of microchannel configurations of (a)square and rectangular channels, (b)circular channels, (c)trapezoidal channels, (d)triangular channels.	13
Figure 2.3	Schematic of microchannel heat sink with fin tip clearance.	14
Figure 2.4	(a)Shrouded array geometry, (b)pin fin with tip clearance, and (c)pin fin without tip clearance.	15
Figure 2.5	(a)Test module, (b)Microchannel heat sink.	16
Figure 2.6	Experimental set-up.	17
Figure 2.7	Schematic diagram of the liquid cooling concept for electronic packages.	18
Figure 2.8	Cross-sectional view of the microchannel heat sink on the flip chip ball grid array packages.	18
Figure 2.9	Schematic diagram of the test section and microchannel heat sink.	19

Figure 2.10	Schematic of the microchannel heat sink: (a)system, (b)microscope image of silicon microchannels, (c)geometric shape of microchannel.	20
Figure 2.11	Structure of rectangular microchannel heat sink.	21
Figure 2.12	Structure and size of heat sinks: (a)structure, (b)size, (c)packaging.	22
Figure 2.13	Schematic of the (a)two-layered MCHS and (b)a repeated section of MCHS.	23
Figure 2.14	The schematic of the heat sink: (a)new design with truncated top channels (b)original design.	24
Figure 2.15	(a)Schematic diagram of computational domain, (b)Cross section of rectangular shaped microchannel.	28
Figure 2.16	(a)Schematic diagram of computational domain, (b)Cross section of trapezoidal shaped microchannel.	29
Figure 2.17	Schematic diagram of computational domain, (a)isometric view of microchannel heat exchanger, (b)cross sectional view of microchannel heat exchanger.	30
Figure 2.18	(a)3D view, (b)top view, (c)side view of the single IMCHS.	32
Figure 3.1	Flow chart of microchannel heat sink model development for simulation analysis.	39
Figure 3.2	Meshing work for various geometrical configurations of microchannels.	42
Figure 3.3	Boundary condition for the 3D modeling of microchannel heat sinks.	43
Figure 3.4	General view of experimental setup.	45
Figure 3.5	Assembly of microchannel heat sink.	46

Figure 3.6	Schematic diagram of equipment system for experimental work.	47
Figure 3.7	(a)rectangular-, (b)triangular-, and (c)trapezoidal microchannel heat sinks.	48
Figure 3.8	Assembly arrangement of microchannel heat sinks with casings and heaters.	50
Figure 3.9	Cross-sectional view of assembly of microchannel heat sink with casings and heaters.	51
Figure 3.10	Comparison of 3% concentration of nanoparticles within nanofluids (SiO_2-H_2O and Al_2O_3-H_2O) with- and without settlement of nanoparticles.	52
Figure 3.11	Geometrical configuration dimensions of microchannel heat sink (all dimensions in mm).	54
Figure 3.12	Dimensions of cross sectional microchannel heat sink (all dimensions in mm) and schematic diagram of various fin configurations without and with vertical fin tip gap.	54
Figure 3.13	Semi - hollow fin and fully closed hollow channels at optimum vertical fin tip gap condition in microchannel heat sink.	55
Figure 3.14	The microchannel heat sink model with dimensions (in mm).	56
Figure 3.15	The cross sectional side view of the heat sink showing the channels (M1 to M11) and fins (H1 to H10), and the dimensions (in mm).	56
Figure 3.16	Solid fin and fins with various hollow geometries.	57
Figure 4.1	Pressure drop within rectangular microchannel heat sink with distilled water.	60

Figure 4.2	Pressure drop within triangular microchannel heat sink with distilled water.	61
Figure 4.3	Pressure drop within trapezoidal microchannel heat sink with distilled water.	61
Figure 4.4	Pumping power for the fluid flow through rectangular microchannel heat sink with distilled water.	62
Figure 4.5	Pumping power for the fluid flow through triangular microchannel heat sink with distilled water.	62
Figure 4.6	Pumping power for the fluid flow through trapezoidal microchannel heat sink with distilled water.	63
Figure 4.7	Heat sink base temperature for rectangular microchannel heat sink with distilled water.	64
Figure 4.8	Heat sink base temperature for triangular microchannel heat sink with distilled water.	64
Figure 4.9	Heat sink base temperature for trapezoidal microchannel heat sink with distilled water.	65
Figure 4.10	Thermal resistance for rectangular microchannel heat sink with distilled water.	66
Figure 4.11	Thermal resistance for triangular microchannel heat sink with distilled water.	66
Figure 4.12	Thermal resistance for trapezoidal microchannel heat sink with distilled water.	67
Figure 4.13	Comparison of pressure drop among various geometrical configurations of microchannels with distilled water, by simulation work.	68

Figure 4.14	Comparison of pumping power among various geometrical configurations of microchannels with distilled water, by simulation work.	69
Figure 4.15	Comparison of heat sink base temperature among various geometrical configurations of microchannels with distilled water, by simulation work.	70
Figure 4.16	Comparison of heat transfer coefficient among various geometrical configurations of microchannels with distilled water, by simulation work.	71
Figure 4.17	Comparison of thermal resistance among various geometrical configurations of microchannels with distilled water, by simulation work.	72
Figure 4.18	Comparison of performance index among various geometrical configurations of microchannels with distilled water, by simulation work.	72
Figure 4.19	Velocity and temperature contour for various geometrical configurations of microchannel heat sinks with distilled water as cooling medium at fluid flow velocity of 0.0298 m/s.	74
Figure 4.20	Pressure drop within rectangular microchannel heat sink with alumina nanofluids with 1% concentration.	77
Figure 4.21	Pumping power for the fluid flow through rectangular microchannel heat sink with alumina nanofluids with 1% concentration.	78
Figure 4.22	Heat sink base temperature for rectangular microchannel heat sink with alumina nanofluids with 1% concentration.	79

Figure 4.23	Heat transfer coefficient for rectangular microchannel heat sink with alumina nanofluids with 1% concentration.	79
Figure 4.24	Thermal resistance for rectangular microchannel heat sink with alumina nanofluid with 1% concentration.	80
Figure 4.25	Pressure drop within rectangular microchannel heat sink with alumina nanofluids with 1%, 2% and 3% concentrations, by simulation work.	82
Figure 4.26	Pumping power for the fluid flow through rectangular microchannel heat sink with alumina nanofluids with 1%, 2% and 3% concentrations, by simulation work.	82
Figure 4.27	Heat sink base temperature for rectangular microchannel heat sink with alumina nanofluids with 1%, 2% and 3% concentrations, by simulation work.	83
Figure 4.28	Heat transfer coefficient for rectangular microchannel heat sink with alumina nanofluids with 1%, 2% and 3% concentrations, by simulation work.	84
Figure 4.29	Thermal resistance for rectangular microchannel heat sink with alumina nanofluids with 1%, 2% and 3% concentrations, by simulation work.	85
Figure 4.30	Comparison of pressure drop among various types of nanofluids within rectangular microchannel at 3% concentration of nanoparticles, by simulation work.	86
Figure 4.31	Comparison of pumping power among various types of nanofluids within rectangular microchannel at 3% concentration of nanoparticles, by simulation work.	87

Figure 4.32	Comparison of heat sink base temperature among various types of nanofluids within rectangular microchannel at 3% concentration of nanoparticles, by simulation work.	88
Figure 4.33	Comparison of heat transfer coefficient among various types of nanofluids within rectangular microchannel at 3% concentration of nanoparticles, by simulation work.	89
Figure 4.34	Comparison of thermal resistance among various types of nanofluids within rectangular microchannel at 3% concentration of nanoparticles, by simulation work.	90
Figure 4.35	Comparison of temperature contour for microchannel heat sink with silica and alumina nanofluids (3% concentration) as cooling medium at fluid flow velocity of 0.0298 m/s.	91
Figure 4.36	Pressure drop comparison as function of vertical fin tip gap, among various fin configurations of microchannel heat sink at volume flow rate of 6.8×10^{-7} m^3/s.	92
Figure 4.37	Total thermal resistance comparison as function of vertical fin tip gap, among various fin configurations of microchannel heat sink at volume flow rate of $6.8 \times 10^{-7} m^3/s$ and heat flux of 300000 W/m^2.	93
Figure 4.38	Convective area of various fin configurations of microchannel heat sink.	94
Figure 4.39	Introduction of new convective area as the vertical fin tip gap is introduced.	94
Figure 4.40	Figure 4.40: Velocity distribution in 6^{th} rectangular channel and in the vertical fin tip gap above 5^{th} rectangular fin at volume flow rate of $6.8 \times 10^{-7} m^3/s$.	96

Figure 4.41	Maximum heat sink base temperature as function of vertical fin tip gap, among various fin configurations of microchannel heat sink at volume flow rate of 6.8 x 10^{-7} m^3/s and heat flux of 300000 W/m^2.	97
Figure 4.42	Temperature contour of heat sink base for various fin configurations of microchannel heat sink at vertical fin tip gap of 0.08mm, volume flow rate of 6.8 x 10^{-7} m^3/s and heat flux of 300000 W/m^2.	98
Figure 4.43	Introduction of horizontal fin convective area as the horizontal fin tip gap decreases.	99
Figure 4.44	Pressure drop as function of different horizontal fin tip gap in microchannel heat sink with optimum vertical fin tip conditions at volume flow rate of 6.8 x 10^{-7} m^3/s.	100
Figure 4.45	Total thermal resistance as function of different horizontal fin tip gap in microchannel heat sink with optimum vertical fin tip conditions at volume flow rate of 6.8 x 10^{-7} m^3/s and heat flux of 300000 W/m^2.	101
Figure 4.46	Comparison of velocity distributions of fluid flow across the channels and hollows among cases A, B1, C1 and D1.	102
Figure 4.47	Comparison of velocity distributions between channel (M6) and hollow (H5).	103
Figure 4.48	Comparison of pressure drop across the heat sink for cases with solid fin and single-hollow fins.	103
Figure 4.49	Temperature contour of heat sink structure with solid and single-hollow fins at volume flow rate of 1.3 × 10^{-5} m^3/s.	104

Figure 4.50 Temperature contour of heat sink base with solid and single-hollow fins at volume flow rate of 1.3 $\times 10^{-5}$ m^3/s. 105

Figure 4.51 Average temperature of heat sink base with solid and single-hollow fins as function of volume flow rate. 105

Figure 4.52 Comparison of total thermal resistance of heat sink with solid and single-hollow fins, as function of volume flow rate. 106

Figure 4.53 Pressure drop across the heat sink with single and double hollow fins as function of volume flow rate. 107

Figure 4.54 Average heat sink base temperature with single and double hollow fins as function of volume flow rate. 107

Figure 4.55 Temperature contours of heat sink base with single and double hollow fins at volume flow rate of 1.3 $\times$ 10^{-5} m^3/s. 108

Figure 4.56 Total thermal resistance of heat sink with single and double hollow fins as function of volume flow rate. 109

LIST OF SYMBOLS

u	Fluid flow velocity component in x-direction
v	Fluid flow velocity component in y-direction
w	Fluid flow velocity component in z-direction
P	Pressure
x, y, z	Cartesian coordinates
T	Temperature
k	Thermal conductivity
c_p	Specific heat capacity
Re	Reynolds Number
h	Heat transfer coefficient
ρ	Density
μ	Dynamic viscosity
φ	Volume fraction of nanoparticle
R	Thermal resistance
ΔT	Temperature difference
Q	Heat input
Q_f	Flow rate
ΔP	Pressure difference
P_{pump}	Pumping power
q	Heat transfer

LIST OF ABBREVIATIONS

FVM	Finite Volume Method
IMCHS	Interrupted Microchannel Heat Sink
MCHS	Mircochannel Heat Sink
3-D	Three-Dimensional

PRESTASI THERMA DALAM MIKRO-PEMPROSSESAN KOMPUTER DENGAN MENGGUNAKAN NANOFLUID DALAM MIKRO PENYERAP HABA

ABSTRAK

Dalam perkembangan teknologi elektronik yang pesat, permintaan terhadap komputer berkapasiti tinggi semakin meningkat setiap tahun. Apabila kapasiti komputer semakin meningkat, haba yang dihasilkan daripada komponen pemprosesan semakin meningkat semasa berfungsi. Dengan ketiadaan pengurusan haba yang sesuai, haba tinggi yang dihasilkan tersebut akan menyebabkan suhu tinggi pada komponen pemprosesan komputer dan akibatnya prestasi komputer akan menurun sehingga pada akhirnya komponen akan mengalami kerosakan. Pada masa yang sama, proses pengecilan saiz komponen elektronik yang berterusan itu menyumbang kesan impak terhadap saiz sistem penyejukkan yang dihubungkan kepada komponen pemprosesan komputer tersebut. Secara amnya, dalam teknologi sistem penyejukkan yang sedia ada, saiz sistem penyejukkan konvensional telah digunakan dalam pasaran and pelbagai jenis medium penyejukkan digunakan untuk menyerap dan membebaskan haba. Walaubagaimanapun, kapasiti penyejukkan bagi sistem penyejukkan konvensional tersebut adalah terhad dan tidak mampu mengeluarkan haba tinggi daripada komponen pemprosesan komputer yang berkapasiti tinggi. Selain itu, saiz yang besar tidak dapat dimuatkan ke atas komponen pemprosesan komputer yang semakin kecil. Dengan itu, langkah - langkah yang sesuai untuk menangani masalah pengurusan haba yang tinggi dan fizikal saiz yang kecil bagi sistem penyejukkan adalah diperlukan. Sebagai penyelesaiannya, mikro penyerap haba telah diperkenalkan. Dalam penyelidikan tersebut, pelbagai parameter (hilang tekanan [range: 20Pa – 38Pa], suhu [range: 342K – 354K] and Reynolds Number [range: 70 – 1150]), fizikal dimensi dan bentuk saluran penyerap haba (segi empat panjang, tiga segi dan trapezoid) telah dipertimbangkan and

dianalisis terhadap impaknya ke atas prestasi mikro penyerap haba. Penyelidikan tersebut telah dijalankan melalui kaedah simulasi. Dalam kaedah eksperimen, pelbagai medium penyejukkan digunakan iaitu air penyulingan dan nanofluid (air penyulingan + alumina Al_2O_3, dan air penyulingan + silica SiO_2) dengan kandungan zarah-zarah nano yang berlainan (1%, 2% and 3% kandungan). Manakala dalam kaedah simulasi, komputer pengisian FLUENT berdasarkan Finite Volume Method (FVM) telah digunakan untuk menyimulasikan keupayaan mikro penyerap haba. Keputusan kajian tersebut menunjukkan bahawa faktor fizikal dimensi dan bentuk memberikan kesan impak yang tinggi terhadap prestasi haba bagi mikro penyerap haba. Dengan itu, saluran berbentuk segi empat panjang mampu memindahkan haba yang tinggi berbanding dengan bentuk saluran mikro yang lain, tetapi ia menunjukkan prestasi hidrodinamik yang rendah. Sebaliknya, mikro saluran segi tiga menunjukkan prestasi pemindahan haba yang rendah walaupun prestasi hidrodinamik yang tinggi. Analisis terhadap kesan jenis zarah – zarah nano (Al_2O_3 dan SiO_2) dan kandungannya (1%, 2% dan 3% kandungan) dalam asas medium penyejukkan ke atas prestasi mikro penyerap haba telah dijalankan dalam kajian tersebut. Hasil analisis tersebut menunjukkan bahawa kehadiran zarah – zarah nano dalam asas medium penyejukkan dapat meningkatkan prestasi penyejukkan sebanyak 40% berbanding dengan penggunaan air penyulingan sahaja. Manakala dengan peningkatan kandungan zarah – zarah nano dalam asas medium penyejukkan, kadar penyejukkan meningkat. Walaubagaimanapun, kuantiti kandungan zarah – zarah nano yang rendah tidak mempengaruhi prestasi hidrodinamik bagi mikro penyerap haba. Sebagai kesimpulannya, kesan fizikal dimensi, bentuk saluran mikro dan kehadiran zarah – zarah nano dalam asas medium penyejukkan merupakan faktor – faktor penting dan menunjukkan impaknya yang jelas ke atas prestasi saluran mikro penyerap haba. Bagi menunjukkan keputusan simulasi yang dihasilkan itu menyakinkan, kaedah eksperimen telah dijalankan bagi mengesahkan keputusan tersebut.

THERMAL PERFORMANCE OF COMPUTER MICRO-PROCESSOR USING MICROCHANNEL HEAT SINK WITH NANOFLUIDS

ABSTRACT

In the rapid development of electronic technology, the demand of high capacity in computer performance is increasing every year. The higher the performance of computer the higher the heat will be released from the computer processor. Without proper management of the heat release, the generated high heat will cause computer performance deteriorate due to high temperature and may cause damage consequently. Furthermore, the continuous miniaturization process of electronic component has contributed impact to the size of cooling system which is incorporated with the electronic component. As commonly found in the current technology of cooling system, the conventional size of cooling system is used, and various medium are applied through the cooling system for heat removal purpose. The heat removal capacity of conventional cooling system is limited which is not able to dispel the high heat that generated from high performance computer processor. Furthermore, the larger size of the conventional cooling system can not be fitted into the smaller size of electronic components of the processor. As a result, a proper approach of managing the high heat issue and proper physical size of cooling system is required, in which microchannel heat sink is introduced. In the research work, various operating conditions (pressure drop [range: 20Pa – 38Pa], temperature [range: 342K – 354K] and Reynolds Number [range: 70 – 1150]), physical dimensions and channel configurations (rectangular, triangular and trapezoidal) are considered and analysed in order to investigate their impact on the microchannel heat sink performance in terms of pressure drop, pumping power, thermal resistance, and heat transfer coefficient. Besides this, various cooling working medium has been used such as distilled water and nanofluid (Distilled Water H_2O + Alumina

Al_2O_3 and Distilled Water H_2O + Silica SiO_2) with various concentrations of nanoparticles (1%, 2% and 3% concentration). Simulation work by applying Finite Volume Method (FVM) in FLUENT software has been carried out to simulate the engineering results for the performance of microchannel heat sink. It is found that the physical dimension and geometrical channel configuration have obvious impact on the microchannel heat sink performance in which the case of rectangular channel that provides the highest heat transfer performance. Besides this, the research work also shows that the effect of different types and concentrations (1%, 2% and 3% concentrations) of nanoparticles within cooling medium plays important role onto the microchannel heat sink performance. The increment of cooling performance by 40% can be achieved by adding nanoparticles into cooling medium as compared with pure distilled water. Furthermore, the increment of cooling rate also can be achieved by the increment of nanoparticles concentration. In the research work, nanofluid Alumina provides the higher cooling rate as compare with pure distilled water and nanofluid Silica due to the effect of high thermal conductivity. However, the small amount of nanoparticles concentration would not affect hydrodynamic performance of microchannel heat sink. As a result, the physical dimension, channel geometrical configurations, existence of nanoparticles within cooling medium are vital factors that able to affect and incur obvious impact on the performances of microchannel heat sink hydrodynamically and thermally. To ensure the result of the simulation work above is reliable, the experimental works have been carried out for validation and comparison.

CHAPTER ONE

INTRODUCTION

1.1 Introduction

Cooling is a very important process in removing the generated heat from an equipment, like electronic components, air-conditioning systems, engine, fuel cells, etc. Without cooling process, the successive generated heat will cause high temperature and the high temperature effect will then causes deterioration in performance and may damage seriously. In order to overcome the high temperature that generated from heat, the cooling process is required. There are various cooling equipments are available in industrial technology such as heat exchanger systems, heat pipe, radiator, condenser, and heat sink. Figures 1.1 and 1.2 show the examples of cooling equipment for electronic component. In conjunction with the use of these cooling equipments, there are various types of working medium are used in these cooling equipments, such as air, water, R-12, R-113, R-141b, R-124, R-134a, ethanol, etc, as coolant to absorb and transport the heat for removal.

In electronic industries for computer technology, cooling process for the electronic components is vital in order to maintain their high performance in function and prevent any damage that caused by the high temperature effect. For instant, microprocessor in CPU (Central Processing Unit) of the high performance computer system. The study of fluid flow and heat transfer for cooling process of the processor has been carried out substantially by various researchers around the world. However, there is still having several issues which have not been investigated. Hence, the related issues have been identified and studied in this research as complimentary for the previous research works, and finally reported / documented in the following chapter in this thesis.

Figure 1.1: Computer processor cooling by heat sink with the application of fan.

(Source: https://en.wikipedia.org/wiki/Computer_cooling#/media/File:AMD_heatsink_and_fan.jpg)

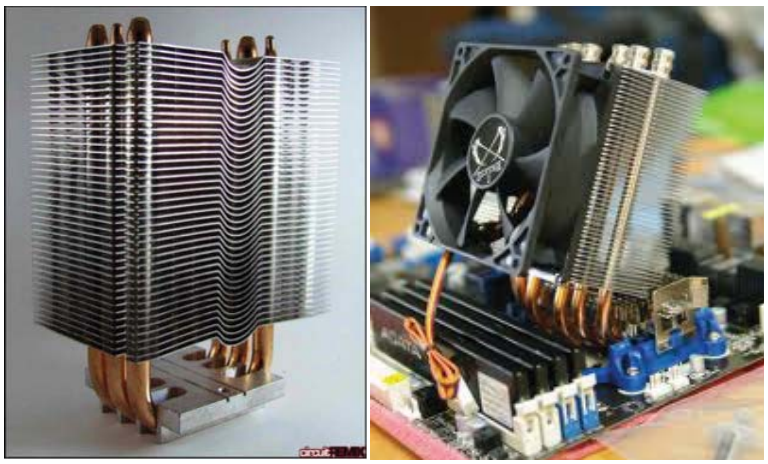

(a) (b)

Figure 1.2: Heat pipe with fins for cooling.

(Source: Figure (a)-http://liquid-cooling.org/wp-content/uploads/2014/05/Figure-9-Sample-heat-sink-with-heat-pipe-Source-circuitremix.com-.png,

Figure (b)- https://en.wikipedia.org/wiki/Computer_cooling#/media/File:Heatsink_with_heat_pipes.jpg)

1.2 Problem Statement

As can be seen in the available cooling heat sink design, various configuration of fin has been designed to suit specific engineering application as shown in Figures 1.3. The example of heat sink assembly onto computer CPU board is also shown in Figure 1.3(e).

a) Circular pin fin type b) Rectangular fin type c) Diverging rectangular fin type

d) Rectangular pin fin type e) Assembly of heat sink on computer CPU board

Figure 1.3: Various configurations of heat sink fin geometry.

(Source: Figures (a), (b) and (c)- https://en.wikipedia.org/wiki/Heat_sink#/media/File:Pin_fin,_straight_fin_and_flared_heat_sinks.png,

Figure (d)- https://en.wikipedia.org/wiki/Heat_sink#/media/File:Pin_fin_heat_sink_with_a_z-clip.png,

Figure (e)- http://i1.wp.com/qats.com/cms/wp-content/uploads/2012/03/QoolPCB.jpg and https://en.wikipedia.org/wiki/Computer_cooling#/media/File:Harumphy.dg965.heatsink.jpg)

Such conventional heat sink design is still being used in cooling electronic component especially for computer system. Normally, such heat sink design is utilized with air flow as cooling medium. Beside the application of air flow, other fluid flow which is in liquid form has been utilized for cooling, i.e. water, alcohol, and Freon. With the utilization of liquid form of cooling medium, package of cooling part that containing the channel heat sink is designed and fabricated with fully concealed.

Figure 1.4 shows the example of the channel heat sink that utilizes liquid cooling medium. The cost of production of this conventional dimension and design of heat sink is low; hence, it is affordable in market place. However, as stated in section 1.1 of this chapter, this conventional heat sink design has limited capacity of removing heat which is about 100W/cm^2 and not able to release or cooling away the high heat that generated by the high performance electronic component.

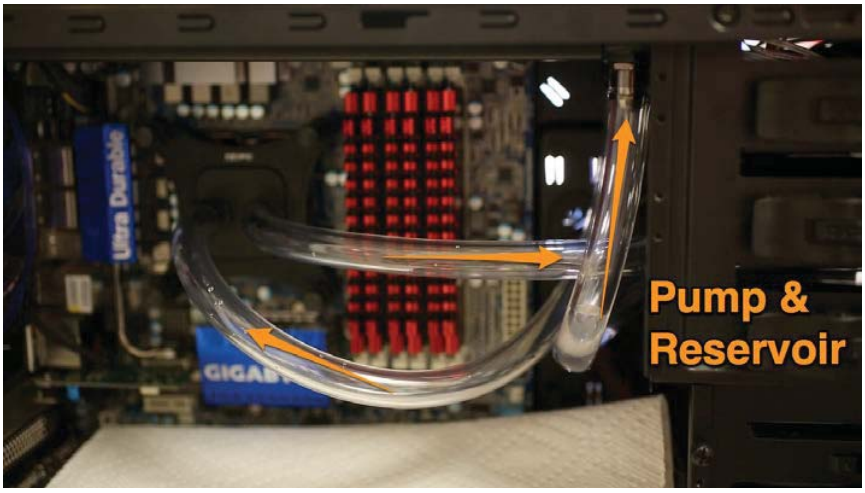

Figure 1.4: Heat sink using liquid medium for cooling in computer CPU.

(Source: http://lifehacker.com/5940236/a-beginners-guide-to-water-cooling-your-computer)

Referring to the assessment of high-heat-flux thermal management schemes that carried out by Mudawar (2001), the high-flux range of heat flux is defined as 100W/cm^2 to 1000W/cm^2. As reported by Harshit et al. (2015), the heat flux dissipation requirement has increased from 100W/cm^2 to 1000W/cm^2 which exceeds the capability of present cooling technology. In order to overcome this limited cooling capacity of conventional heat sink, the microchannel heat sink has been proposed. Such new heat sink design can dissipate the heat as high as capacity of 790W/cm^2 as reported by Tuckerman and Pease (1981). They also stated that single phase forced convective cooling in microchannels should be feasible for circuit power densities of more than 1000 W/cm^2. As a result, the

microchannel heat sink has high potential and able to meet high heat flux dissipation requirement.

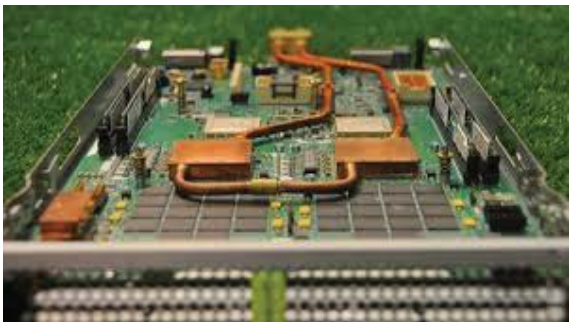

a) Microchannel heat sinks that assembled onto processor.

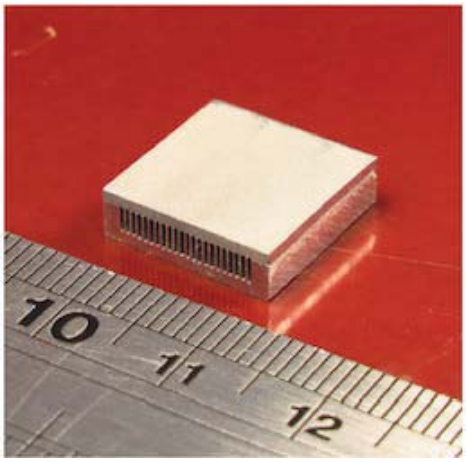

b) Microchannel heat sink size measurement.

Figure 1.5: Microchannel heat sink.

(Source: Figure (a) http://newatlas.com/using-hot-water-to-cool-internet-servers/14830/pictures and Figure (b) http://liquid-cooling.org/tag/liquid-immersion-cooling-theory/)

Referring to Figure 1.5, microchannel heat sink has been designed in various form in the purpose to dissipate the high heat that generated by high performance computer processor.

Although there are various researches have been carried out by other researchers, there are still several research gaps that haven't been explored. As refer to Chapter 2,

various configurations of microchannel heat sink fins have been studied individually, in which it is including the number of fin, fin arrangement (especially for pin fin), physical dimension of fin, type of cooling medium, fluid flow velocity and phase type of cooling medium flow during heat dissipation (single- phase: gas or liquid only, or two-phase flows: boiling condition in which vapor and liquid exist in the same time within microchannel).

The present study has carried out like comparison of cooling performance among various microchannel configurations and effect of nanofluid application as cooling medium on the various configurations of microchannel.

1.3 Objectives of the study

The objectives of the present study are as follow:

1. To provide understanding on the cooling performance by comparison of various configurations of microchannel heat sink fin as well as fin modification by adding hollow section into each fin configuration.
2. To provide understanding on the effect of fin tip gap on the various configurations of microchannel heat sink fin that may exist after assembled with substrate.
3. To explore the effect of nanofluid application on the various configurations of microchannel heat sink.

1.4 Scope of research work

The following are the work scope of the present study:

1. Three configurations of microchannels are investigated such as rectangular microchannel, triangular microchannel and trapezoidal microchannel.

2. The fluid flow within microchannel is laminar flow as for the range of Reynolds Number of 70 to 1150.
3. The fluid flow is incompressible.
4. The fluid flow is analyzed in steady state condition.
5. Three types of cooling mediums such as distilled water, alumina nanofluid (Al_2O_3 - H_2O) and silica nanofluid (SiO_2 – H_2O) are used in microchannel heat sink.
6. Three concentrations of 1%, 2% and 3% of nanoparticles within nanofluid are analyzed.

Referring to the work scope above, the following studies have been carried out to investigate the performance of microchannel heat sink:

1. To investigate numerically and experimentally the effects of various geometrical configurations of microchannel on heat sink hydrodynamic and thermal performances by using distilled water (base fluid) as cooling medium.
2. To investigate numerically and experimentally the effect of nanofluid (distilled water + 1% concentration of Al_2O_3 nanofluid) on the performance of microchannel heat sink with various geometrical configurations of microchannels.
3. To investigate numerically and experimentally the effect of nanoparticle concentration (distilled water + 1%-, 2%-, and 3% concentrations of Al_2O_3 nanofluid) in nanofluid on the performance of selected high thermal performance geometrical configuration of microchannel heat sink.
4. To investigate numerically and experimentally the effect of nanoparticles types (distilled water + 3% concentration of Al_2O_3 nanofluid, and distilled water + 3% concentration of SiO_2 nanofluid) on the performance of

selected high thermal performance geometrical configuration of microchannel heat sink with various geometrical configurations of microchannels.

5. To investigate numerically the effect of vertical and horizontal fin tip gaps on the performance of microchannel heat sinks with various geometrical configurations of microchannels.
6. To investigate numerically the effect of geometry and number of hollow on the performance of microchannel heat sinks.

Both of simulation and experimental works have been carried within the work scope. In simulation work, three types of geometrical configurations of microchannel have been designed and these geometrical configurations are analyzed accordingly. In order to ensure the result of simulation is convincing, the result is verified with experimental result. In experimental work, microchannel heat sinks with different geometrical configurations have been fabricated for analysis in order to study the hydrodynamic and thermal performances of various geometrical configurations of microchannels as compared with the result of simulation. The cooling medium that used in the analysis is distilled water. The analysis of heat transfer in microchannel heat sink is further analyzed by using nanoparticles which is added into base fluid (distilled water) to form nanofluid as cooling medium. In the analysis of applying nanoparticles, only two types of nanoparticles are used, i.e. silica SiO_2 and alumina Al_2O_3. This is because various previous studies have been carried out by simulation and experimental methods for different types of nanoparticles within different types of base fluid in single geometrical configuration of microchannel, and it is well known about their cooling effect among these two parameters. Hence, in the present study, it is important to focus on the effect of nanoparticles application among various geometrical configurations of microchannels at same hydraulic diameter, which is has not been explored by any other studies currently.

Of course, the pure cooling medium of distilled water is also being analyzed for comparison with the application of nanoparticles. As a result, the right effective geometrical configuration of microchannel can be determined and how well of cooling rate between the interaction of nanoparticles effect and geometrical configurations microchannel parameters.

1.5 Thesis Outline

There are five chapters have been arranged subsequently. In chapter 1 for introduction section, general description about the microchannel heat sink and other related heat sink that have been used and analyzed for cooling purpose. For further understanding about the status analysis of microchannel heat sink, literature review has been carried out as compiled in chapter 2. Methodology for simulation work in mathematical modeling and numerical method that been applied to simulate the fluid flow and heat transfer in mirochannel heat sink has been described systematically in chapter 3. Furthermore, the fundamental of experimental work is also been described in the chapter as well in which both simulation and experimental works are related each other as complement to fulfill the research work. In chapter 4, the results and discussion will highlight the verification of simulation result with the experimental result. Besides this, a thorough description of analysis and discussion are highlighted within the scope of this research work. Optimization work is also been carried out to determine the optimum performance of microchannel heat sink. In the final chapter, conclusion is made to conclude the finding of the research.

CHAPTER TWO
LITERATURE REVIEW

2.1 Introduction

In the current status of cooling system for electronic component, especially for computer microprocessor, the demand of higher performance and stability for continuous function, the high capacity of high heat dissipation of microchannel heat sink is required to meet the requirement. As a result, a thorough study about the microchannel heat sink is essential in order to ensure proper design of microchannel heat sink can meet the demand effectively. As refer to the following subsequent subtopic in this chapter, various studies have been carried out by researchers around the world for microchannel heat sink. By the way, in their studies, various geometrical configurations of microchannel have been designed and analyzed accordingly. Furthermore, the effect and type of fluid flow, i.e. laminar flow, turbulent flow and boiling, in microchannel also been analyzed in detail. For advance case in cooling method, the application of nanofluid in microchannel is also been studied extensively. All of these studies are carried out experimentally; of course, simulation is not exempted in this research as well, which is also a vital part of research work in simulating the result of research work in detail at the point where experimental work that not able to provide the detail result. To further understand the trend of the research works on microchannel heat sink, the related previous research works have been summarized and arranged accordingly as in the following subsequent subtopic.

2.2 Study on the effect of fluid flow, various microchannel heat sink configurations and physical channel dimensions

As reported in the study by Chein and Chen (2008), the different arrangements of inlet and outlet for microchannel heat sink have been designed as shown in Figure 2.1.

Simulation work has been applied in their study and using Finite Volume Method to simulate the hydrodynamic and thermal performances of microchannel heat sink. In their finding, for the arrangement of inlet and outlet of N-, S-, D-, U-, and V-type, the velocity maldistribution is more obvious and it is not preferable in which the flow rate in each heat sink channel become different obviously. Hence, such fluid flow condition causes more serious uneven temperature distribution over the heat sink body. Comparatively, they conclude that the V-type arrangement of inlet and outlet of heat sink contributes the best hydrodynamic and thermal performances in terms of pressure drop and overall heat transfer coefficients respectively.

.

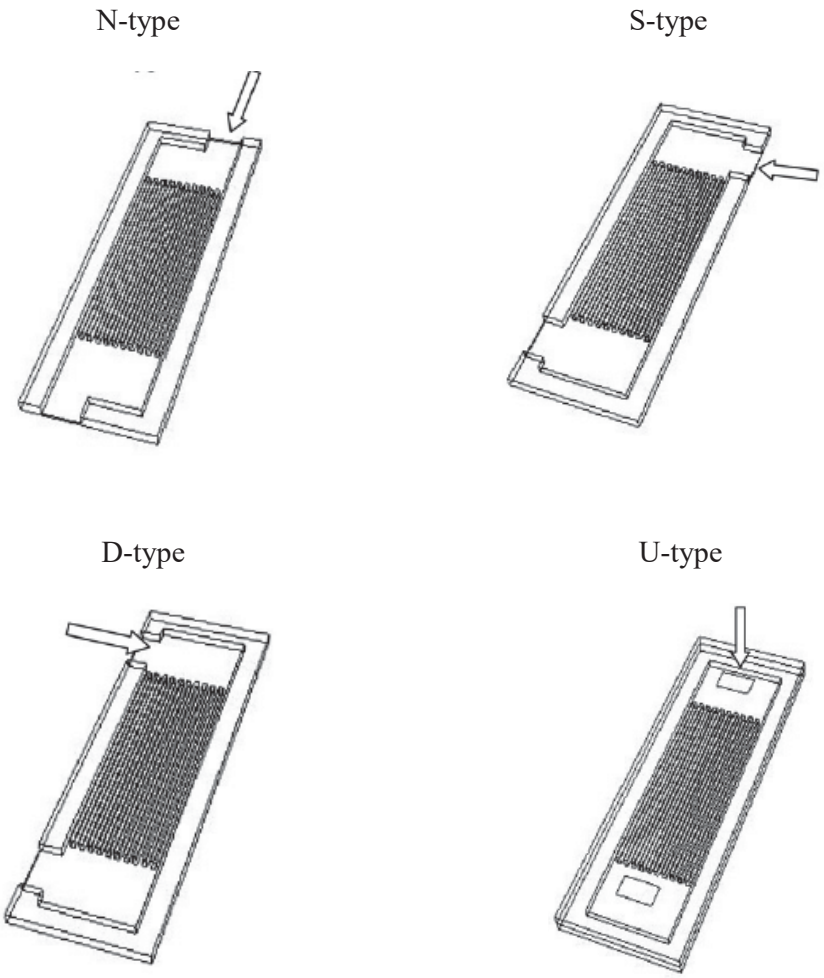

Figure 2.1: Geometric configurations of N-, S-, D-, U-, and V-type arrangement of inlet and outlet of microchannel heat sink (Chein and Chen, 2008).

V-type

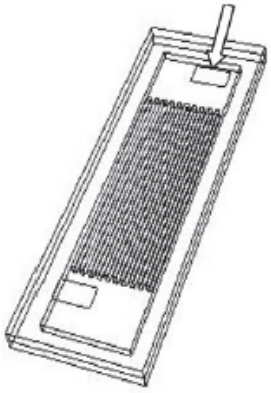

Figure 2.1 (Cont'd): Geometric configurations of N-, S-, D-, U-, and V-type arrangement of inlet and outlet of microchannel heat sink (Chein and Chen, 2008).

Mushtaq et al. (2009) also carried out their study by applying numerical solution of finite volume method in their simulation work. In their study, various configurations of channels have been designed i.e. circular, square, rectangular, iso-triangular and trapezoidal as shown in Figure 2.2. Their study objective is to evaluate the effect of size and shape of channels on microchannel heat sink performance, and their analysis result shows that at the same volume of a microchannel heat sink, both effectiveness and pressure drop will increase at the increment of channel quantity. Furthermore, they found that circular channels give the highest overall performance in hydrodynamic and thermal among various channel configurations.

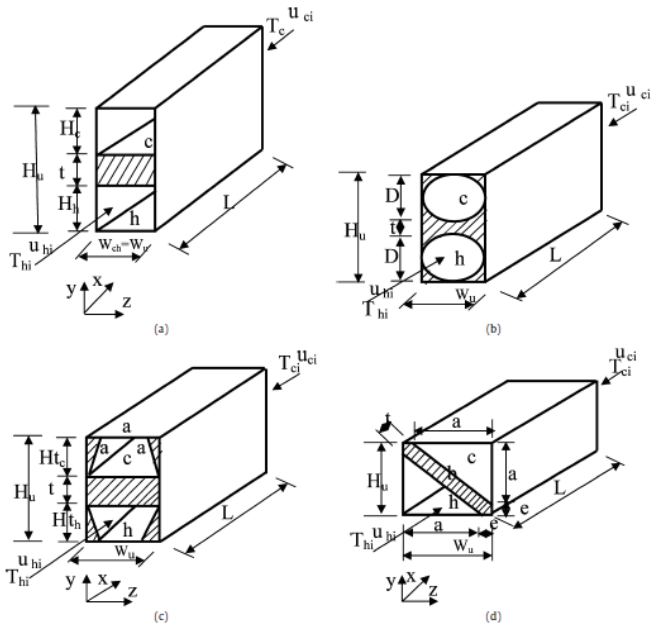

Figure 2.2: Schematic of microchannel configurations of (a) square and rectangular channels, (b) circular channels, (c) trapezoidal channels, (d) triangular channels (Mushtaq et al., 2009).

In the study by Jung and Kwak (2008), they carried out their experiment on various width of microchannel i.e. 100, 150, and 200 micron with the same height of 100 micron and length of 15mm. They found that the measured friction factors for laminar regime are comparable to the theoretical value from the correlation for the flow in macrochannels. But the convective heat transfer coefficients are found to be linearly dependent on the wall temperature and the Reynolds Number dependence on the Nusselt Number is much higher than those for the corresponding flow in macrochannels.

Lee et al. (2005) had carried out their experiment study for the heat transfer in rectangular microchannels with the channel width range from 194μm to 534μm, and the channel depth of fine times the the width in each case. The test piece was made of copper and deionized water was used as cooling medium with the Reynolds Number ranging from approximately 300 to 3500. They also carried out numerical prediction based on the classical-continuum approach and they found that the numerical prediction to be in good agreement with their experimental data which showed average deviation of 5%. Hence,

they suggested that conventional analysis approach can be employed in predicting heat transfer behaviorinmicrochannels.

In the research by Jung et al. (2004), they carried out their study on the effect of fin tip clearance on the cooling performance of microchannel heat sink. Figure 2.3 shows the schematic of microchannel heat sink with fin tip clearance. The effect of fin tip clearance was investigated numerically and optimized tip clearance was determined for which the thermal resistance was minimum. They concluded that the presence of fin tip clearance can improve the cooling performance of microchannel heat sink when the fin tip clearance was smaller than a channel width.

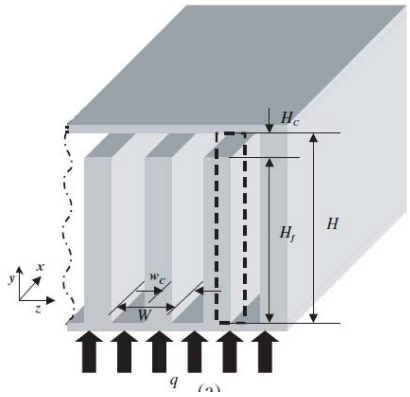

Figure 2.3: Schematic of microchannel heat sink with fin tip clearance (Jung et al., 2004).

For the other study on fin tip clearance effect, Moores et al. (2009) had carried out their investigation on the heat transfer and fluid flow in shrouded pin fin arrays with and without fin tip clearance as shown in Figure 2.4.

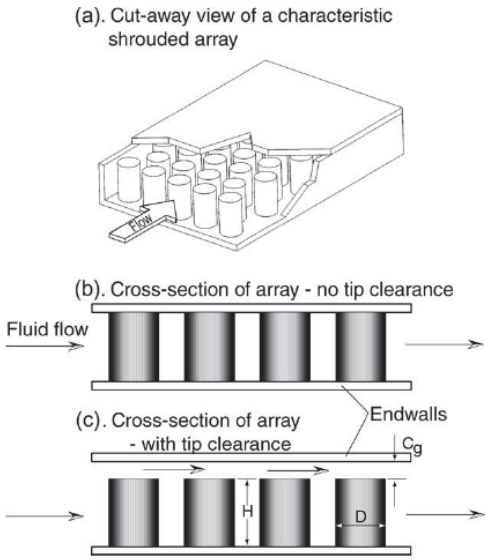

Figure 2.4: (a) Shrouded array geometry, (b) pin fin with tip clearance, and (c) pin fin without tip clearance (Moores et al., 2009).

In their investigation, the tip clearance was found to influence pressure drop performance to the greatest extent at low Reynolds Number ($<5 \times 10^3$). But the effect was being significantly diminished by Reynolds Number of 1.5×10^4. In thermal performance, higher heat transfer rates were found for dimensionless clearances (tip clearance / pin diameter) less than 0.2 as compared with the non-clearance case.

Qu and Mudawar (2002) had carried out experimental and numerical study of pressure drop and heat transfer in single phase fluid flow in microchannel heat sink. The heat sink was fabricated from copper and fitted with polycarbonate plastic cover plate as shown in Figure 2.5. The heat sink consisted of an array of rectangular microchannel with dimensions of 231μm wide and 713μm deep, and deionized water was used as cooling medium. The heat sink was tested at various ranges of heat flux and Reynolds Numbers. They found that the measured pressure drop and temperature distributions show good agreement with the numerical predictions, and they concluded that the conventional Navier – Stokes and energy equations are able to predict the fluid flow and heat transfer characteristics of microchannel heat sinks.

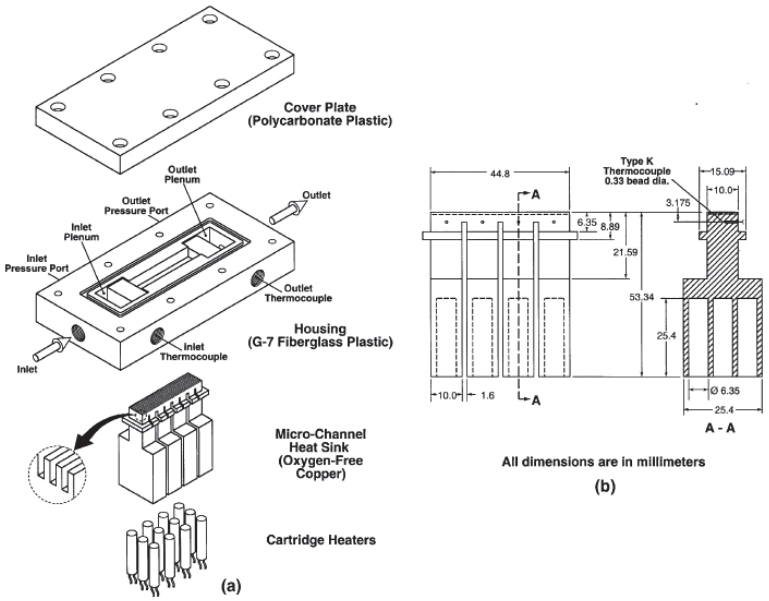

Figure 2.5: (a) Test module, (b) Microchannel heat sink (Qu and Mudawar, 2002).

In the analysis of developing convective heat transfer in deep rectangular microchannels, Harms et al. (1999) had investigated the microchannel performance experimentally by using deionized water as cooling medium. They also found that the experimentally obtained local Nusselt Number agrees well with the classical developing channel flow theory.

Li et al. (2007) carried out their study of liquid flow and heat transfer in microtubes by experiment and simulation. The smooth fused silica and rough stainless steel microtubes with hydraulic diameters of 50 – 100μm and 373 - 1570μm respectively are investigated by using deionized water as coolant at Reynolds Number range from 20 to 2400.Their experimental data showed that the friction factor was well predicted with conventional theory for smooth fused silica tubes. But for the rough stainless steel tubes, the friction factor was higher than the prediction of conventional theory and it was increasing as surface relative roughness increased. Besides this, they also found that the conventional theory for friction was valid for water flow through microtube with relative

surface roughness less than 1.5%. In thermal analysis, the local Nusselt Number approaches the conventional theory prediction when the axial heat conduction effect is gradually weakened with the increase of Reynolds Number and the decrease of the relative tube wall thickness.

In the experimental work that carried out by Sara et al. (2009), investigation of laminar forced convective mass transfer and pressure drop in microtubes was performed on the circular tube size with dimension of 0.20mm and the L/d values in the range of 100 – 500 at Reynolds Number range of 40 – 1400. Their experiment equipment setup is in shown in Figure 2.6. Distilled water had been used as cooling medium. Their experimental results had shown that friction factors were good agreement with the classical Poiseuille flow theory.

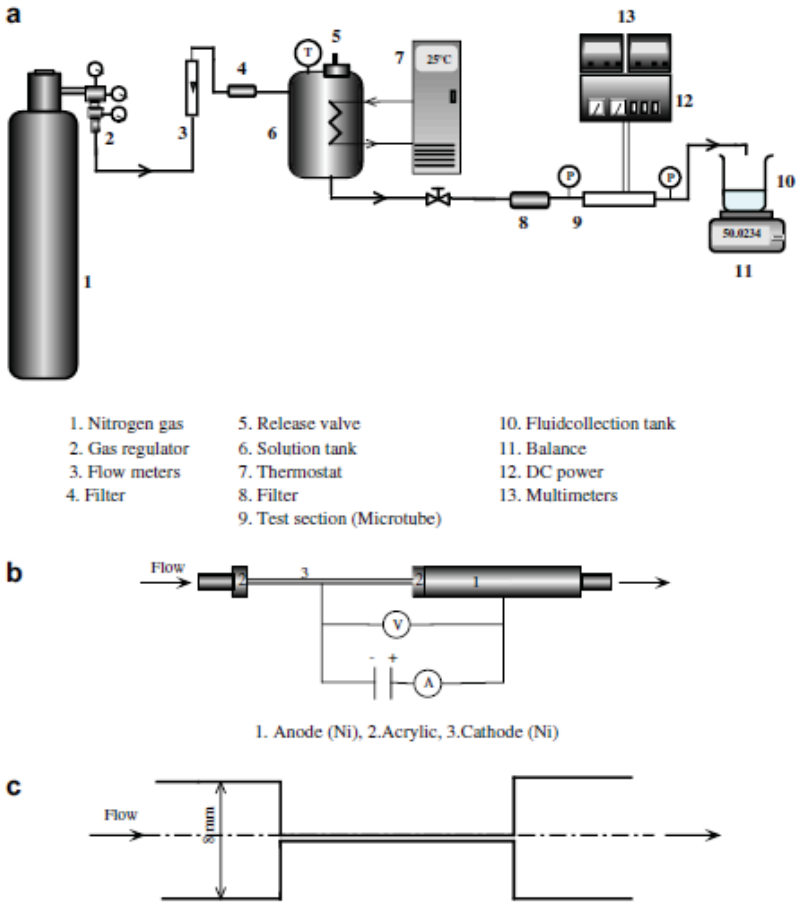

Figure 2.6: Experimental set-up (Sara et al., 2009).

In the study of single phase liquid cooled microchannel heat sink, Zhang et al. (2005) has reported that analytical prediction of pressure drop and thermal resistance through microchannel heat sink was in good agreement with deviation of ≤15% and ≤6% respectively based on their experiment set-up as shown in Figures 2.7 and 2.8.

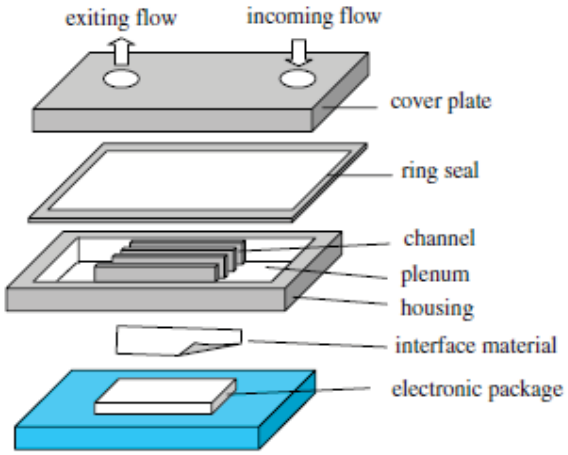

Figure 2.7: Schematic diagram of the liquid cooling concept for electronic packages (Zhang et al., 2005).

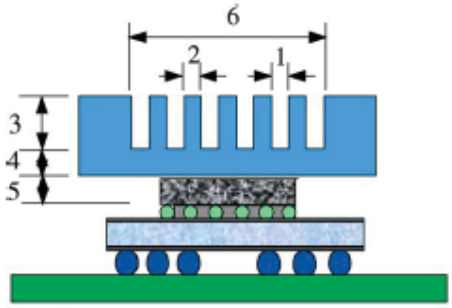

Figure 2.8: Cross-sectional view of the microchannel heat sink on the flip chip ball grid array packages (Zhang et al., 2005).

In the study by Naphon and Khonseur (2009) for the convective heat transfer and pressure drop in microchannel heat sink, experiment had been carried out for different channel heights and channel widths at Reynolds Number of 200 – 1000 and heat flux of 1.80 – 5.40 kW/m^2. Their experiment results had revealed that the microchannel geometry configuration has significant effect on the enhancement of heat transfer and

pressure drop. The following figure shows the schematic diagram of microchannel heat sink for their experimental work.

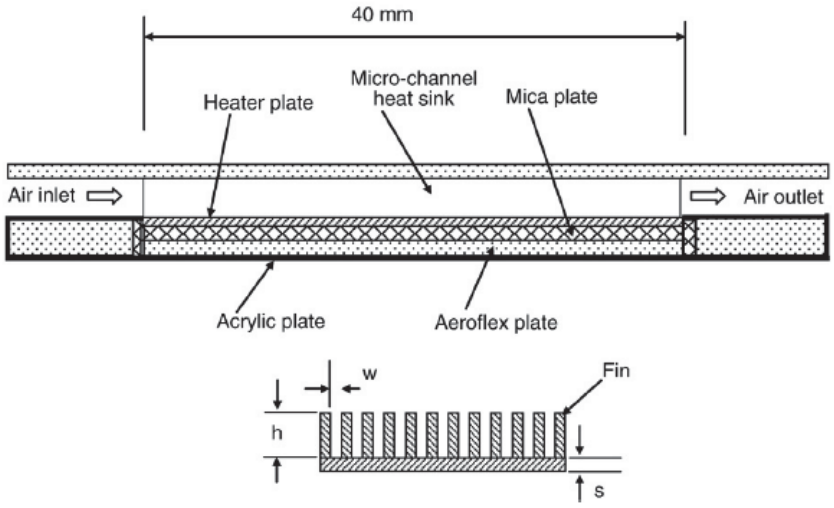

Figure 2.9: Schematic diagram of the test section and microchannel heat sink (Naphon and Khonseur, 2009).

In the simulation work by Chen et al. (2009), they carried out studied for 3-dimensional numerical analysis of heat and fluid flow in noncircular microchannel heat sinks as shown in Figure 2.10. Their study had shown that the value of Nusselt Number was much higher at the inlet region and approaches the constant fully developed value quickly. Besides this, they also found that the triangular microchannel contribute to the highest thermal efficiency.

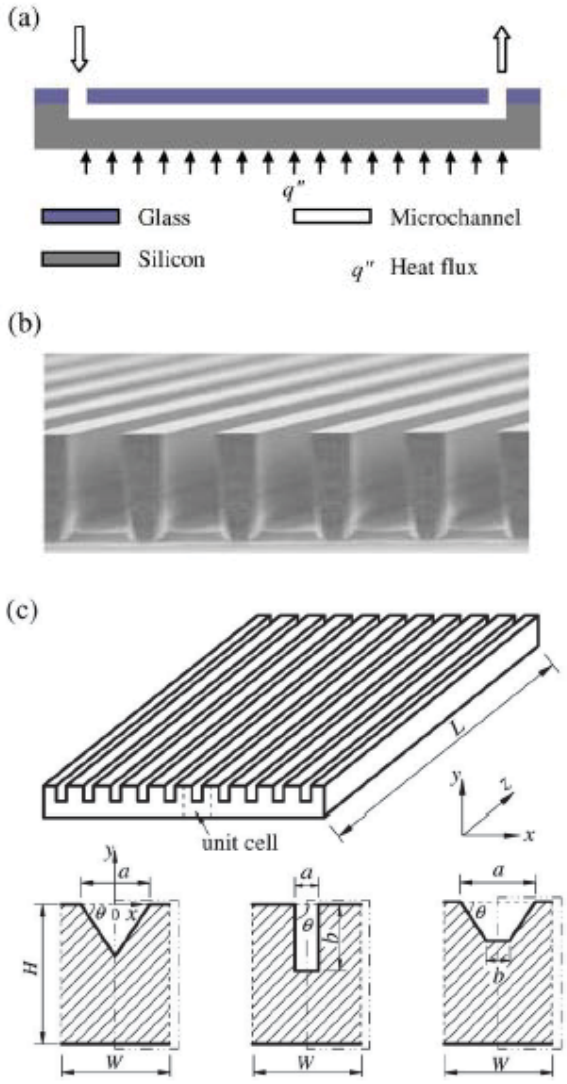

Figure 2.10: Schematic of the microchannel heat sink: (a) system, (b) microscope image of silicon microchannels, (c) geometric shape of microchannel (Chen et al., 2009).

In the research work by Park and Punch (2008), they had carried out study on friction factor and heat transfer in multiple rectangular microchannels with uniform flow distribution. The rectangular microchannels were tested at laminar flow with Reynolds Number of 59 – 800, and their finding showed that conventional theory for fully-developed flow is applicable within the range of their experiments. But in thermal analysis, they found that the average Nusselt Number showed deviation between experimental and theoretical values of heat transfer rate in microchannels. Hence, they

proposed an empirical correlation that confined to their experimental range and expected to be useful to design the microchannel devices related to heat transfer.

Li et al. (2004) had carried out their study in 3-dimensional analysis of heat transfer in a microchannel heat sink with single phase flow as shown in Figure 2.11.

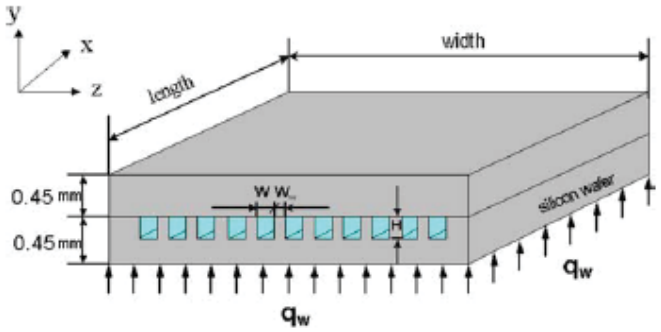

Figure 2.11: Structure of rectangular microchannel heat sink (Li et al, 2004).

They employed a finite difference numerical code with Tri-Diagonal Matrix Algorithm (TDMA) to solve governing equations. The influence of geometric al channel parameters and thermophysical properties of fluid on the flow and heat transfer were investigated by evaluating thermophysical properties at a reference bulk temperature. Their work results showed that thermophysical properties of the liquid can significantly influence both the flow and heat transfer in microchannel heat sink.

Xie et al. (2009) had reported that the microchannel flow geometry provides large surface area of heat transfer and high convective heat transfer coefficient. In their study, minichannel with bottom size of 20mm x 20mm was analyzed numerically for single phase laminar flow for water as cooling medium. Their study results revealed that narrow and deep channel with thin bottom wall thickness and relatively thin channel wall thickness contributes to improvement of heat transfer performance. However, the pressure drop was relatively high but acceptable. Beside this, they also highlighted that

the simulated thermal resistance agrees quite well with the result of conventional correlations method with maximum deviation of 12%.

The research work by Chai et al. (2013) has revealed that the heat transfer enhancement can be achieved by using the microchannel heat sink with periodic expansion – constriction cross-section. Their design of microchannel heat sink is shown in Figure 2.12. Both numerical and experimental works were carried out in their research. They found that the heat transfer is enhanced remarkably for the newly proposed heat sinks with periodic expansion-constriction cross-section (F-type and T-type microchannels) in which showing the averaged Nu number could be increased by about 1.8 times as compared with the R-type microchannel.

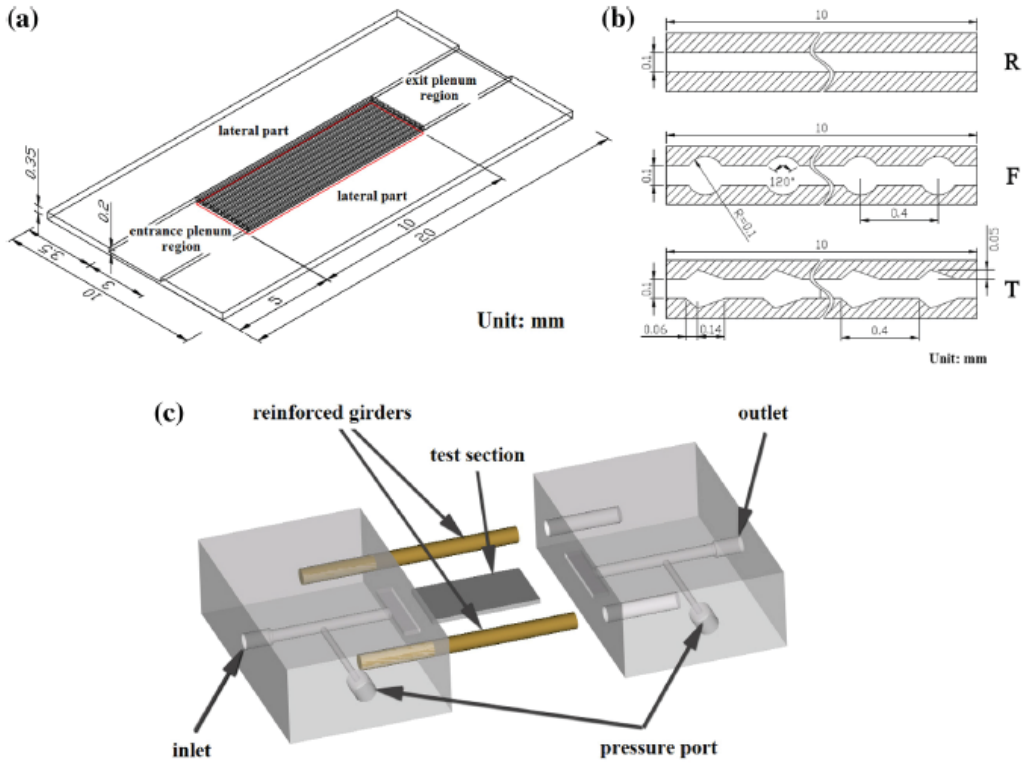

Figure 2.12: Structure and size of heat sinks. (a) Structure, (b) Size, (c) Packaging (Chai et al., 2013).

Wong and Fashli (2013) have carried out numerical analysis on parallel flow two-layered microchannel heat sink. Their modelling of microchannel heat sink for their analysis work is shown in Figure 2.13.

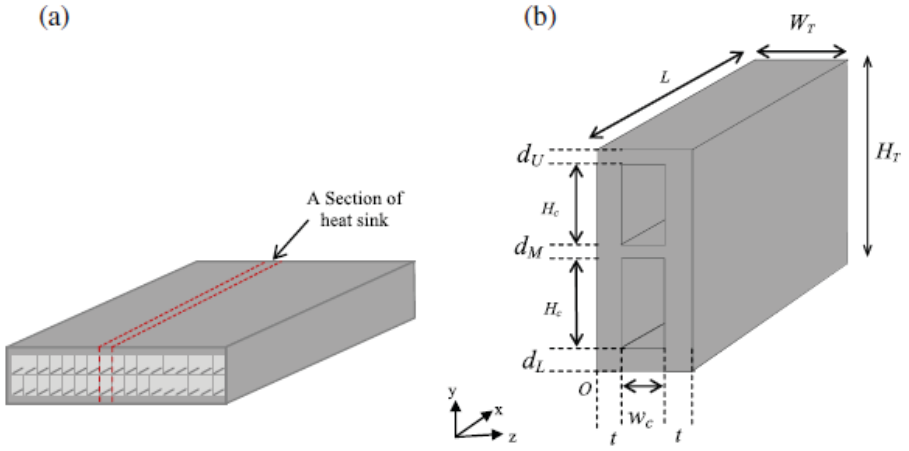

Figure 2.13: Schematic of the (a) two-layered MCHS and (b) a repeated section of MCHS (Wong and Fashli, 2013).

Their findings has shown that the parallel flow configuration leads to better heat transfer performance as compared with the case of counterflow, except for high Reynolds number and high channel aspect ratio. By reducing the thickness of middle rib, lower thermal resistance can be achieved in parallel flow two-layered microchannel heat sink.

As compared with the work by Wong and Fashli (2013), Chuan et al. (2015) has conducted their research work with an improved design of double-layered microchannel heat sink with truncated top channels as shown in Figure 2.14. They reported that there exists an optimal truncation position for the top channel to achieve the best double-layered microchannel heat sink performance. Their finding has shown that for the original double-layer microchannel heat sink with larger L_x, the cooling effect and heating effect of the top coolant are both enhanced compared to the design with smaller L_x. As a result, an appropriate truncated design for the top channel can reduce the top coolant heating effect significantly without the loss of cooling effect. Hence, the

advantages of the truncated concept become more obvious when applied in a double-layered microchannel heat sink with larger L_x.

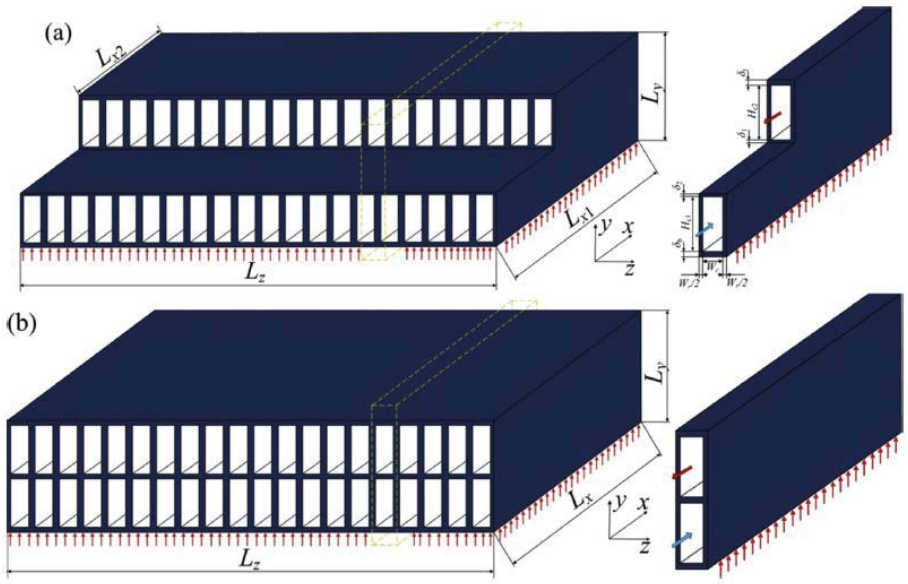

Figure 2.14: The schematic of the heat sink: (a) new design with truncated top channels (b) original design (Chuan et al., 2015).

2.3 Study on the effect of nanofluid in cooling performance of microchannel heat sink

In the experiment work by Ho et al. (2010), analysis of forced convective cooling performance of microchannel heat sink by using alumina nanofluid was carried out. The alumina nanofluid had been employed in 25 parallel rectangular microchannels with dimensions of 50mm length, 283μm width and 800μm height. It was tested at the Reynolds Number range of 226 – 1676. Their experimental results revealed that nanofluid had cooled the heat sink outperforms the water-cooled one in which it was showing significantly higher heat transfer coefficient, and markedly lower the thermal resistance and wall temperature at high pumping power. In hydrodynamic performance of the heat sink, the friction factor for nanofluid-cooled heat sink was found slightly increased.

For other study work for the case nanofluid, Chein and Huang (2005) had carried out analysis based on theoretical model and experimental correlations for pure water-Cu nanofluid with various volume fractions of Cu nanoparticles as cooling medium in microchannel heat sink. The microchannel heat sinks with different dimensions were examined. Their experimental results showed that the heat sink performance was greatly improved by using nanofluid as coolant. This is because of the increased thermal conductivity and thermal dispersion effects. Furthermore, the existence of nanoparticles in the base fluid did not affect any extra pressure drop which is due to small particle size and low volume fraction of the particle.

In the research work by Lee and Mudawar (2007), they also used alumina nanofluid as cooling medium in microchannel heat sink. Their study had found that the high thermal conductivity of nanoparticles is able to enhance the single phase heat transfer coefficient in laminar flow. In analyzing the heat transfer along the microchannels, higher heat transfer coefficient is achieved mostly in the entrance region of channels, but the enhancement becomes weak in the fully developed region. It was proving that nanoparticles have appreciable effect on thermal boundary layer development. In the case of higher concentration of nanoparticles in nanofluid, the nanofluid produced greater sensitivity to heat flux. However, for two-phase cooling, nanoparticles caused catastrophic failure by depositing effect that can lead to the formation of large cluster near the channel exit due to localized evaporation once boiling commenced.

In the work by Jang and Stephen Choi (2006), numerical analysis was carried out to study the cooling performance of microchannel heat sink with nanofluids. Two types of nanofluids were employed in their work, i.e. 6nm copper-in-water and 2nm diamond-

in-water. They reported that the nanofluids reduced both the thermal resistance and the temperature difference between the heated microchannel wall and the coolant.

Chein and Jason (2007) had carried out their analysis experimentally to investigate microchannel heat sink performance using nanofluids. They employed CuO-H_2O mixture as coolant in silicon microchannel heat sink and the CuO particle volume fraction was in the range of 0.2% to 0.4%. It was found that the nanofluid could absorb more heat than water when the flow rate was low. For the case of high flow rates, the heat transfer was dominated by volume flow rate and the nanoparticles did not contribute to additional heat absorption. In their experimental work for low flow rate, the measured wall temperature variations agreed with the theoretical prediction. But for high flow rate, the wall temperature measurement could not agree with the theoretical prediction which is due to the particle agglomeration and deposition. By further analyzing the nanoparticles within the base fluid, they found that raising the nanofluid bulk temperature could prevent the particles from agglomeration into larger particle clusters. In term of hydrodynamic performance of the microchannel heat sink, the pressure drop was slightly increased due to the existence of nanoparticles in microchannel heat sink operation.

In the analysis of forced convective heat transfer of nanofluids in microchannels, Jung et al. (2009) had carried out experimental analysis to investigate the effect of volume fraction of nanoparticles to convective heat transfer and fluid flow in microchannels. They used aluminum dioxide Al_2O_3 nanofluid as coolant in microchannel heat sink. They found that the convective heat transfer coefficient of aluminum dioxide nanofluid increased up to 32% as compared with the distilled water as coolant.

In the numerical analysis for thermal performance of nanofluid flow in microchannels, Li and Kleinstreuer (2008) employing the commercial Navier-Stokes

solver CFX-10 (Ansys Inc., Canonsburg, PA) and user-supplied pre- and post-processing software to analyze the nanofluid flow in trapezoidal microchannel. Pure water and CuO nanofluid with volume fraction of 1% and 4% CuO were used as coolant in the microchannel heat sink. Their study revealed that nanofluids enhanced the thermal performance of microchannel heat sink with small amount increment of pumping power. As the concentration of CuO nanoparticle increased in nanofluid, the thermal performance also increased.

Anoop et al. (2009) research work had reported that the effect of particle size in nanofluid could affect the convective heat transfer in the developing region. Two particle sizes were used in their study, i.e. 45nm and 150nm. Their study had showed that both nanofluids enhanced higher heat transfer characteristics than the base fluid and the nanofluid with 45nm particles showed higher heat transfer coefficient that that with 150nm particles. In the fluid flow region, they also found that the heat transfer coefficients showed higher enhancement than in the developed region.

In the study by Wen and Ding (2004), they also reported that nanofluid was able to enhance convective heat transfer significantly in the entrance region. They used Al_2O_3 nanoparticles and de-ionized water as coolant flowing through a copper tube and fluid flow in the laminar flow regime.

Liu and Yu (2011) had analyzed various concentrations of Al_2O_3 nanoparticles within Al_2O_3 nanolfluid in circular minichannel with 1.09mm inner diameter and at Reynolds Number range of 600 to 4500. In their research, three observations were made for nanofluids in transition and turbulent flow regions. 1st observation, the onset of transition to turbulent flow is delayed. 2nd observation, both of the friction factor and the convective heat transfer coefficient are below than the case of water at the same

Reynolds Number in the transition flow. 3rd observation, at fully developed turbulence flow, the difference in the flow and heat transfer of nanofluids and water will diminish. Besides this, their analysis also revealed that particle-fluid interaction has significant impact on flow of nanofluids, particularly in the transition and turbulent regions. Hence, nanofluids should be used in either the laminar flow or the fully developed turbulent flow in order to yield increment of heat transfer performance.

In the simulation analysis by Mohammed et al. (2010), rectangular microchannel heat sink is numerically analyzed by using alumina-water (Al_2O_3-H_2O) nanofluid as cooling medium with concentration of volume fraction ranged from 1% - 5%. Figure 2.15 shows the modeling of rectangular microchannels for their simulation analysis.

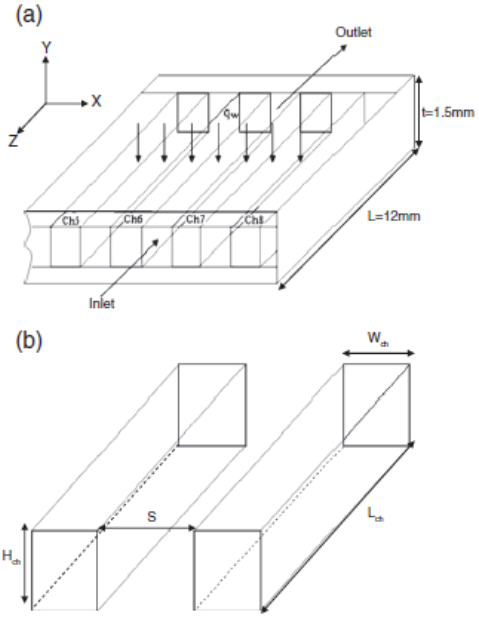

Figure 2.15: (a) Schematic diagram of computational domain, (b) Cross section of rectangular shaped microchannel (Mohammed et al., 2010).

The microchannel heat sink was tested at Reynolds Number that ranged from 100 – 1000. In their simulation work, 3-dimensional of governing equations were solved by using finite volume method (FVM). Their simulation results revealed that heat transfer

coefficient and wall shear stress were increased when the concentration of alumina nanoparticles within nanofluid increased. But thermal resistance of the microchannel heat sink showed decrement. However, when the concentration of alumina nanoparticles was at 5% volume fraction, the alumina nanofluid was not able to increase heat transfer performance. For hydrodynamic performance of the microchannel heat sink, their finding showed slight increase of pressure drop in nanofluid application as compared with base fluid.

Mohammed et al. (2011) continued analyzed the influence of nanofluid in microchannel heat sink by simulation work. 3-dimensional trapezoidal microchannel heat sink had been modeled as shown in Figure 2.16, and four types of base fluids are considered namely water, ethylene glycol, oil and glycerin.

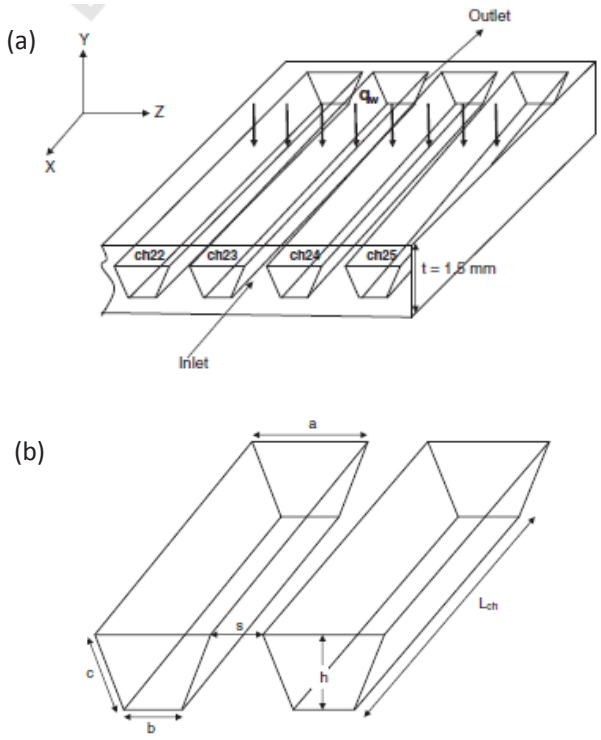

Figure 2.16: (a) Schematic diagram of computational domain, (b) Cross section of trapezoidal shaped microchannel (Mohammed et al., 2011).

Each of these base fluids were mixed with 2% volume fraction of diamond particle. Furthermore, four types of substrate materials for the microchannel heat sink were also

been analyzed, i.e. copper, aluminum, steel and titanium. In their simulation work, conventional governing equations were solved by finite volume method. Their simulation results has shown that the best uniformities in heat transfer coefficient and temperature in microchannel heat sink could be obtained by using glycerin-base nanofluid in which followed by oil-base nanofluid, ethylene glycol-base nanofluid and water-base nanofluid. Comparatively, water-base nanofluid able greatly enhanced the heat transfer performance of the heat sink in which substrate was made of steel.

Besides the works that had been done as mentioned above, Mohammed et al. (2011) had further analyzed the influence of nanofluids in microchannel heat sink by simulation work. In this research work, 3-dimensional square microchannel heat exchanger was modeled as shown in Figure 2.17.

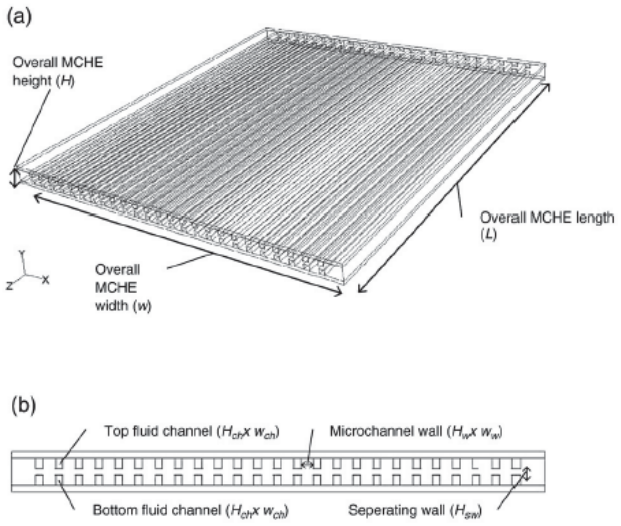

Figure 2.17: Schematic diagram of computational domain, (a) Isometric view of microchannel heat exchanger, (b) Cross sectional view of microchannel heat exchanger (Mohammed et al., 2011).

Four types of nanofluids had been analyzed with the heat exchanger, i.e. aluminum oxide Al_2O_3, silicon dioxide SiO_2, silver Ag and titanium dioxide TiO_2, with different concentration of nanoparticle in nanofluid range of 2%, 5% and 10%. Their results had

shown that the nanofluids were able to enhance thermal properties and performance of the heat exchanger. But the pressure drop in the heat exchanger showed slight increment.

In the research work by Hung et al. (2012), numerical study had been carried out by using 3-D modelling of microchannel heat sink (MCHS). The Al_2O_3-H_2O nanofluid had been used as cooling medium within the microchannel heat sink. They reported that heat transfer enhancement can be obtained by using the nanofluid. Furthermore, they also reported that by using base fluid with lower dynamic viscosity and substrate materials with high thermal conductivity can enhance the thermal performance of the microchannel heat sink. Their analysis results show that as the nanoparticle volume fraction of the nanofluid increases, the thermal resistance decreases and then increases. Hence, the volume fraction of nanoparticle in nanofluid and pumping power under given geometry conditions need to be properly adjusted in order to obtain lowest thermal resistance. Within the range of particle sizes in their analysis, they found that the nanofluids with smaller nanoparticles enable the microchannel heat sink to yield better thermal performance. Moreover, the thermal resistance of the microchannel heat sink can be reduced significantly by increasing the pumping power.

Tokit et al. (2012) has carried out numerical study on an interrupted microchannel heat sink (IMCHS) using nanofluids as cooling medium and their 3-D modelling of IMCHS as shown in Figure 2.18. In their research work, the three dimensional equations of continuity, momentum and energy were solved by using finite volume method (FVM). Difference of nanoparticle volume fraction (1% to 4%), nanoparticle types (Al_2O_3, CuO and SiO_2) and nanoparticle size (30nm to 60nm) are examined at Reynolds number range of 140 to 1034. Their research work reveals that the Nu number for IMCHS is higher than the conventional MCHS with a slight increase of pressure drop. They also found that the highest thermal augmentation is for Al2O3 followed by CuO and SiO2 in

IMCHS. The Nu number increased with the increment of nanoparticle volume fraction and decrement of nanoparticle size.

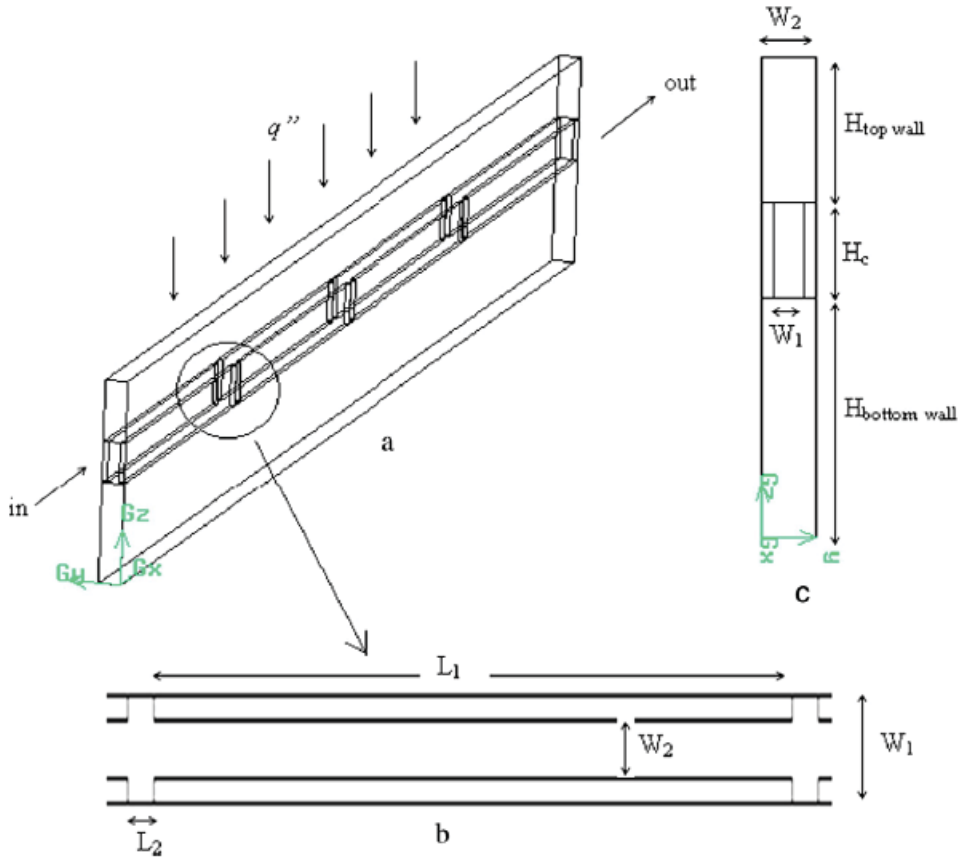

Figure 2.18: (a) 3D view, (b) top view, (c) side view of the single IMCHS (Tokit et al., 2012).

In the research work by Behzad et al. (2013), Eulerian-Eulerian two-phase numerical approach is utilized for forced convection laminar, incompressible and steady three dimensional flow of copper-oxide nanoparticles in base fluid of water at 100 to 200 nm diameter and 1% to 4% volume concentration range within trapezoidal microchannel heat sink. Their research result has shown that by increasing the volume concentration of nanoparticles, the nanoparticles size effect become more prominent and the pressure drop is intensified for above 150 nm particles diameter. Unlike the pressure drop, heat transfer decreases with an increase in nanoparticles diameter. Furthermore, with an increase in nanoparticles diameter, the average Nusselt Number of base fluid decreases

more than nanoparticles. This signifies that base fluid has more efficacy on thermal performance of copper-oxide nanofluid.

Wang et al. have carried out investigation on the effects of temperature-dependent thermophysical properties for the nanofluid Al_2O_3 – H_2O with 1% particle volume fraction under constant pumping power constraint. Their investigation has revealed that increase in viscosity of the nanofluid did not always lead to enhancement of microchannel heat sink (MCHS) performance under fixed pumping power constraint. The optimal MCHS design is closely to the assigned pumping power. However, in high pumping power regime, the performance enhancement is not as effective as in low pumping power regime.

In the findings by Mostafa and Maziar (2013), their numerical analysis on microchannel heat sink by utilizing nanofluid Al_2O_3 – H_2O as cooling medium has revealed that enhancement in heat transfer and increase in friction factor have been obtained by the used of the nanofluid. Heat transfer enhancement is more obvious by the use of variable properties in which the effects of temperature variation on nanofluid heat transfer are greater than the pure water.

Tiew et al. (2014) have conducted their research work by investigating the effect of streamwise conduction on the thermal performance of nanofluid flow in microchannel heat sinks under exponentially decaying wall heat flux. They reported that the significance of the streamwise conduction which is prevalent in low Peclet Number flow is greatly amplified when the volume fraction of nanoparticle is increased. At low Peclet Number, the contribution of the streamwise conduction in nanofluid is found to be more than twofold of that in its base fluid. The effect of streamwise conduction on the

nanofluid flow in microchannel heat sink is significant albeit not dominant particularly for low Peclet Number and high nanoparticle volume fraction of the nanofluid.

For the research that carried out by Yun et al. (2015), numerical analysis by using finite volume method is utilized to investigate the hydraulic and thermal performance of manifold microchannel heat sink (MMHS) with and without nanofluids as working fluids. Their results showed that with increasing volume fraction of nanoparticles, Nusselt Number and pumping power increase, but total entropy generation decreases. Increasing particle size leads to decreasing Nusselt Number, pumping power, and performance index, but increasing the total entropy generation. By increasing the Reynolds number, the Nusselt Number and pumping is increasing but decreasing performance index and total entropy generation.

Bahram et al. (2015) have conducted their research on the performance of an enhanced microchannel heat sink with sectional oblique fins as shown in Figure 2.19, and with a coolant that contains Nano-Encapsulated Phase Change Material (NEPCM) particles. The effect of introducing tip-clearance to the heat sink on thermal and hydrodynamic performances is examined at low Reynods Number. They have found that by using of NEPCM slurry in contrast with pure base fluid, enhanced the cooling performance of the heat sink but increased the Euler Number. Moreover, they also found that the introduction of tip-clearance to the heat sink, if the clearance is chosen properly, has the potential to enhance the cooling performance and reducing the Euler Number simultaneously.

2.4 Summary

As review for the previous research works which had been carried out by researchers in this chapter, most of researchers had claimed that conventional governing

equations, i.e. Continuity equation, Navier-Stokes equations and Energy equations can be solved that able to simulate the hydrodynamic and thermal performances of microchannel heat sink. The previous works also shows that the geometrical configurations of microchannels also play an important role that can affect the performances of microchannel heat sink. Comparatively, it is found that most of these works were carried out onto single type of microchannel heat sink, like rectangular, triangular and circular channel individually. Except for the research work by Chen et al. (2009), they have made comparison of microchannel heat sink performance between rectangular, trapezoidal and triangular channels but each of these channel configurations has different hydraulic diameter which is not proper approach for comparison purpose. Referring to the analysis work by Jung et al. (2004), the vertical fin tip gap has been analyzed. But they have not carried out any analysis onto vertical fin tip gap effect for triangular and trapezoidal for comparison as well as horizontal fin tip gap. Hence, this is the gap of knowledge to be explored for comparison of microchannel heat sink performance (at same hydraulic diameter) and fin tip gap among various channel configurations.

Besides using various types of base fluids for cooling in microchannel heat sink, researchers had carried out innovation approach to add nanoparticle into base fluid to form nanofluid that able to enhance thermal performance of the heat sink with slight changes in hydrodynamic performance, i.e. small increment of pressure drop as compared with base fluid as coolant. Various types of nanofluids were also been analyzed in both experimental and simulation works. Although various researches have been carried out by researchers on the microchannel heat sink by using various types of nanofluids, the experimentally comparison of nanofluid application among various configurations of microchannel heat sink still have not been explored. As referring to the research work by Mohammed et al. (2010 and 2011), numerical analysis have been carried out on the various types of nanofluids within rectangular and trapezoidal

microchannel heat sinks, in which each types of microchannel hear sink configuration was analyzed individually. Besides this, other researchers also carried out their numerical analysis on single configuration of microchannel heat sink. Furthermore, the research work by Lee and Mudawar (2007), Ho et al. (2010), Jung et al. (2009) and other researchers also carried out their experimental work on single configuration of microchannel heat sink and no comparison was made for the various configurations of microchannel heat sink. Hence, this is also a gap of knowledge to be explored to analyze the comparison of performance among various configurations of microchannel heat sink.

In the current work, rectangular-, triangular- and trapezoidal-microchannels have been designed and fabricated for analysis experimentally. Besides this, the 3-dimensional modeling of the same dimension as actual microchannel heat sink is also been carried out for validation with the experimental results and simulation analysis in order to further analyze the performance of the microchannel heat sink in which for the condition that not be able to be determined by the experiment work. Base fluid of distilled water and nanofluids (Al_2O_3-H_2O nanofluid and SiO_2-H_2O nanofluid) with different concentrations of nanoparticles are employed in the analysis of performance of various geometrical configurations of microchannel heat sink. The purpose is to determine the best configuration of microchannel that able contribute to high thermal performance.

CHAPTER THREE
METHODOLOGY

3.1 Introduction

The thermal management of electronic components by using mirochannel heat sinks has been analyzed by both simulation and experimental works in this research study. There are three types of geometrical configurations of microchannels have been designed, such as rectangular, triangular and trapezoidal microchannels, in order to study their comparative contribution in thermal management improvement. In order to enable heat dissipation away from the microchannel heat sinks, various cooling mediums are used within these microchannels and analyzed systematically to determine the cooling effectiveness among the various of cooling mediums. Types of cooling mediums which have been analyzed are as follow: distilled water, alumina (Al_2O_3) nanofluid and silica (SiO_2) nanofluid. Furthermore, the nanofluids are studied in different content of nanoparticle concentration.

In the experimental work, three types of microchannel configurations are fabricated using material of aluminium. The micro-pump is used to pump the cooling medium through microchannel to dissipate heat from the heat sink. Based on the available capacity of the micro-pump, the Reynolds Number of the fluid flow shows that the flow within the microchannels is laminar flow type. The hydrodynamic and thermal performances of the microchannel heat sink are determined and analyzed based on the measurement of pressure and temperature of fluid flow and heat sinks.

In simulation work, Finite Volume Method (FVM) has been applied to simulate the hydrodynamic and thermal performances of microchannel heat sink. Such solution method is carried out by using the FLUENT software. The modeling of the microchannel heat sink in simulation is exactly according to the experimental model for each type of

microchannel configurations. The simulation work has been carried out based on the same value of parameters, i.e. Reynolds Number, microchannel heat sink material and heat input to the heat sink base.

Both of the study works above are discussed in detail in the subsequent sub-chapters.

3.2 Model Development

The solid modeling of microchannel heat sink is carried out in AutoCAD software and save the file into the format that can be exported for further edit in other software. Gambit 2.4.6 has been employed to import the file which is created by AutoCAD software and further edit the solid modeling microchannel heat sinks. In the Gambit software, the fluid and solid volumes are defined in which then these volumes are meshed accordingly. Boundary conditions for the related areas of the heat sinks and fluid flow are defined. After complete all of the necessary works of defining the heat sink model in Gambit software, the meshed model has been exported to FLUENT 6.3.26 software for fluid flow analysis. In the FLUENT software, there are various parameters are set and defined for fluid and solid volumes, for instant, material properties, pressure, heat input, fluid flow velocity, etc. In order to have a clear picture about the model development as described, Figure 3.1 shows the summary of the development process.

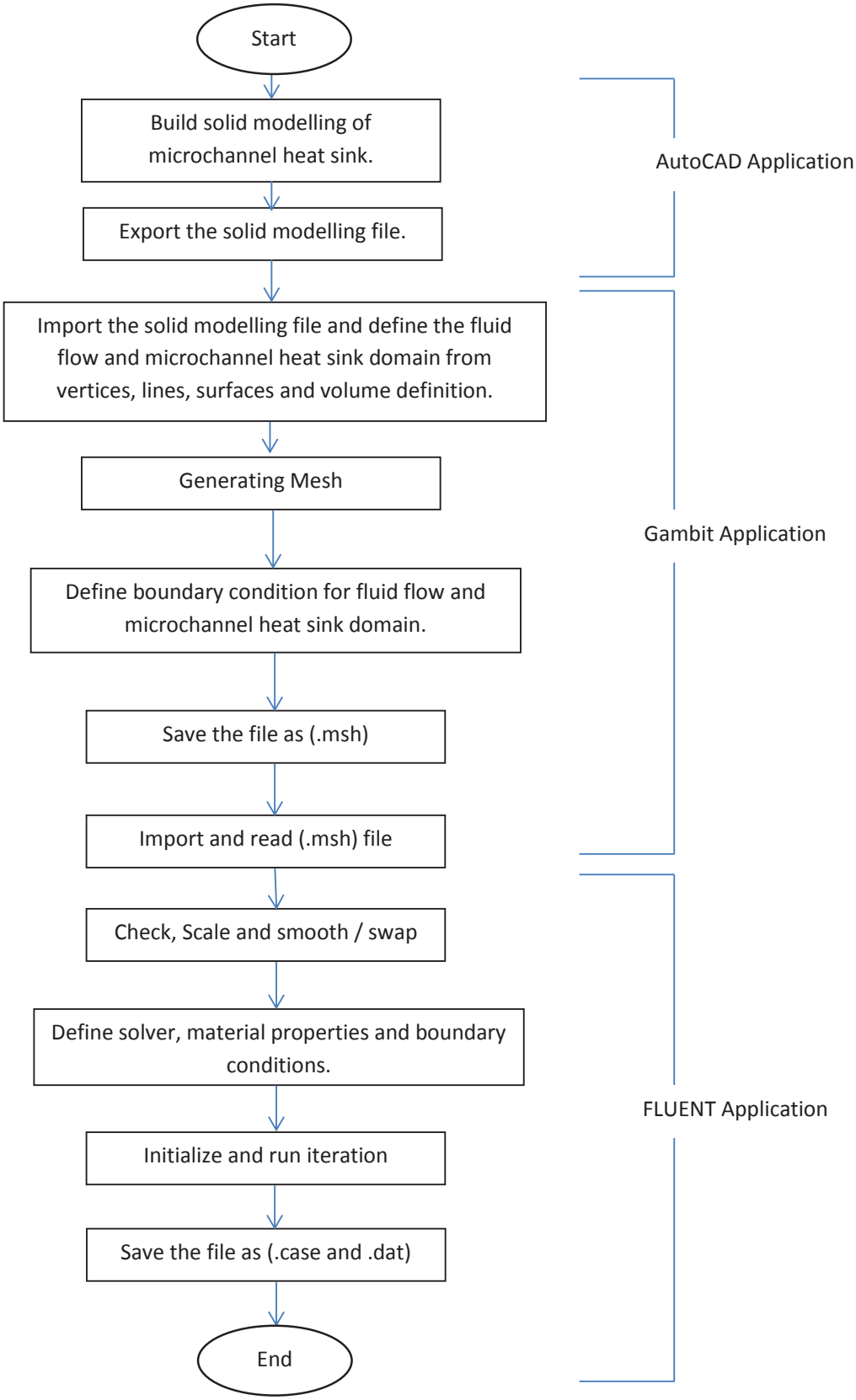

Figure 3.1: Flow chart of microchannel heat sink model development for simulation analysis.

3.2.1 Equations solution for modeling

In the simulation work, the following assumptions are made:

a. Fluid flow and heat transfer are in steady state condition.

b. The cooling medium is a single phase fluid flow.

c. The flow is laminar within Reynolds number range of 70 to 1150.

d. Properties of the fluid and microchannel heat sink are constant due to not large changes temperature between inlet and outlet of microchannel heat sink.

e. Heat sink surfaces which are exposed to the surrounding are assumed as adiabatic, except the heat sink base surface where heat flux is applied.

Based on the assumptions above, the following equations of Continuity equation, Navier-Stokes equations and Energy equation are solved by Finite Volume Method in FLUENT software for the cooling medium of distilled water.

Continuity equation:

$$\frac{\partial u}{\partial x} + \frac{\partial v}{\partial y} + \frac{\partial w}{\partial z} = 0 \tag{3.1}$$

where *u*, *v* and *w* is fluid flow velocity in *x*-, *y*-, and *z*-directions respectively.

Momentum equation:

$$u\frac{\partial u}{\partial x} + v\frac{\partial u}{\partial y} + w\frac{\partial u}{\partial z} = -\frac{1}{\rho_f}\frac{\partial P}{\partial x} + \frac{\mu}{\rho_f}\left(\frac{\partial^2 u}{\partial x^2} + \frac{\partial^2 u}{\partial y^2} + \frac{\partial^2 u}{\partial z^2}\right) \tag{3.2a}$$

$$u\frac{\partial v}{\partial x} + v\frac{\partial v}{\partial y} + w\frac{\partial v}{\partial z} = -\frac{1}{\rho_f}\frac{\partial P}{\partial y} + \frac{\mu}{\rho_f}\left(\frac{\partial^2 v}{\partial x^2} + \frac{\partial^2 v}{\partial y^2} + \frac{\partial^2 v}{\partial z^2}\right) \tag{3.2b}$$

$$u\frac{\partial w}{\partial x} + v\frac{\partial w}{\partial y} + w\frac{\partial w}{\partial z} = -\frac{1}{\rho_f}\frac{\partial P}{\partial z} + \frac{\mu}{\rho_f}\left(\frac{\partial^2 w}{\partial x^2} + \frac{\partial^2 w}{\partial y^2} + \frac{\partial^2 w}{\partial z^2}\right) \tag{3.2c}$$

where ρ is density, μ is viscosity and *P* is pressure.

Fluid flow - Energy equation:

$$u\frac{\partial T}{\partial x}+v\frac{\partial T}{\partial y}+w\frac{\partial T}{\partial z}=\frac{k_f}{\rho_f c_{pf}}\left(\frac{\partial^2 T}{\partial x^2}+\frac{\partial^2 T}{\partial y^2}+\frac{\partial^2 T}{\partial z^2}\right) \tag{3.3}$$

where k is thermal conductivity and c_p is specific heat capacity.

Solid – Conduction equation:

$$\frac{\partial^2 T}{\partial x^2}+\frac{\partial^2 T}{\partial y^2}+\frac{\partial^2 T}{\partial z^2}=0 \tag{3.4}$$

In order to simulate the case of silica and alumina nanofluid cooling mediums, the properties of density ρ, dynamic viscosity μ, specific heat capacity c_p and thermal conductivity k need to be determined by the following equations:

Density (Mohammed et al., 2010):

$$\rho_{nf}=(1-\varphi)\rho_{bf}+\varphi\rho_p \tag{3.5}$$

Specific heat capacity (Mohammed et al., 2010):

$$(\rho c_p)_{nf}=(1-\varphi)\left(\rho c_p\right)_{bf}+\varphi(\rho c_p)_p \tag{3.6}$$

Thermal conductivity (Mohammed et al., 2010):

$$k_{nf}=\frac{k_p+2k_{bf}+2(k_p-k_{bf})\varphi}{k_p+2k_{bf}-(k_p-k_{bf})\varphi}k_{bf} \tag{3.7}$$

Viscosity (Mohammed et al., 2010):

$$\mu_{nf}=\mu_{bf}(1+2.5\varphi) \tag{3.8}$$

where φ is the volume fraction of nanoparticles, the subscript of '*bf*' is referred as base fluid, the subscript of '*nf*' is referred as nanofluid, the subscript of '*p*' is referred as nanoparticle.

3.2.2 Development of mesh modeling

In developing the mesh for microchannel heat sink modeling, the Gambit 2.4.6 software is used by creating vertices as the beginning step for the physical dimension of microchannel heat sink. Then, lines are created to link between vertices to form an area in which then defined as surface. The fluid flow and microchannel heat sink volume domains are created based on the surface. Figure 3.2 shows the meshing result for rectangular, triangular and trapezoidal microchannel.

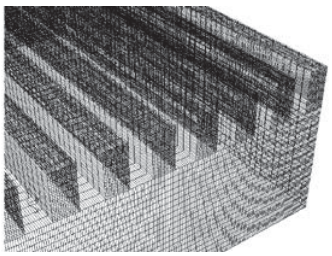

a) Meshing for rectangular microchannels

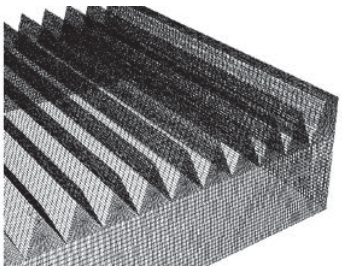

b) Meshing for triangular microchannels

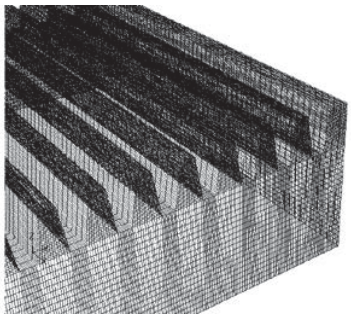

c) Meshing for trapezoidal microchannels

Figure 3.2: Meshing work for various geometrical configurations of microchannels.

After complete the meshing for the microchannel heat sink model as shown in the figure above, they will be saved into the file format (.msh) that will be imported into FLUENT software for analysis.

3.2.3 Boundary conditions

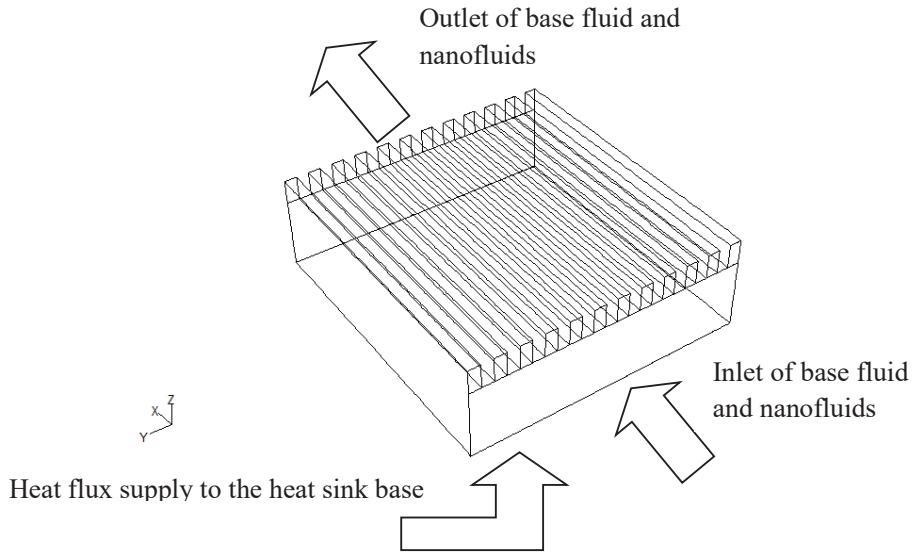

Figure 3.3: Boundary condition for the 3-D modeling of microchannel heat sinks.

As shown in Figure 3.3, the boundary conditions are set as follow:

At inlet of microchannel heat sink:

$$u = u_{in};\ T = T_{in} \tag{3.9}$$

Interface between solid and fluid:

$$u = v = w = 0\ ms^{-1};\ T = \frac{T_s + T_f}{2} \tag{3.10}$$

$$-k_s \frac{\partial T_s}{\partial n} = -k_f \frac{\partial T_f}{\partial n} \tag{3.11}$$

At the heat sink base:

$$q'' = -k_s \frac{\partial T_s}{\partial n} \tag{3.12}$$

At the outlet of microchannel heat sink:

$$P = P_{out} \tag{3.13}$$

$$\frac{\partial T}{\partial n} = 0 \tag{3.14}$$

where the subscript of 's' is referred as solid and subscript of 'f' is referred as fluid.

The boundary conditions above have been set in both Gambit and FLUENT softwares for analysis. Furthermore, these boundary conditions are set based on the actual condition from experimental work.

3.2.4 Grid independency

In the grid independency analysis, the effect of grid size is important and need to be analyzed before analysis of microchannel heat sink performance can be carried out. This is because different size of grid can affect the numerical results. As shown in Table 1, there are three grid sizes have been studied i.e. 4.99 x 10^5, 11.30 x 10^5, and 21.49 x 10^5 grids by analyse rectangular microchannel heat sink. Comparatively, it is found that the maximum deviation of heat sink base temperature for experimental result, grid 4.99 x 10^5, and grid 11.30 x 10^5 as compared with the grid 21.49 x 10^5 are 0.887%, 3.281% and 0.893% respectively. Since the deviation between the grid sizes of 11.30 x 10^5 and 21.49 x 10^5 is less than 1%, and the 11.30 x 10^5 grid size is sufficient and chosen throughout the numerical analysis with less computing time and memory usage as compared with the grid size of 21.49 x 10^5.

Table 1: Comparison of experimental result with simulation result at various grid sizes.

Reynolds Number, Re	Experimental Result for Heat Sink Base Temperature, K	% Difference as compared with the Case 3	Simulation Result for Heat Sink Base Temperature, K				
			Grid Size				
			Case 1: 4.99×10^5	% Difference as compared with the Case 3	Case 2: 11.30×10^5	% Difference as compared with the Case 3	Case 3: 21.49×10^5
73	350.72	0.887	342.250	3.281	350.700	0.893	353.860
83	348.02	0.778	339.880	3.099	347.960	0.795	350.750
94	345.60	0.844	338.040	3.013	345.570	0.852	348.540
105	343.38	0.875	334.999	3.294	343.390	0.872	346.410

3.3 Experiment Setup

3.3.1 Equipment Setup

With reference to the research work by Qu and Mudawar (2002), the experimental equipment, the design of microchannel heat sink and computer system have been set up as shown in Figures 3.4 and 3.5.

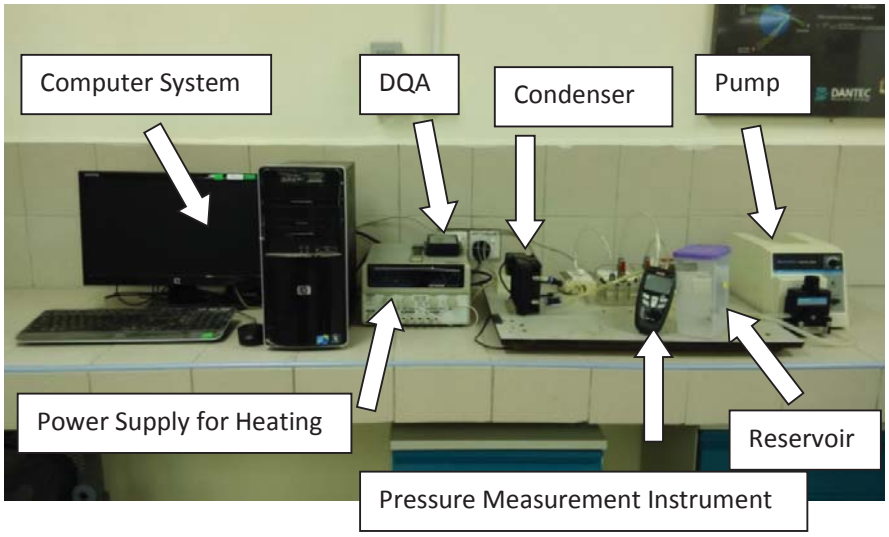

Figure 3.4: General view of experimental setup.

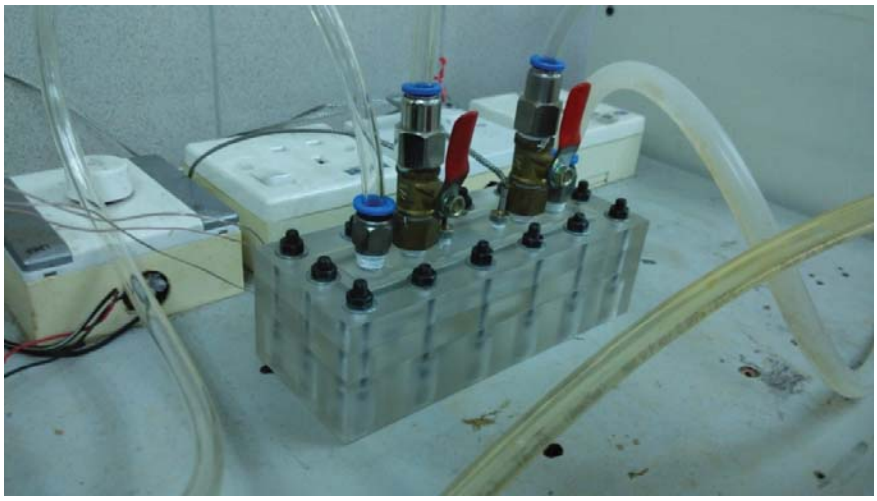

Figure 3.5: Assembly of microchannel heat sink.

To have a clear picture about the whole system of the experimental work, a schematic diagram is shown as in Figure 3.6.

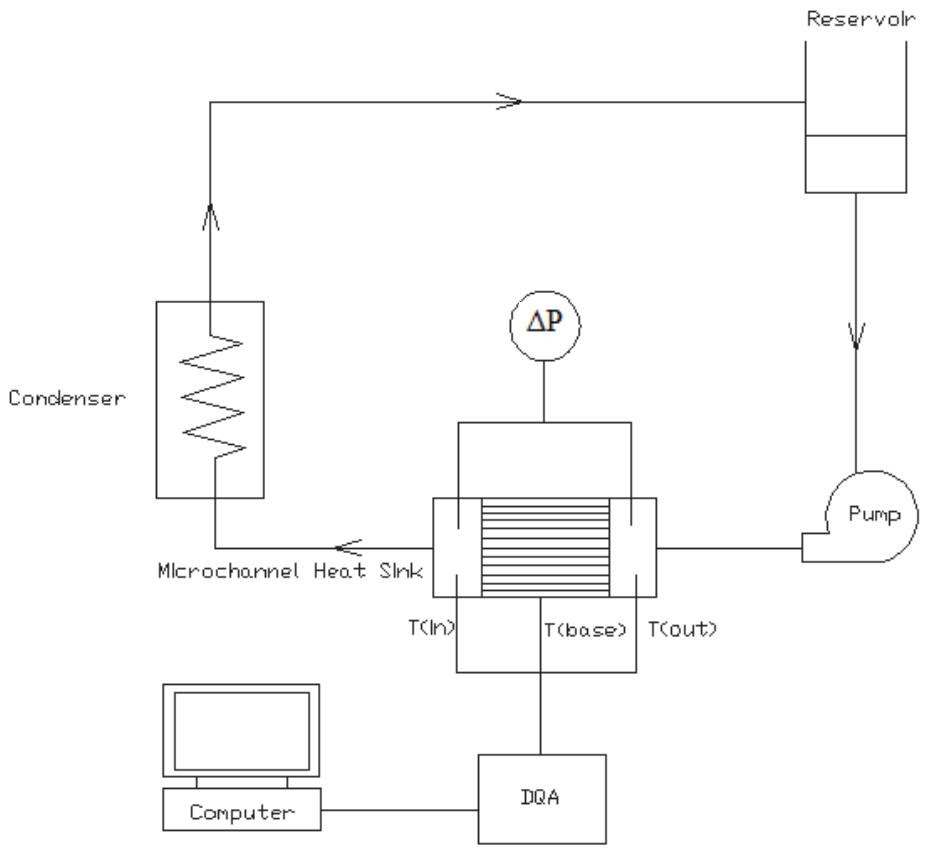

Indications:

ΔP – Pressure measurement by digital pressure indicator (on differential pressure)

T(in) – Inlet flow temperature measurement by thermocouple

T(out) – Outlet flow temperature measurement by thermocouple

T(base) – Microchannel heat sink base temperature measurement by thermocouple

Figure 3.6: Schematic diagram of equipment system for experimental work.

Generally, the dimension of the experiment rig that has been in the experiment work is shown in Figure 3.9. For microchannel design, three types of geometrical configurations of microchannels have been fabricated as shown in Figure 3.7 with the detail of dimension. These heat sinks are made by aluminium material.

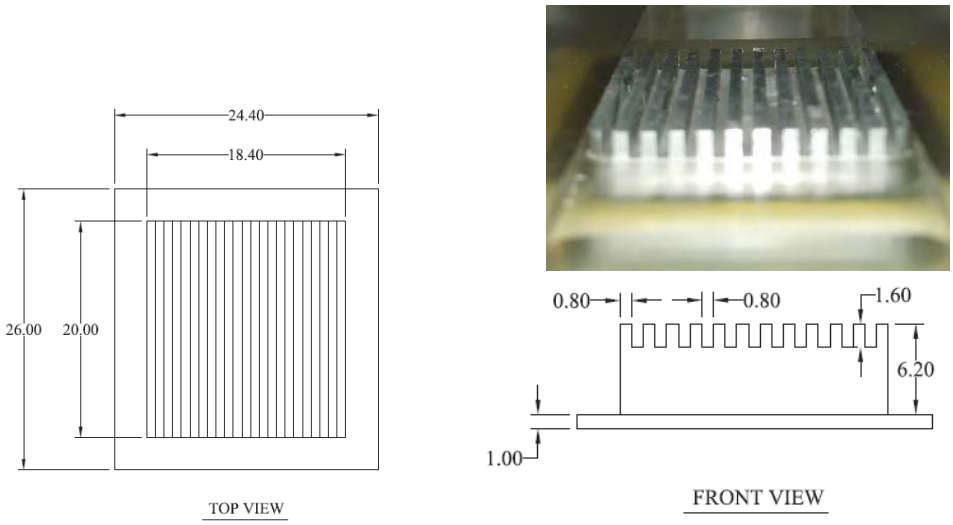

(a) Rectangular microchannel heat sink

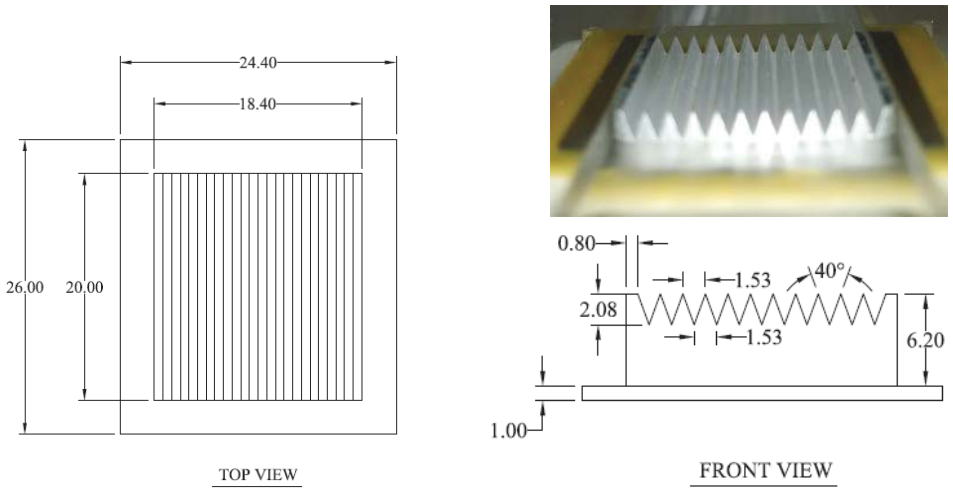

(b) Triangular microchannel heat sink

Figure 3.7: (a) Rectangular-, (b) Triangular-, and (c) Trapezoidal- microchannel heat sinks.

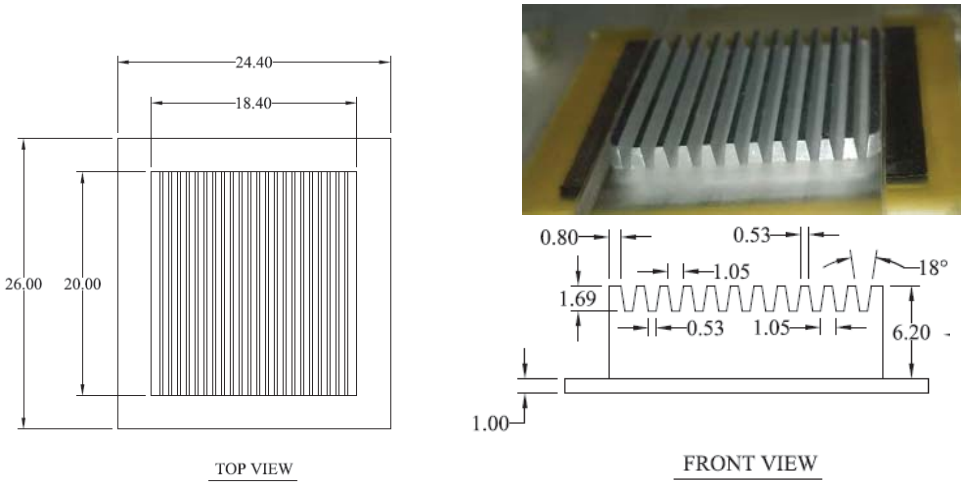

(c) Trapezoidal microchannel heat sink

Figure 3.7 (Cont'): (a) Rectangular-, (b) Triangular-, and (c) Trapezoidal- microchannel heat sinks.

In order to enable these microchannel heat sinks to be analyzed experimentally, the casings of top (thickness of 12mm), middle (thickness of 12mm) and bottom (thickness of 26mm) have been designed and fabricated to contain the microchannel heat sink as shown in Figure 3.5 and Figure 3.8. The casing parts are made of Perspex with low thermal conductivity. By surrounding the microchannel heat sinks with such low thermal conductivity material, the heat loss to the environment is small and assumed to be neglected.

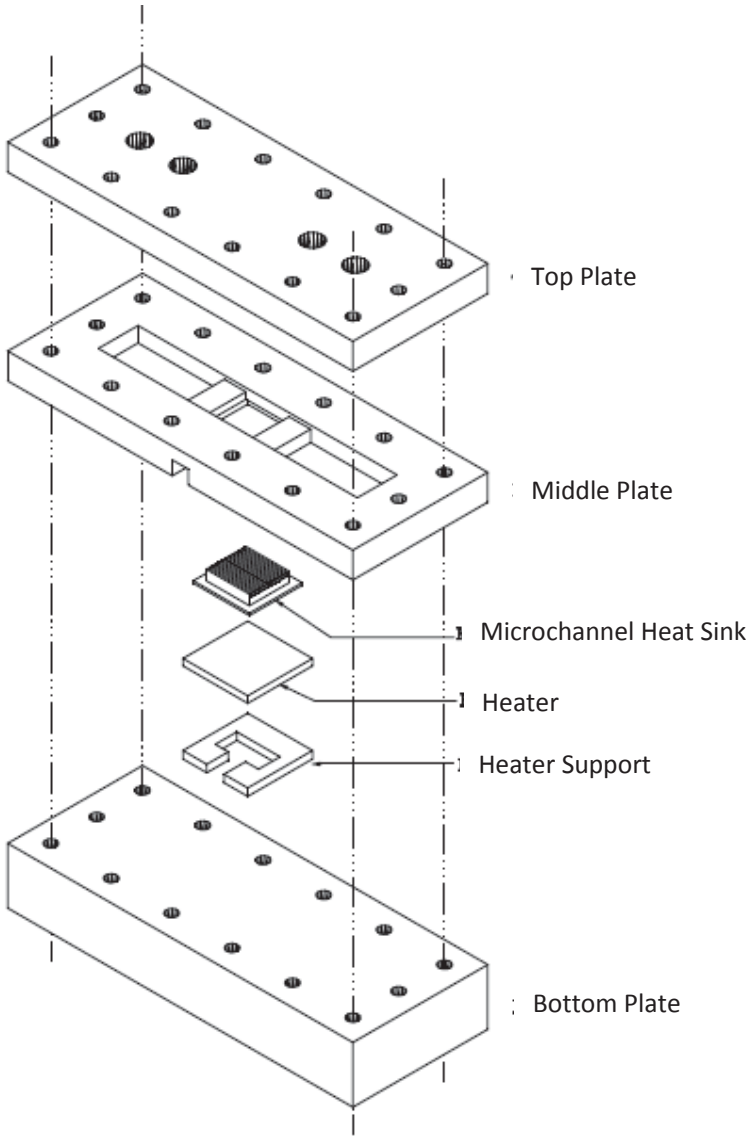

Figure 3.8: Assembly arrangement of microchannel heat sink with casing and heater.

As refer to Figure 3.9, the cooling medium will flow into the manifold of middle plate and then flow through microchannel heat sinks to transfer away the heat from the heated heat sink, and the cooling medium flow is driven by using the micro-pump MasterFlex L/S Drive PTFE Tubing Pump. There are three types of cooling mediums are tested in this experiment work, namely distilled water, silica nanofluid and alumina nanofluid. The preparation of silica and alumina nanofluid will be described further in the following section of this chapter. The heat sink is heated by heater at the bottom of the heat sink. During the cooling medium flows through the microchannel heat sink, the

temperature of the heat sink base, fluid flow inlet and fluid flow outlet are measured by using K-type thermocouple that linked to DQA in which the temperature measurement is collected by computer system. Besides this, the pressure measurement of fluid flow inlet and outlet is carried out by using digital MP120 Pressure Indicator. Based on the available capacity of micro-pump, it is found the range of dimensionless Reynolds Number is between 70 and 110. Such value of Reynolds Number is indicating that the fluid flow is laminar flow.

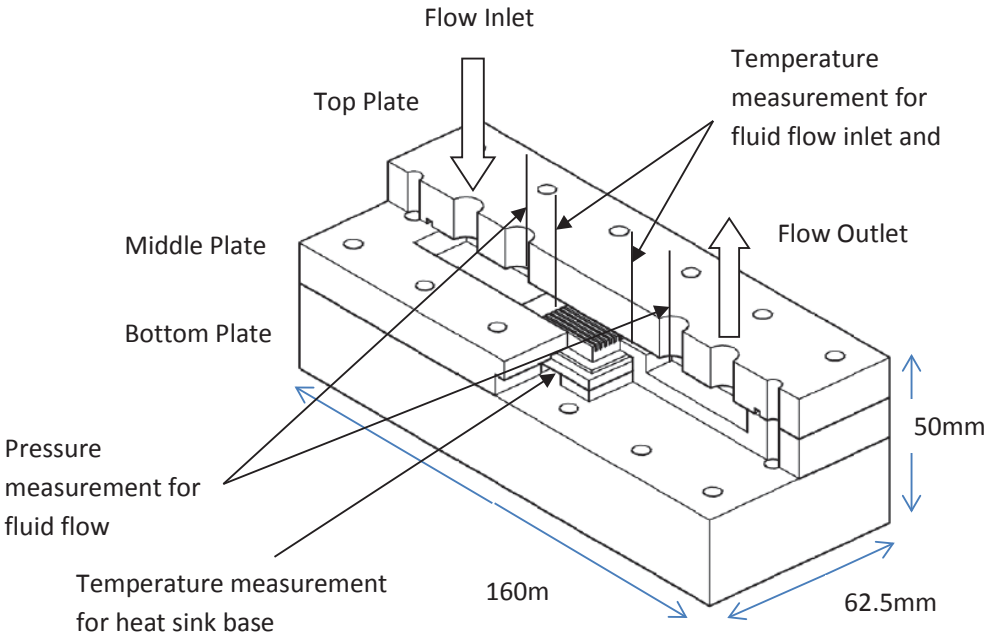

Figure 3.9: Cross-sectional view of assembly of microchannel heat sink with casings and heaters.

3.3.2 Nanofluids preparation

Two – step production method is carried out to prepare the silica and alumina nanofluid cooling medium. In this method, the nanoparticles of silica SiO_2 (with particle size of 7 nm) and alumina Al_2O_3 (with particle size of 7 nm) are added directly into base fluid (distilled water) and then the nanoparticles will be dispersed within the base fluid by ultrasonic vibration using Q700 Sonicator. The time requirement of particle

dispersion for these two types of nanoparticles is different. For silica nanoparticles, the time duration of 1 hour ultrasonic vibration is required to disperse the silica nanoparticles within base fluid evenly; whereas for alumina nanoparticles, the time requirement is longer that is 2 hours of ultrasonic vibration. After ultrasonic vibration has been done on these two types of nanoparticles as shown in Figure 3.10 for 3% concentration of nanoparticles, the silica and alumina nanofluids are left for few days. After 5 days, it is found that settlement of some silica and alumina nanoparticles can be seen in the figure. However, the settlement of alumina nanoparticles is more obvious as compared with silica nanoparticle as shown in the figure. As for the current experiment purpose, three volume fraction of 1%, 2% and 3% nanoparticles concentration within base fluid are prepared by the same preparation method and tested for all geometrical configurations of microchannels at various Reynolds Numbers.

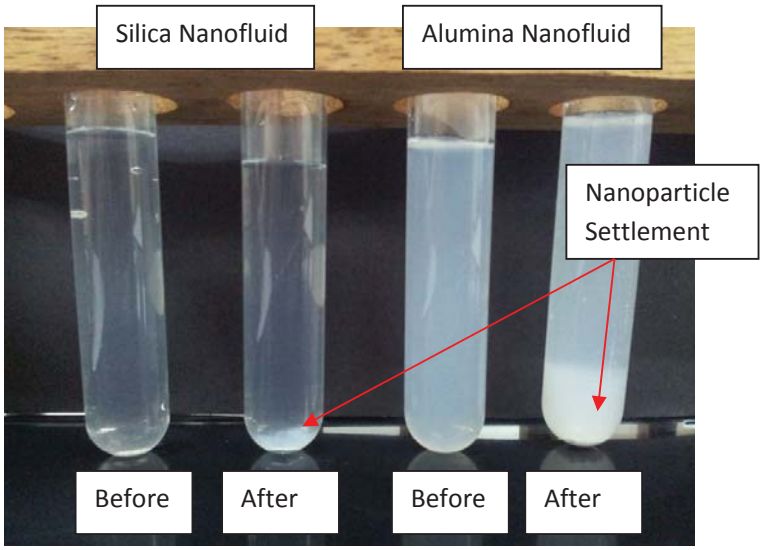

Figure 3.10: Comparison of 3% concentration of nanoparticles within nanofluids (SiO_2-H_2O and Al_2O_3-H_2O) with- and without settlement of nanoparticles.

3.4 Work flow of experimental and simulation analysis

Before proceed to the detail of results and discussion chapter 4, it is important to have a clear picture about the flow of experimental and simulation analysis as stated sequentially as follow, in order to be able to understand the content of chapter 4.

a. Analysis of various geometrical configurations of microchannels by considering base fluid (distilled water) as cooling medium on the heat sink performances.
b. Analysis of various geometrical configurations of microchannels by considering the effect of nanofluid (distilled water + 1% concentration of Al_2O_3 nanofluid) as cooling medium on the heat sink performances.
c. Analysis of selected high thermal performance for the geometrical configuration of microchannel by considering the effect of nanofluid concentrations (distilled water + 1%-, 2%-, and 3% concentrations of Al_2O_3 nanofluid) as cooling medium on the heat sink performances.
d. Analysis of selected high thermal performance for the geometrical configuration of microchannel by considering the effect of nanofluid types (distilled water + 3% concentration of Al_2O_3 nanofluid, and distilled water + 3% concentration of SiO_2 nanofluid) as cooling medium on the heat sink performances.
e. Analysis of the effect of vertical and horizontal fin-tip gaps for the various geometrical configurations of microchannels.

In this analysis, various geometrical configurations of microchannel heat sink have been sizing down and analysed by simulation. As shown in Figure 3.11, 3 – dimensional microchannel heat sink has been modelled. The dimension of the microchannel heat sink is 16.00mm (length, L) x 7.0809mm (width, W) x 0.50mm (height, H). There are three types of fin configurations have been analysed in this study, i.e. rectangular, triangular and trapezoidal fins. The physical dimension of the microchannel heat sink is same for all fin configurations except fin dimension.

The hydraulic diameter for each channel configuration is also the same. In order to analyse the effect of the vertical fin tip gap on the heat sink performance, the height of each fin configuration is reduced at the certain gap as denoted as H_c and its limit is within channel width.

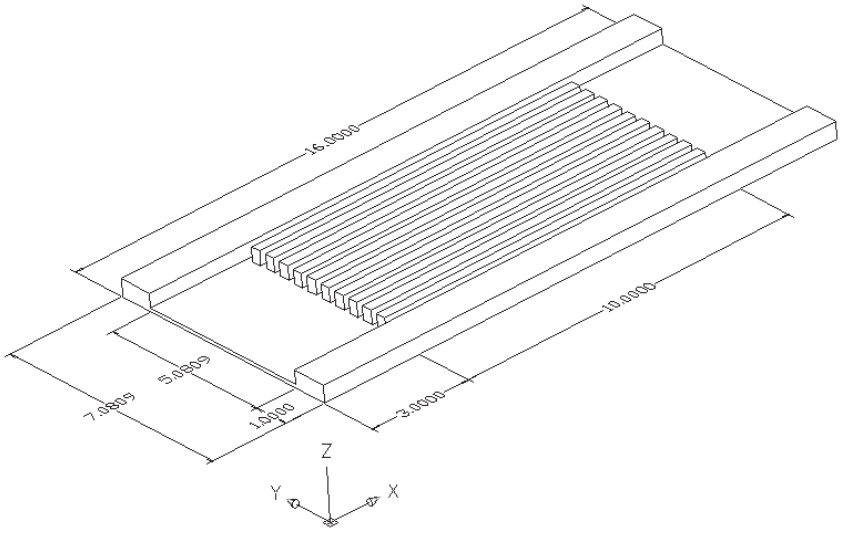

Figure 3.11: Geometrical configuration dimensions of microchannel heat sink (all dimensions in mm).

Figure 3.12 shows the cross section view of various geometrical configurations of microchannels with and without vertical fin tip gap.

(a)Rectangular fin without fin tip gap

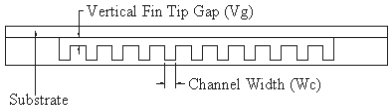

(b)Rectangular fin with vertical fin tip gap

(c) Triangular fin without fin tip gap

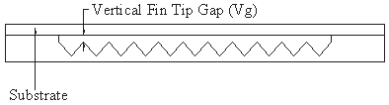

(d) Triangular fin with vertical fin tip gap

Figure 3.12: Dimensions of cross sectional microchannel heat sink (all dimensions in mm) and schematic diagram of various fin configurations without and with vertical fin tip gap.

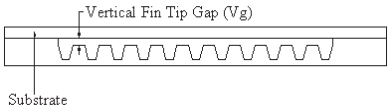

(e) Trapezoidal fin without fin tip gap (f) Trapezoidal fin with vertical fin tip gap

Figure 3.12 (Cont'): Dimensions of cross sectional microchannel heat sink (all dimensions in mm) and schematic diagram of various fin configurations without and with vertical fin tip gap.

After the optimum vertical fin tip gap has been firmly determined, the horizontal sub-fin is introduced at the both sides of each rectangular fin tip as shown in Figure 3.13. It is also convenient to express the horizontal fin tip gap in terms of the dimensionless parameter ratio of the horizontal fin tip gap to channel width, G_c/W_c.

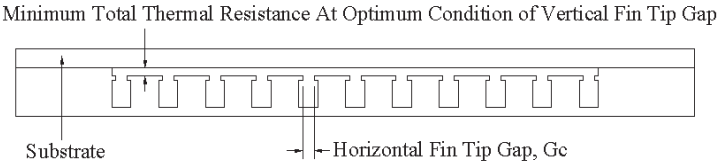

(a) Semi – hollow fin at optimum condition of vertical fin tip gap

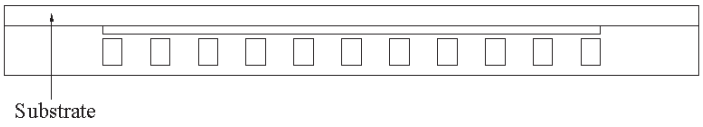

(b) Fully closed hollow channels at optimum condition of vertical fin tip gap

Figure 3.13: Semi - hollow fin and fully closed hollow channels at optimum vertical fin tip gap condition in microchannel heat sink.

f. Analysis of the effects of geometry and number of hollow on the performance of rectangular fins in microchannel heat sinks.

The three dimensional (3D) model of the microchannel heat sink, of size 60 mm (length, L) × 24.8mm (width, W) × 2 mm (height, H), is shown in Fig. 3.14. It consists of 11 channels (M1 to M11) with the dimensions of 42mm (length) ×

0.80mm (width) × 1.60mm (height) and 10 fins (H1 to H10), as indicated in Figure 3.15. Keeping the dimensions of the channels and the fins fixed, simulations are performed on various configurations, such as solid fin, and fins with single and double hollows of rectangular, circular and trapezoidal geometries, as illustrated in Figure 3.16 (cases A, B1, B2, C1, C2, D1 and D2).

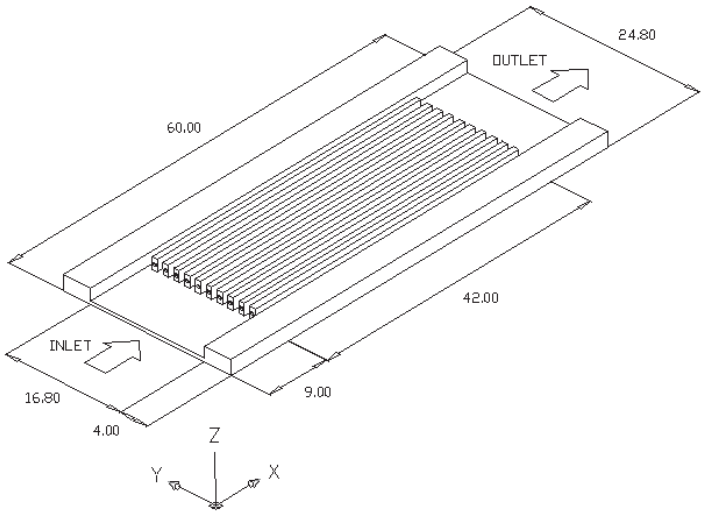

Figure 3.14: The microchannel heat sink model with dimensions (in mm).

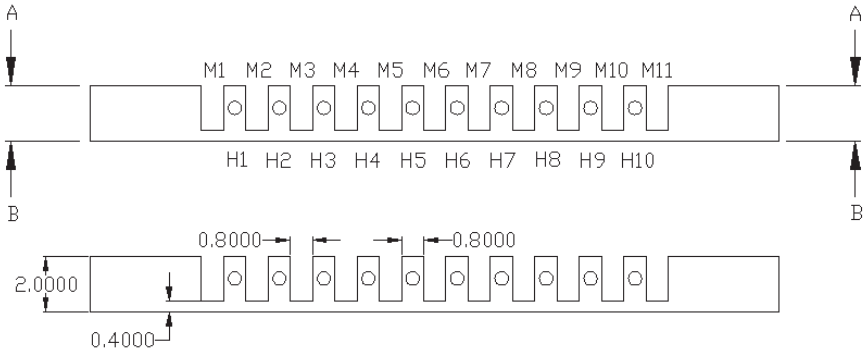

Figure 3.15: The cross sectional side view of the heat sink showing the channels (M1 to M11) and fins (H1 to H10), and the dimensions (in mm).

Case A : Solid fin

Single – hollow fin

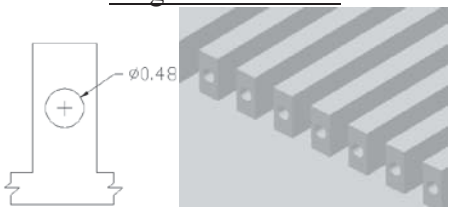

Case B1: One circular hollow

Double- hollow fin

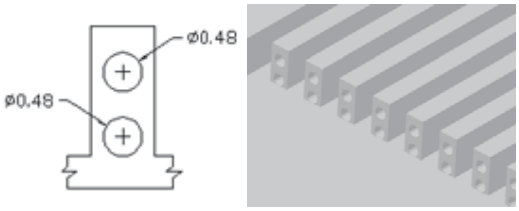

Case B2: Two circular hollows

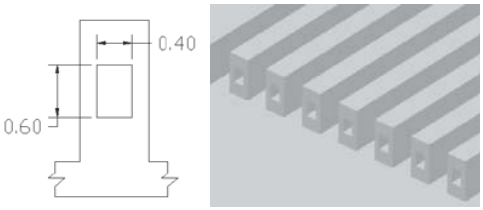

Case C1: One rectangular hollow

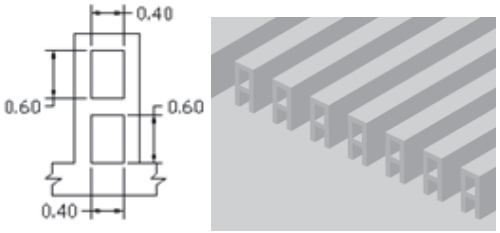

Case C2: Two rectangular hollows

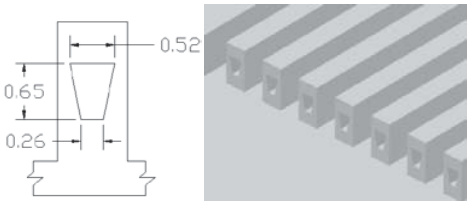

Case D1: One trapezoidal hollow

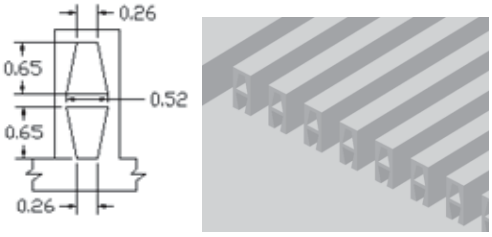

Case D2: Two trapezoidal hollows

Figure 3.16: Solid fin and fins with various hollow geometries.

3.5 Summary

The model of rectangular, triangular and trapezoidal microchannels have been designed and developed in AutoCAD and Gambit software, and analyzed by FLUENT software by solving the governing equation with Finite Volume Method. Besides this, the actual microchannel heat sinks also have been fabricated for experimental analysis. The purpose of experimental work is carried out for both cases of distilled water and nanofluids are to ensure the simulation results are acceptable through validation. However, the main limitations of the experiment set up in carrying out the research are the limitation of fluid flow rate due to available capacity of water pump and size of microchannel heat sink. As a result, simulation work is required to simulate the performance of microchannel heat sink with smaller size and cooling medium flow of higher flow rate.

Once the simulation results are validated, the simulation can employed further to explore the thermal parameters which are not able to be determined in experimental work, i.e. maximum heat sink temperature, visualization of temperature contour of heated heat sink etc. The results that obtained from experiment and simulation works have been compiled in chapter 4, and they will be discussed in detail in that chapter.

CHAPTER FOUR
RESULT AND DISCUSSION

4.1 Introduction

The results of experimental and simulation works are presented in chapter. The method that has been applied to obtain the results is according to the methodology which has been discussed in the previous chapter. The simulation results have been validated successfully with the experimental results as will be presented in the following sub-section. The good agreement of simulation results with the experimental results is showing that the simulation work is able to predict the hydrodynamic and thermal performances of the microchannel heat sinks. In the subsequence sub-section, the study on the hydrodynamic performance on various geometrical configurations of microchannels has been discussed in detail for the base fluid and nanofluid on the parameters of pressure drop, friction factor and pumping power. Besides this, the thermal performance also has been discussed in detail on the parameters of heat sink base temperature, heat transfer coefficient and thermal resistance.

4.2 Validation of simulation work through experimental work

For validation purpose in this section, the base fluid of distilled water as cooling medium is considered in the microchannel heat sink. In hydrodynamic performance of microchannel heat sink, it is found that the simulation results are fit well with the experimental results as shown in Figures 4.1 through 4.6. The maximum difference between them is about 1%. Hence, it is showing that the simulation results are well validated by the experimental results, and the simulation work is able to predict the acceptable result for the hydrodynamic performance of the microchannel heat sink. As refer to Figures 4.1 through 4.3, in experimental work, the pressure drop ΔP at given Reynolds Number is directly measured through the use of digital pressure measurement instrument between inlet and outlet of microchannels. For simulation work, the pressure drop ΔP is determined by the differential pressure between inlet and outlet of microchannels as to the equation of $\Delta P = P_{in} - P_{out}$.

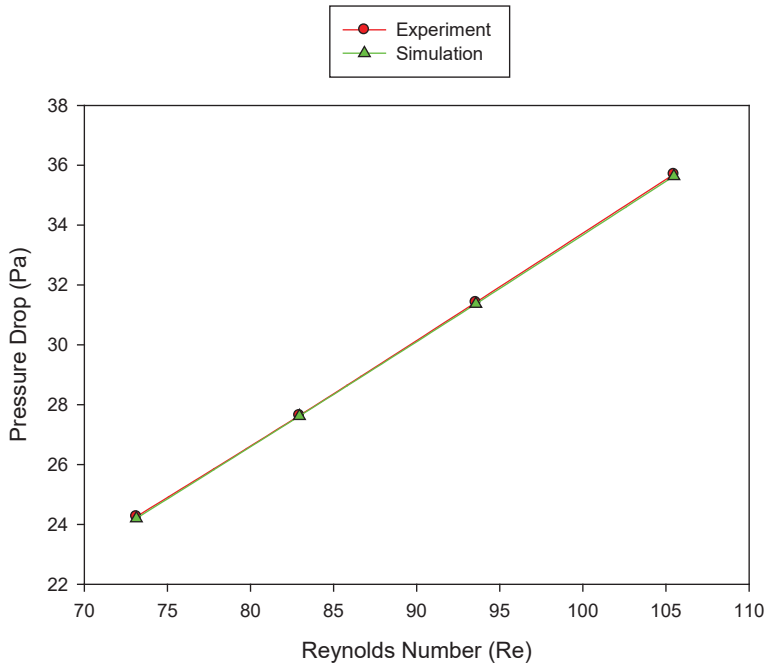

Figure 4.1: Pressure drop within rectangular microchannel heat sink with distilled water.

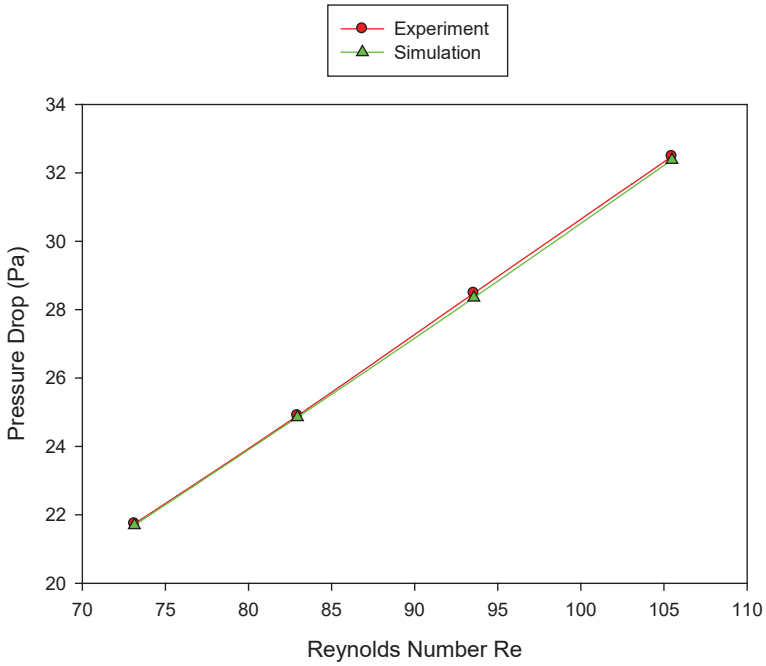

Figure 4.2: Pressure drop within triangular microchannel heat sink with distilled water.

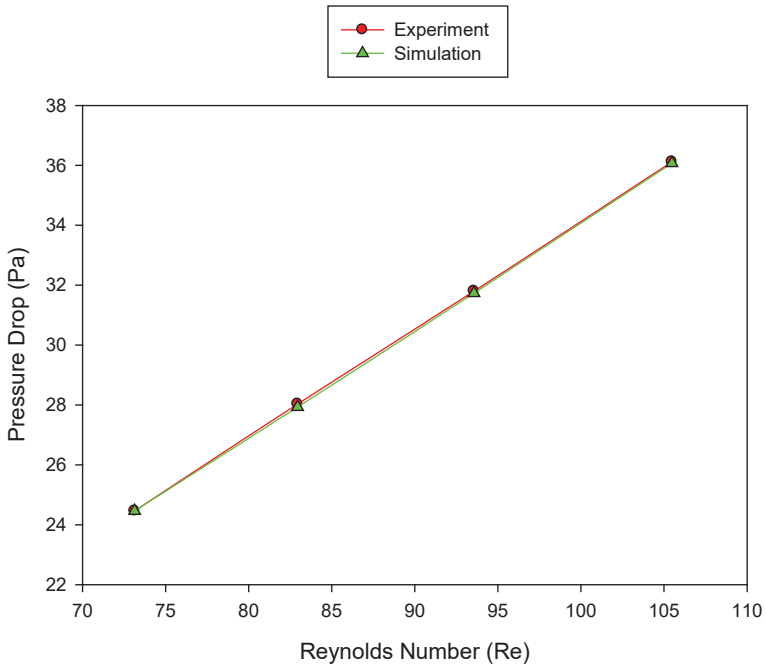

Figure 4.3: Pressure drop within trapezoidal microchannel heat sink with distilled water.

After the determination of pressure drop ΔP, the pumping power is calculated for both experimental and simulation works through the equation of pumping power = $\Delta P \bullet Q_f$, where Q_f is volume flow rate of fluid flow. The calculated pumping power is compiled

and comparison is made for both experimental and simulation results as shown in Figures 4.4 through 4.6.

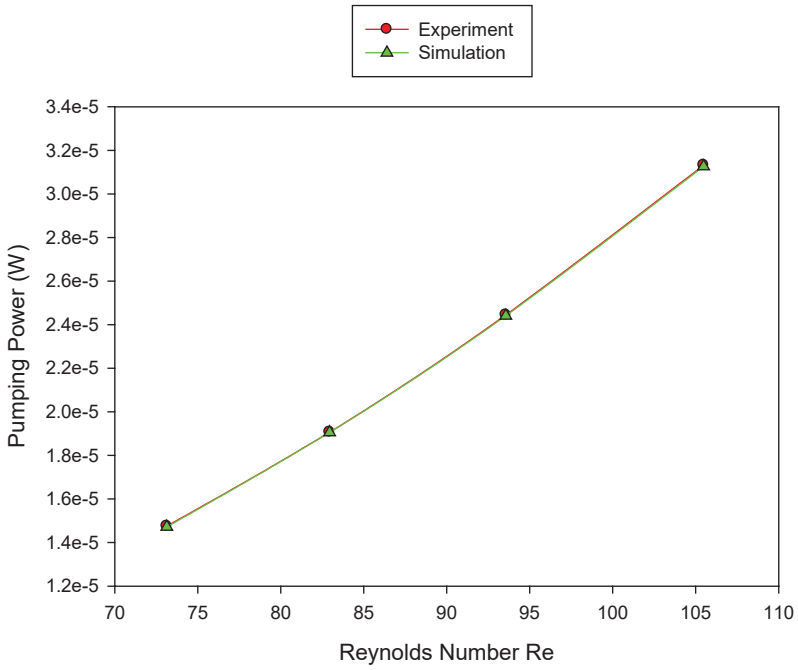

Figure 4.4: Pumping power for the fluid flow through rectangular microchannel heat sink with distilled water.

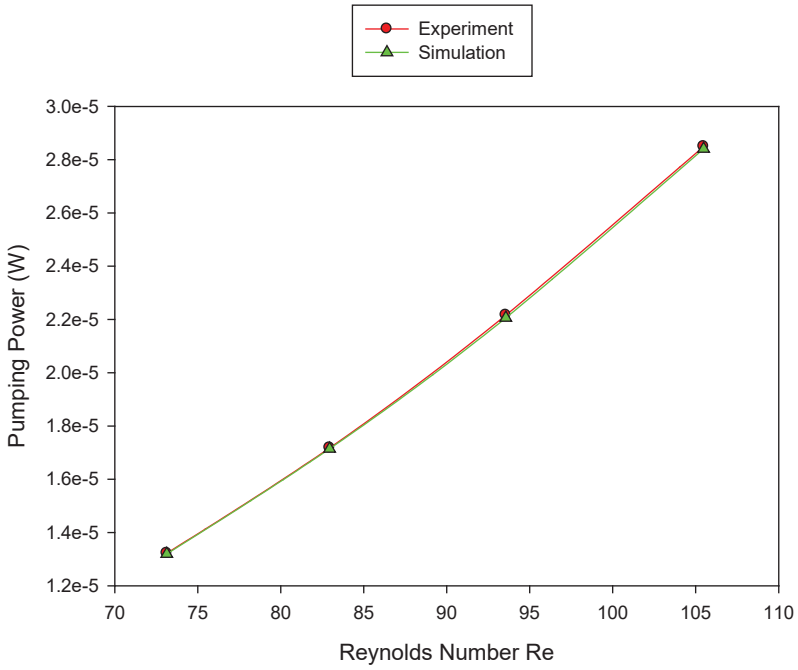

Figure 4.5: Pumping power for the fluid flow through triangular microchannel heat sink with distilled water.

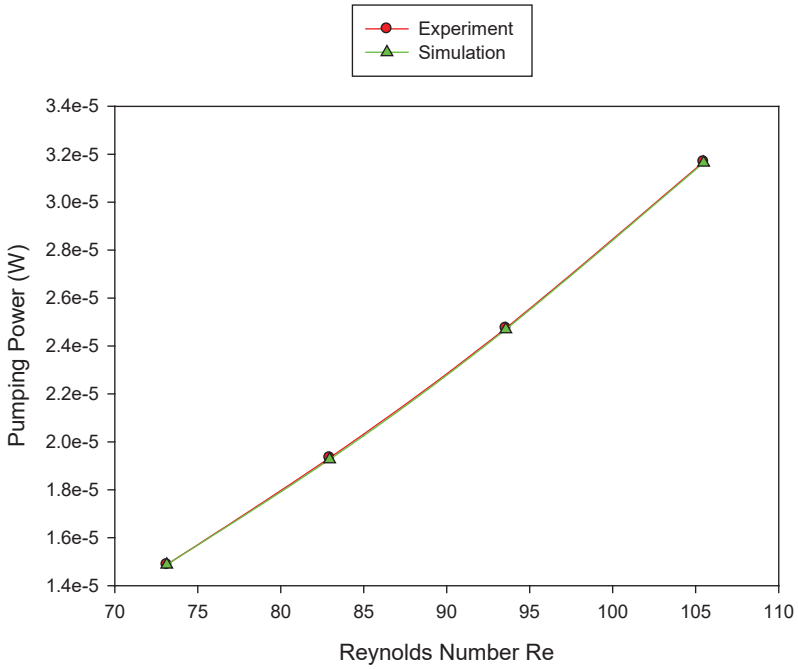

Figure 4.6: Pumping power for the fluid flow through trapezoidal microchannel heat sink with distilled water.

For thermal performance of microchannel heat sink, the result comparison of heat sink base temperature between experimental and simulation results is found to be well fit to each other as referring to the Figures 4.7 through 4.9. The maximum difference is 1.1%. Hence, the simulation results are well validated by the experimental results, and showing that the simulation work is able to predict the acceptable result for the thermal performance of microchannel heat sink.

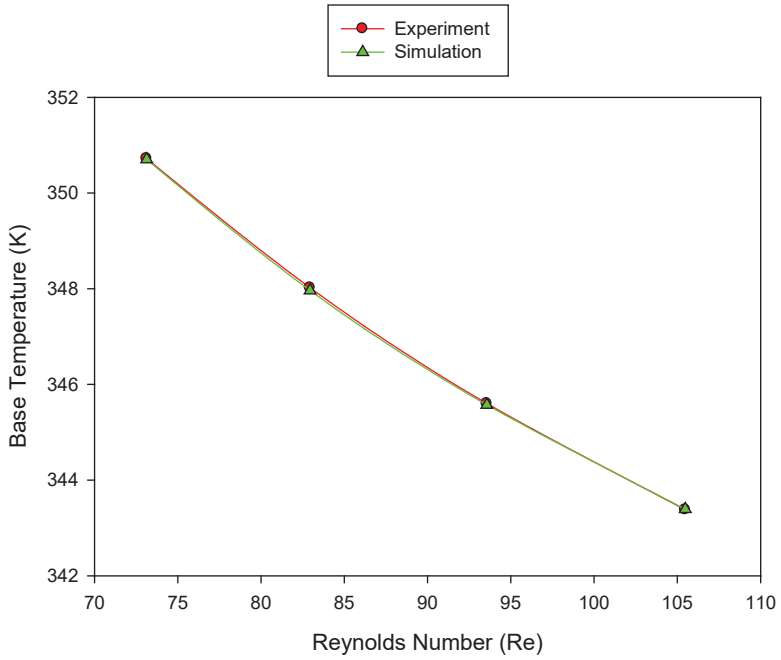

Figure 4.7: Heat sink base temperature for rectangular microchannel heat sink with distilled water.

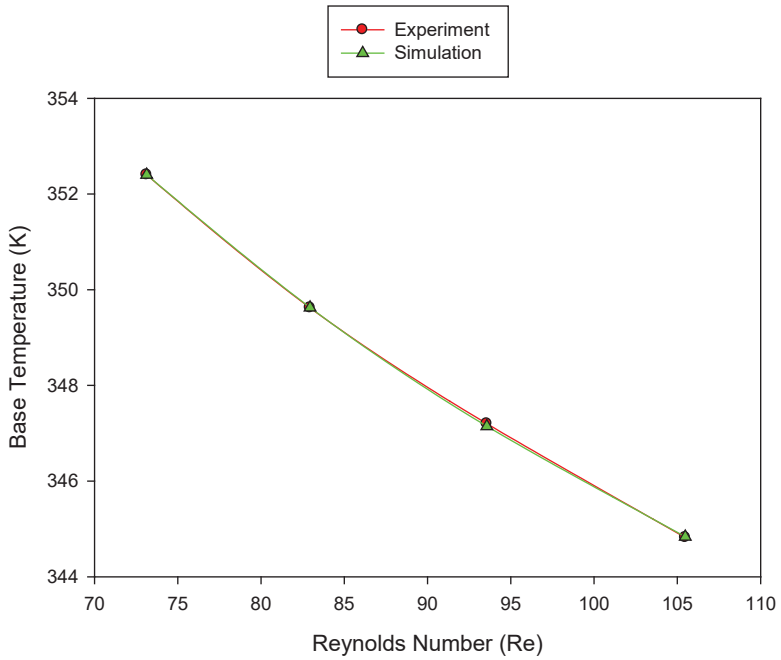

Figure 4.8: Heat sink base temperature for triangular microchannel heat sink with distilled water.

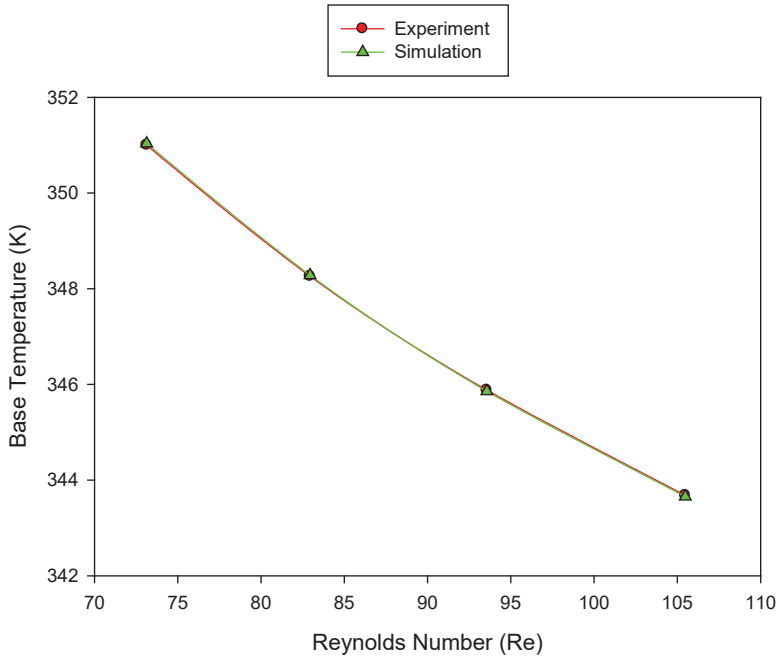

Figure 4.9: Heat sink base temperature for trapezoidal microchannel heat sink with distilled water.

As refer to the Figures 4.10 through 4.12, in both experimental and simulation works, the thermal resistance is determined through the equation of $R = \frac{\Delta T}{Q}$ and is compiled accordingly in the figures. Comparatively, it is also found that the experimental and simulation results of thermal resistance are well fit to each other in which the maximum difference is about 1.0%, and showing that the simulation work is able to simulate the thermal performance of microchannel heat sink.

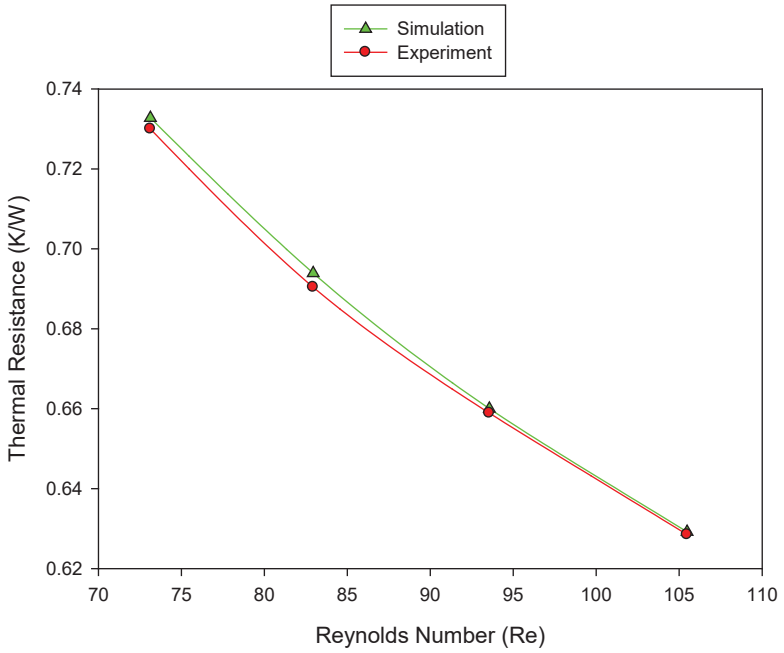

Figure 4.10: Thermal resistance for rectangular microchannel heat sink with distilled water.

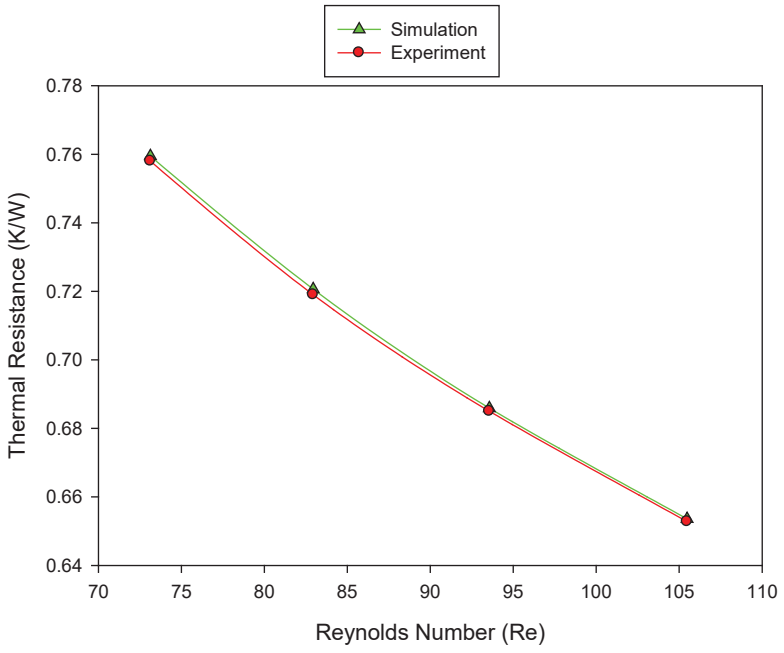

Figure 4.11: Thermal resistance for triangular microchannel heat sink with distilled water.

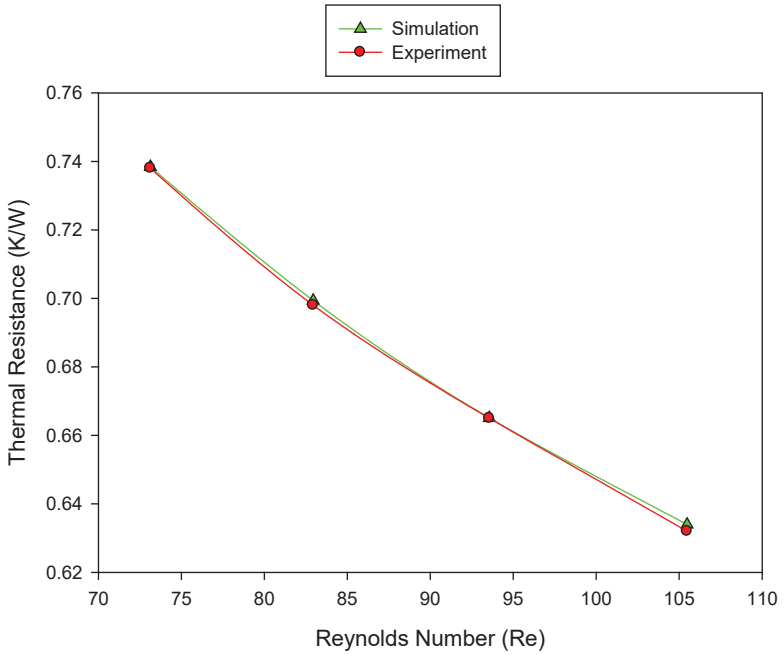

Figure 4.12: Thermal resistance for trapezoidal microchannel heat sink with distilled water.

4.3 Analysis of the effect of various geometrical configurations of microchannels on the heat sink performances

Referring to the discussion that has been made for validation of simulation results with experimental results, it is practically that the simulation results are used for result and discussion as for following sections. For the analysis in this section, the base fluid of distilled water is considered as cooling medium within various configurations of microchannels.

a) Hydrodynamic performance

Figure 4.13 shows the comparison of pressure drop among various geometrical configurations of microchannels. The pressure drop for rectangular and trapezoidal microchannels shows small difference between them in which the average difference is about 1.15% only. But these configurations of microchannels have shown obvious

difference of pressure drop as compared with triangular microchannel. Although triangular microchannel has same hydraulic diameter as rectangular and trapezoidal microchannels, the triangular microchannel has shown better hydrodynamic performance in term of pressure drop with improvement of average 12.12%. The improvement of hydrodynamic performance can be explained by the effective fin surface area of triangular microchannel which is smaller than the effective fin surface area of rectangular and trapezoidal microchannels. Hence, the friction force between fluid flow and effective fin surface area is smaller, and the pressure drop for the triangular microchannel becomes lower.

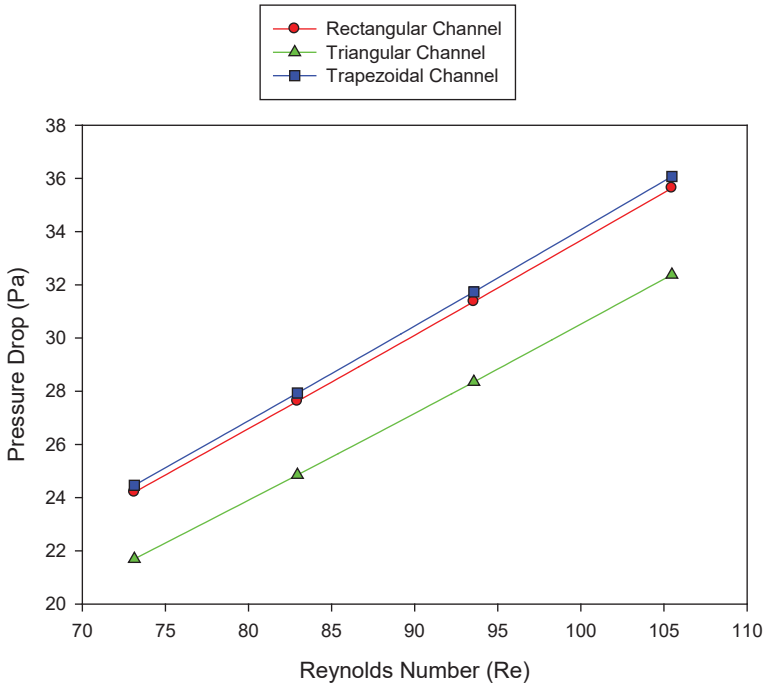

Figure 4.13: Comparison of pressure drop among various geometrical configurations of microchannels with distilled water, by simulation work.

Referring to Figure 4.14, the pumping power for triangular microchannel is the lowest along Reynolds Number, and it is consistent with the result of pressure drop as indicated in Figure 4.13. This is because lesser pumping power is required to overcome the friction force between fluid flow and effective fin surface area. As can be seen in the figure, the

pumping power for the rectangular and trapezoidal microchannels are almost close to each other along the Reynolds Number and the difference between them is about 1.15% only. Both of them are indicating average 11.48% higher pumping power than the triangular microchannel.

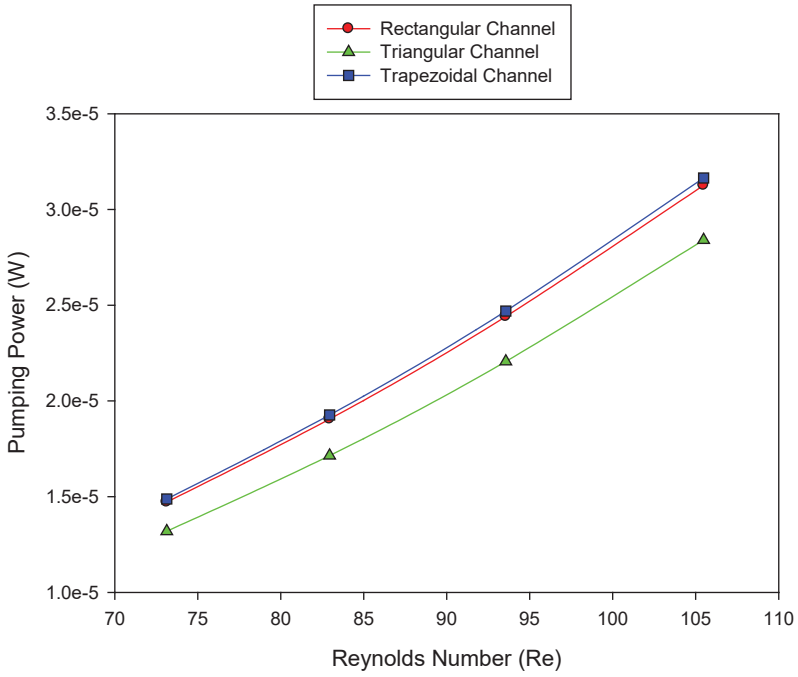

Figure 4.14: Comparison of pumping power among various geometrical configurations of microchannels with distilled water, by simulation work.

b) Thermal performance

By analysing the heat sink base temperature, it is found that the heat sink base temperature for triangular microchannel is the most highest as indicated in Figure 4.15. It is followed by trapezoidal microchannel and rectangular microchannel. Such result can be explained by heat transfer coefficient as shown in Figure 4.16. As refer to the figure, the heat transfer coefficient for triangular microchannel is the lowest and it is indicating that the heat transfer between fluid flow and fin is low which is due to the low contact of fluid flow with effective fin surface area. For rectangular microchannel, the fin surface area is high and it allows more contact with fluid flow that enables more heat can be

transferred convectively into the fluid flow. As a result, the rectangular microchannel has shown improvement of 40% in thermal performance as compared with the triangular microchannel. For the case of trapezoidal microchannel, it is comparatively not obvious difference as compared with rectangular microchannel which is 7.8% only.

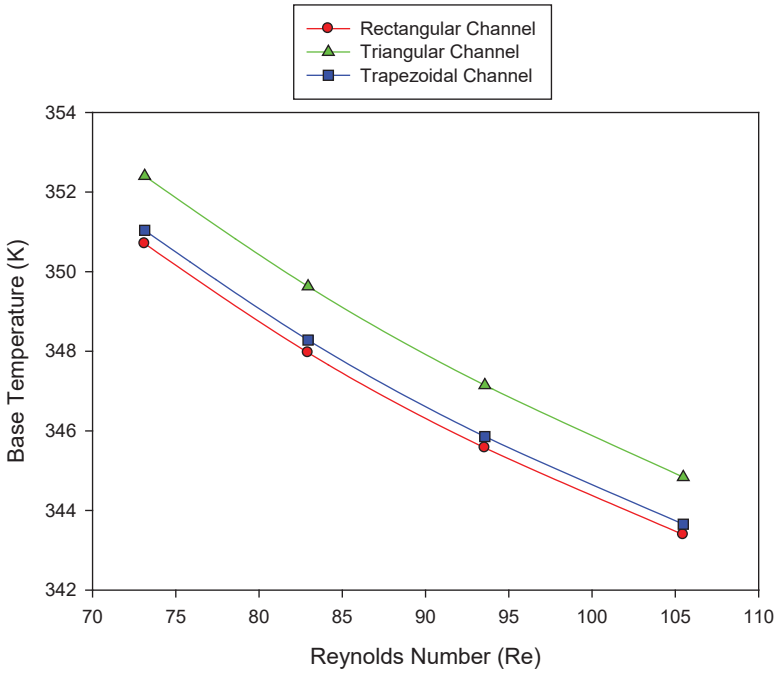

Figure 4.15: Comparison of heat sink base temperature among various geometrical configurations of microchannels with distilled water, by simulation work.

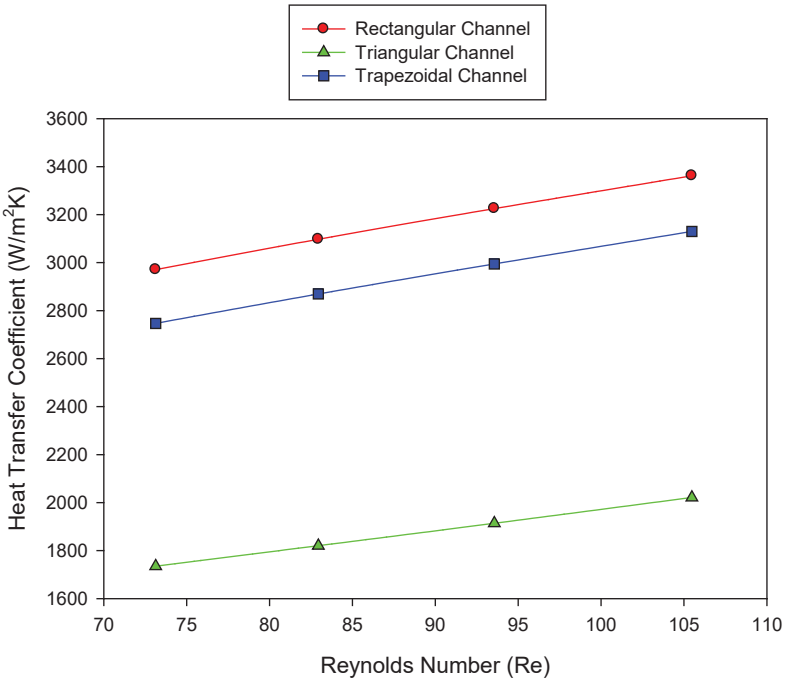

Figure 4.16: Comparison of heat transfer coefficient among various geometrical configurations of microchannels with distilled water, by simulation work.

Referring to Figure 4.17, it is expected that the thermal resistance for the triangular microhannel is the highest. It is due to the low heat transfer as already been indicated as low heat transfer coefficient in Figure 4.16. As a result, there is a high temperature portion within the heat sink structure which is not effectively removed.

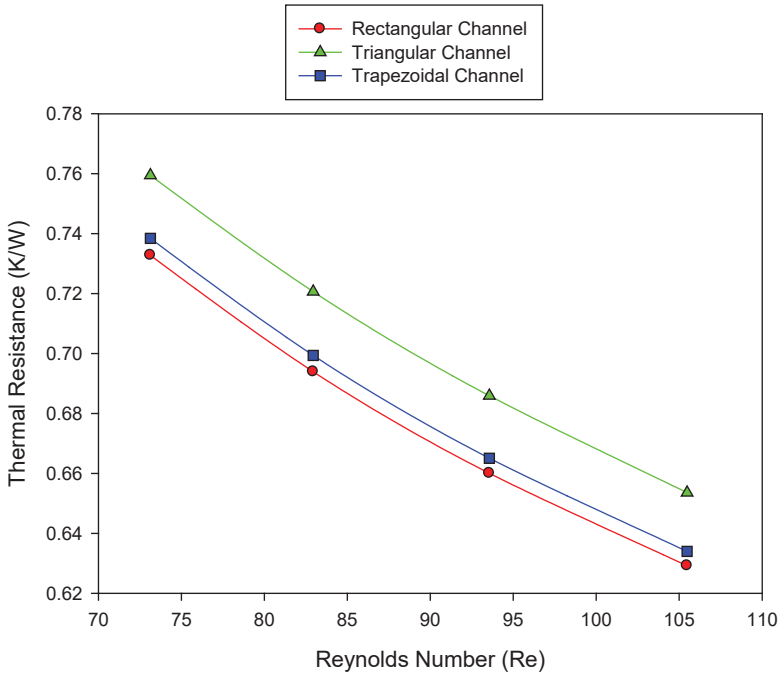

Figure 4.17: Comparison of thermal resistance among various geometrical configurations of microchannels with distilled water, by simulation work.

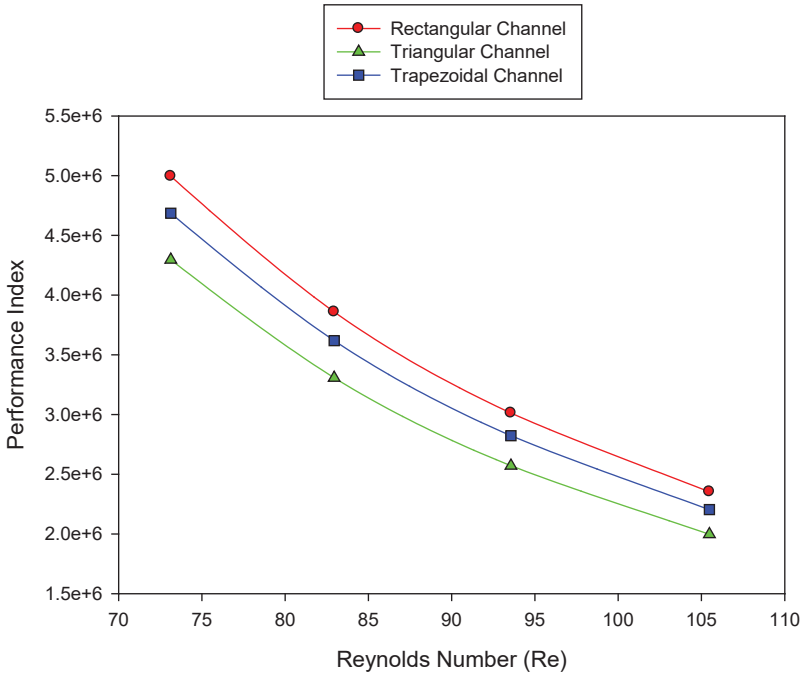

Figure 4.18: Comparison of performance index among various geometrical configurations of microchannels with distilled water, by simulation work.

In order to considering the overall performance of microchannel heat sink among various configurations of microchannels, the performance index is analysed and it is calculated through the equation of $\eta = \frac{q}{P_{pump}}$ (Mohammed et al., 2011), where q is heat transfer rate and P_{pump} is pumping power. As refer to Figure 4.18, the calculated performance index for various configurations of microchannels has been compiled. Comparatively, it is found that the rectangular microchannel shows the highest performance whereas the triangular microchannel shows the lowest performance index. As a result, the performance index has shown that the rectangular microchannel able to remove heat effectively instead of higher pumping power consumption as compared with the triangular microchannel.

To visualize the thermal performance in temperature contour as for comparison among various geometrical configurations of microchannels, Figure 4.19(a) shows that the rectangular microchannel can effectively remove the heat which is indicated by the cool area that spread widely as compared with triangular and trapezoidal microchannels. These visualization results are consistent with the results which have been shown and discussed previously for heat sink base temperature and thermal resistance.

Microchannel Configuration	Iso View	Bottom View
Rectangular Microchannel	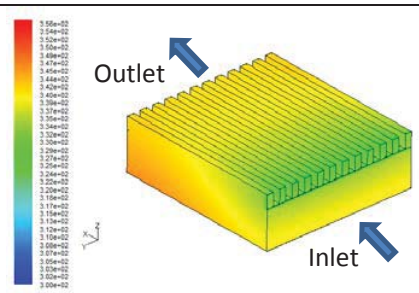	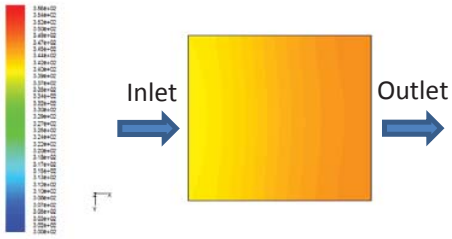
Triangular Microchannel	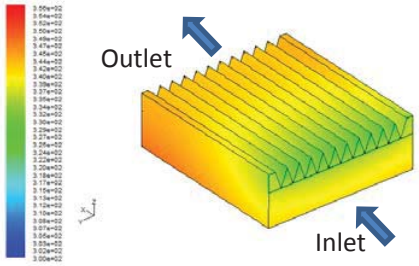	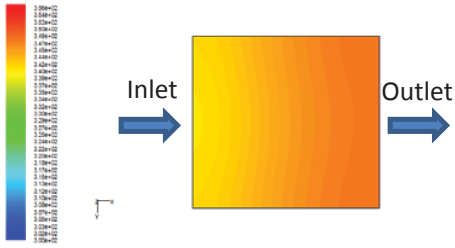
Trapezoidal Microchannel	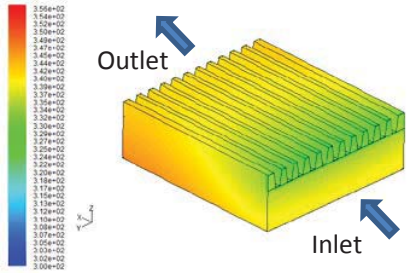	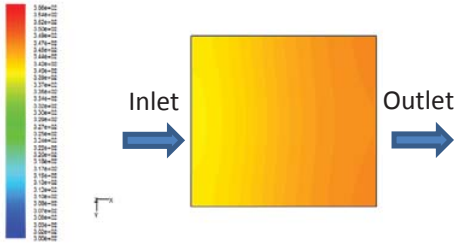

(a) Comparison of temperature contour of physical structure of heat sink among various geometrical configurations of microchannels.

Figure 4.19: Velocity and temperature contour for various geometrical configurations of microchannel heat sinks with distilled water as cooling medium at fluid flow velocity of 0.0298 m/s.

Microchannel Configurations	Contour	
	Fluid Flow Velocity	Temperature
Rectangular Microchannel	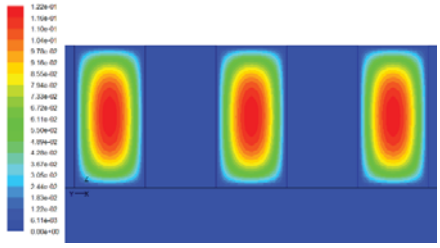	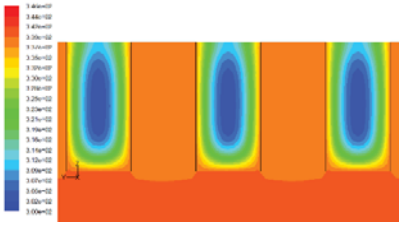
Triangular Microchannel	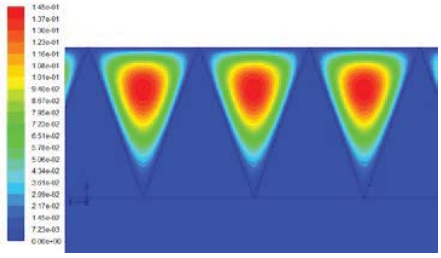	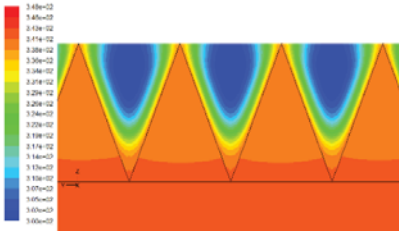
Trapezoidal Microchannel	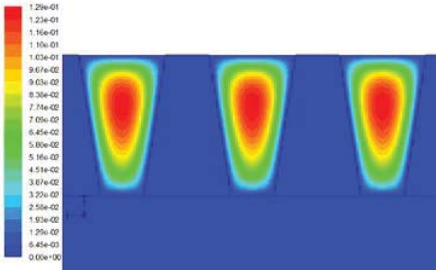	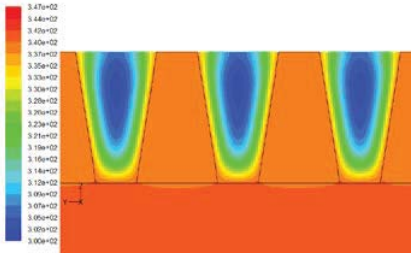

(b) Comparison of velocity and temperature contours at the cross section of heat sinks among various geometrical configurations of microchannels.

Figure 4.19 (Cont'): Velocity and temperature contour for various geometrical configurations of microchannel heat sinks with distilled water as cooling medium at fluid flow velocity of 0.0298 m/s.

The main reason of the rectangular microchannel that able to remove heat effectively is due to the effect of fluid flow distribution across the cross – section of the microchannel. As refer to Figure 4.19(b), the effective fluid flow velocity (as indicated in green colour) has shown wide coverage to the fin surface area. As a result of the high contact area between fluid flow and fin surface area, high heat can be transferred into fluid flow as shown by the fluid flow temperature contour across the cross – section of rectangular

microchannel. There is almost same condition is shown in the trapezoidal microchannel. In the trapezoidal microchannel, the coverage area of effective fluid flow velocity to the trapezoidal fin is lower as compared with the case of rectangular microchannel. Hence, lower heat can be transferred into fluid flow as indicated by the fluid flow temperature contour, in which the thermal performance of trapezoidal microchannel becomes lower with the indication of higher thermal resistance. However, the triangular microchannel has shown the poorest thermal performance which is due to the lowest coverage of effective fluid flow velocity to the fin surface area. As can be seen to the bottom of the cross – sectional triangular microchannel, there is a large area of low fluid flow velocity in which the effective fluid flow velocity (as indicated by in green colour) is far away from the bottom surface. As a result, the heat is not effectively absorbed into fluid flow from the bottom part of the triangular microchannel as shown by the temperature contour in the figure. So, the thermal resistance of the microchannel is the highest.

4.4 Analysis of performance of microchannel by considering the effect of nanofluid on the heat sink performances

Referring to the analysis in section 4.3 above, the rectangular microchannel is found to be the highest performance as heat removing heat sink. Hence, the fin configuration is further considered for analysis of the effect of nanofluid as discussed in the following section. In the analysis of the effect of nanofluid as cooling medium, the Al_2O_3 nanofluid with 1% concentration of Al_2O_3 nanoparticles within base fluid is analysed as compared the microchannel heat sink performance using base fluid of distilled water.

a) Hydrodynamic performance

For the analysis of nanofluid application as cooling medium in microchannel heat sink, small quantity of 1% volume fraction of Al_2O_3 nanoparticles is added into base fluid (distilled water). As refer to Figure 4.20, pressure drop for nanofluid as cooling medium in microchannel heat sink is not much difference with the case of using base fluid (distilled water) as cooling medium. The difference between them is 3% only. As a result, the pumping power also shows the same trend in which it is not much difference with the case of base fluid as indicated in Figure 4.21, and the difference is only 2.5%. It is found that the effect of nanofluid will not affect the hydrodynamic performance and this is the advantage of using nanofluid as cooling medium. By the way, it can be seen that the simulation result is fit well with experimental result, and showing that the simulation work is able to simulate the acceptable result of hydrodynamic performance of microchannel heat sink.

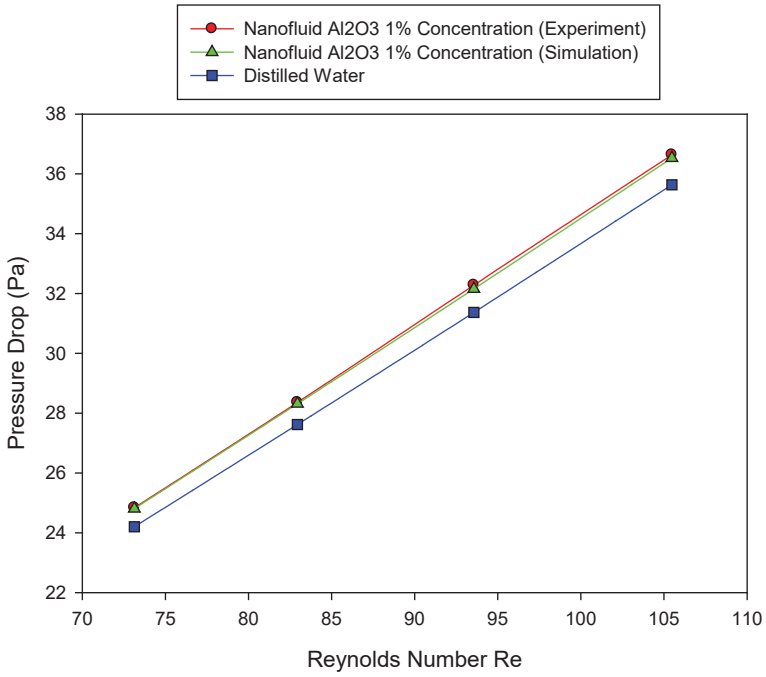

Figure 4.20: Pressure drop within rectangular microchannel heat sink with alumina nanofluids with 1% concentration.

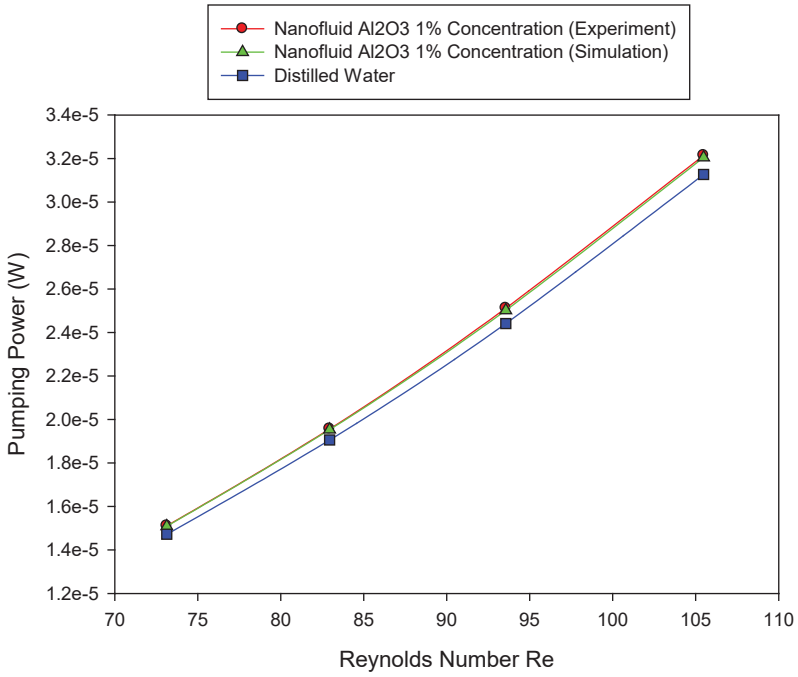

Figure 4.21: Pumping power for the fluid flow through rectangular microchannel heat sink with alumina nanofluids with 1% concentration.

b) Thermal performance

As shown in Figure 4.22, the microchannel heat sink base temperature is further reduced by using the Al_2O_3 nanofluid as cooling medium. This is because the existence of nanoparticles within base fluid can further increase the thermal conductivity of cooling medium in which more heat can be absorbed. Such condition can be explained by Figure 4.23. As refer to the figure, the heat transfer coefficient for the application of nanofluid is higher than the case of base fluid in which more heat can be removed by using nanofluid. By further analyse the result in the figure, the difference between them increases as Reynolds Number increases. Hence, the application of nanofluid can increasingly remove the heat from the heat sink at higher Reynolds Number and this is the advantage of nanofluid application in thermal performance.

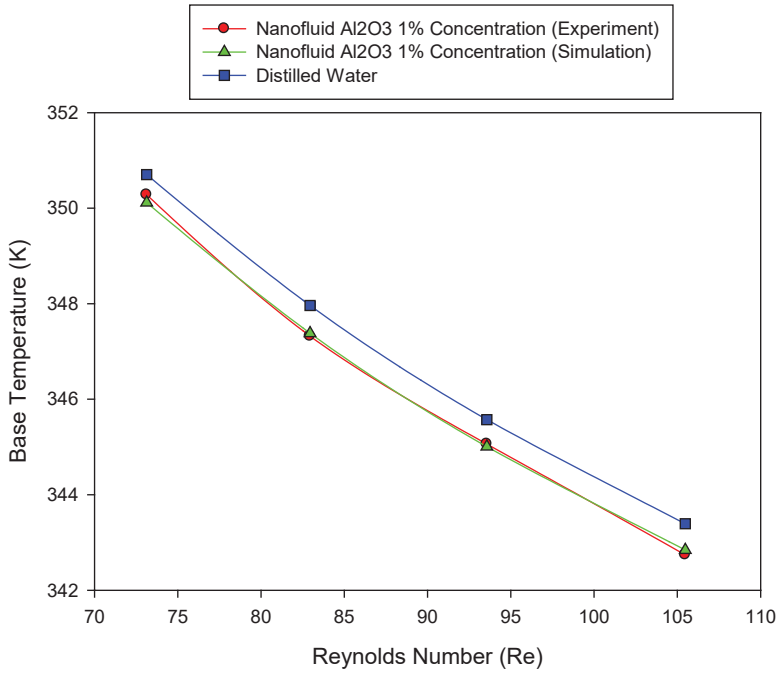

Figure 4.22: Heat sink base temperature for rectangular microchannel heat sink with alumina nanofluids with 1% concentration.

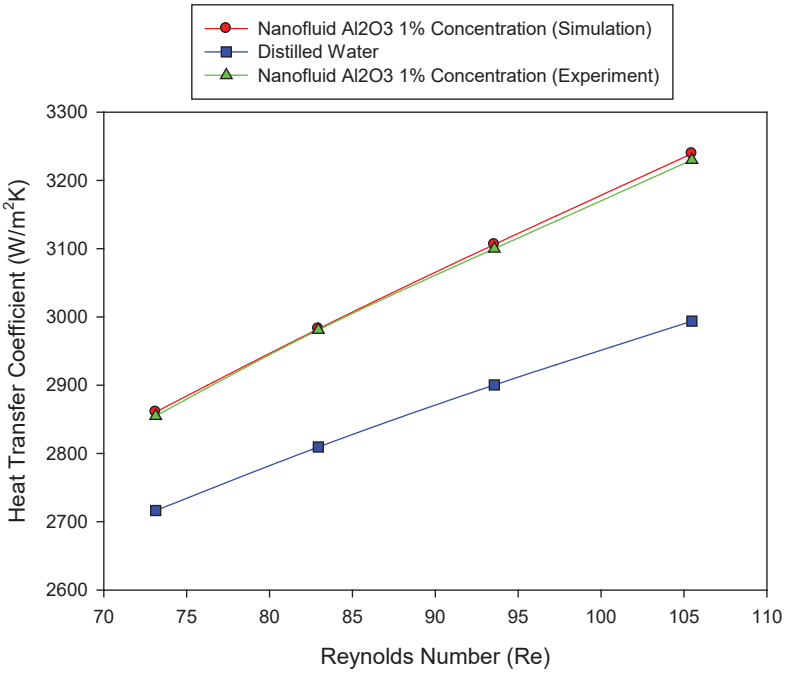

Figure 4.23: Heat transfer coefficient for rectangular microchannel heat sink with alumina nanofluids with 1% concentration.

Since the heat transfer is higher by using nanofluid, it is no doubt that the thermal resistance of heat sink will become lower by using nanofluid as cooling medium as shown in Figure 4.24. This is because the nanofluid is effectively absorbing the heat from the microchannel heat sink, hence the temperature of the whole structure of the heat sink is further reduced and it is definitely that thermal resistance will be further reduced as well.

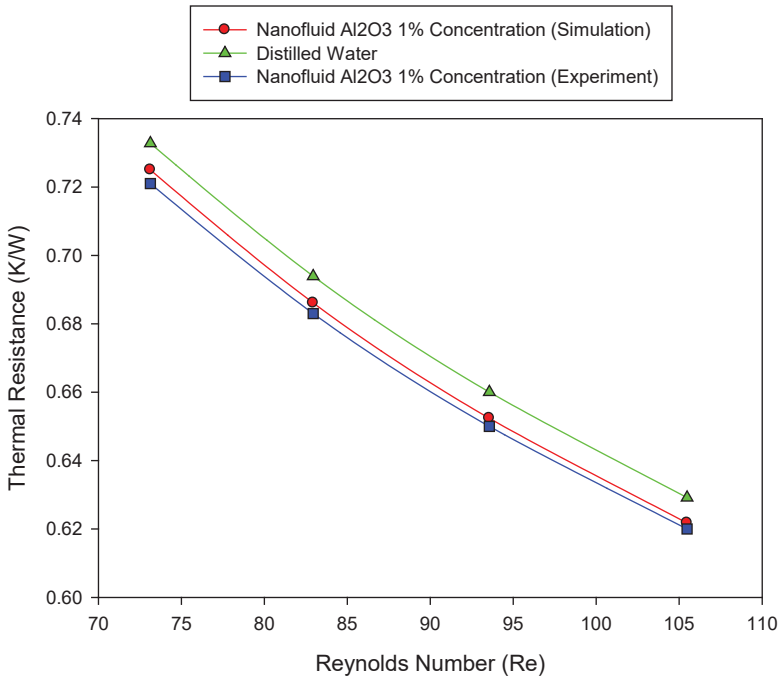

Figure 4.24: Thermal resistance for rectangular microchannel heat sink with alumina nanofluid with 1% concentration.

Referring to the experimental and simulation results in Figures 4.22, 4.23, and 4.24, it is found that the difference between them is small, and it is also showing that the simulation is also able to simulate the acceptable result of thermal performance of microchannel heat sink.

4.5 Analysis of performance of microchannel by considering the effect of nanofluid concentrations

The microchannel heat sink performance is further analyzed by the increase the concentration of Al_2O_3 nanoparticle to the base fluid from 1% to 2%, and up to 3% concentrations. Comparison of microchannel heat sink performance with these various concentrations of nanoparticle has been made with the case of base fluid.

a) Hydrodynamic performance

The rectangular microchannel heat sink is further analyzed for various concentration of nanoparticle within nanofluid. Figure 4.25 shows the comparison of the effect of various nanoparticle concentrations within base fluid (distilled water). It is found that the pressure drop of various nanoparticle concentrations is not much difference as compared with base fluid. As refer to Figure 4.26, the same condition also found for the case of pumping power in which the effect of nanoparticles existence will not much affect the pumping power in small quantity until the 3% volume fraction concentration.

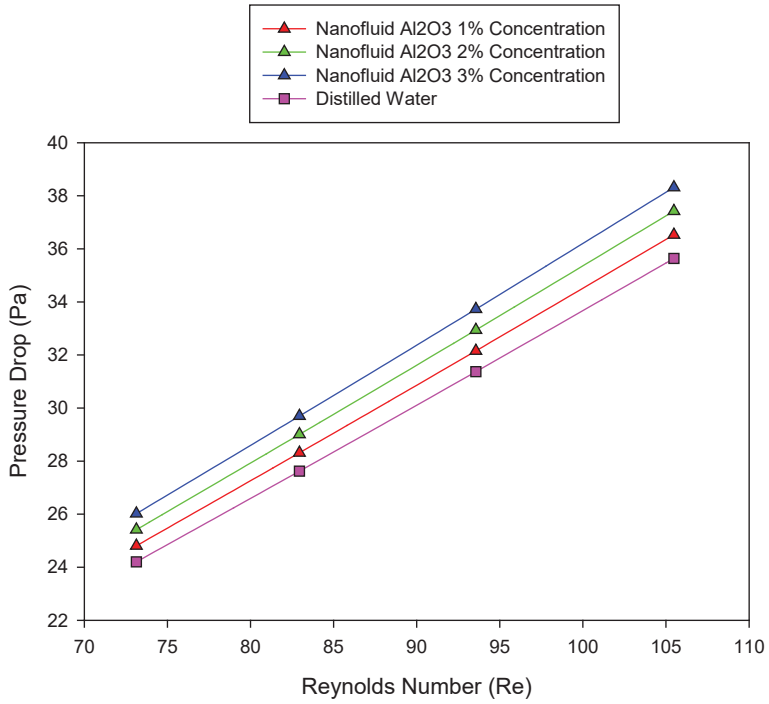

Figure 4.25: Pressure drop within rectangular microchannel heat sink with alumina nanofluids with 1%, 2% and 3% concentrations, by simulation work.

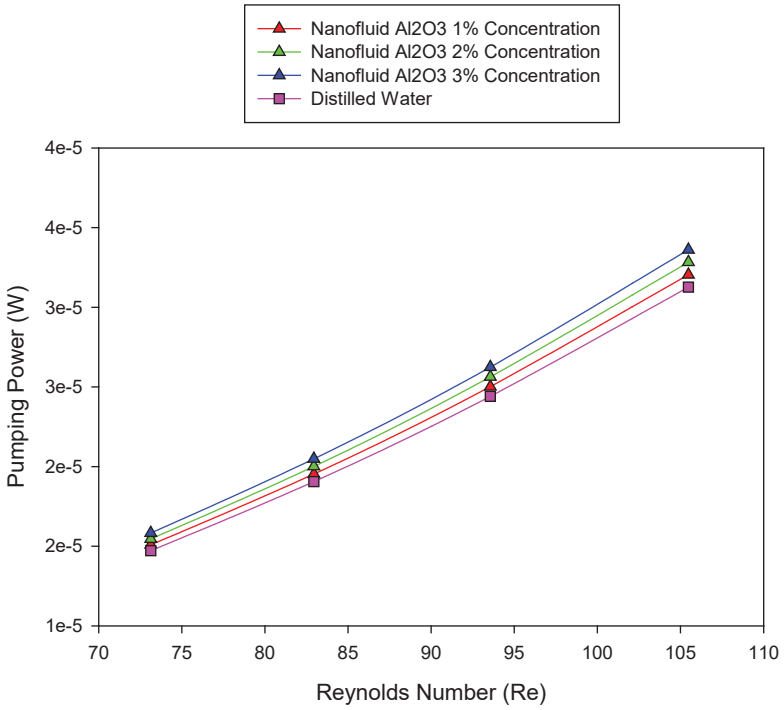

Figure 4.26: Pumping power for the fluid flow through rectangular microchannel heat sink with alumina nanofluids with 1%, 2% and 3% concentrations, by simulation work.

b) Thermal performance

As the concentration of nanoparticles within base fluid increases, the heat sink base temperature decreases as shown in Figure 4.27. This is because of the increasing thermal conductivity of the nanofluid in which more heat can be absorbed into fluid flow. Furthermore, as shown in Figure 4.28, the heat transfer coefficient increases in which heat is effectively transferred into fluid flow by convective heat transfer. At the highest Reynolds Number, it is found that 11% improvement of heat transfer can be achieved at 3% concentration of nanoparticles.

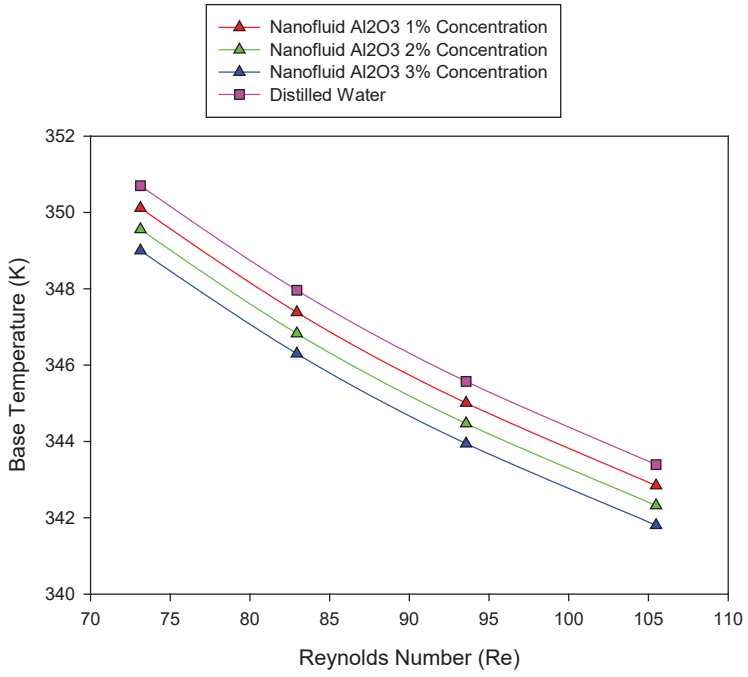

Figure 4.27: Heat sink base temperature for rectangular microchannel heat sink with alumina nanofluids with 1%, 2% and 3% concentrations, by simulation work.

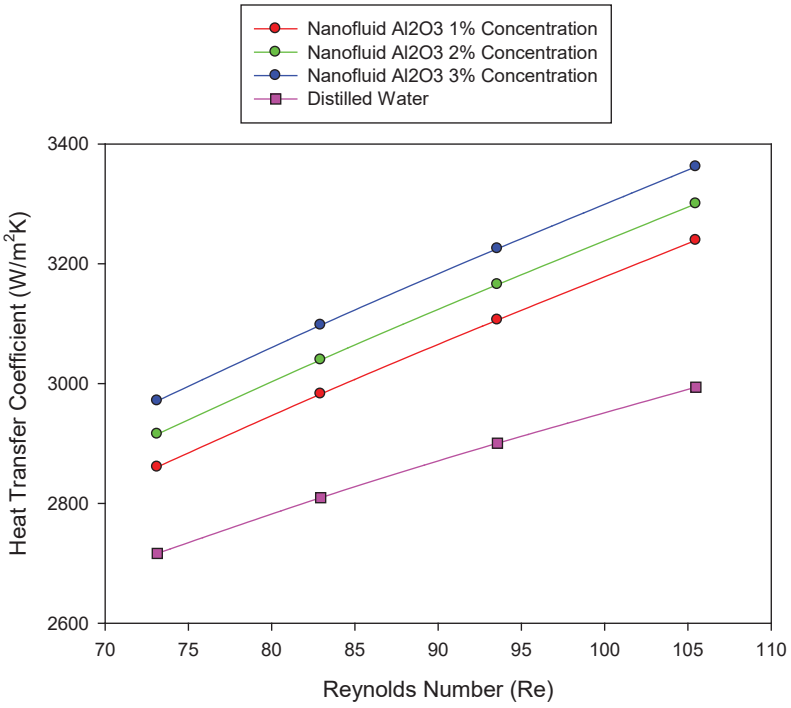

Figure 4.28: Heat transfer coefficient for rectangular microchannel heat sink with alumina nanofluids with 1%, 2% and 3% concentrations, by simulation work.

With the increasing of heat transfer rate as described previously, the thermal resistance of the heat sink is decreased with increment of nanoparticle concentration as shown in Figure 4.29. Hence, the thermal performance of the heat sink can be further improved by increasing the concentration of nanoparticles.

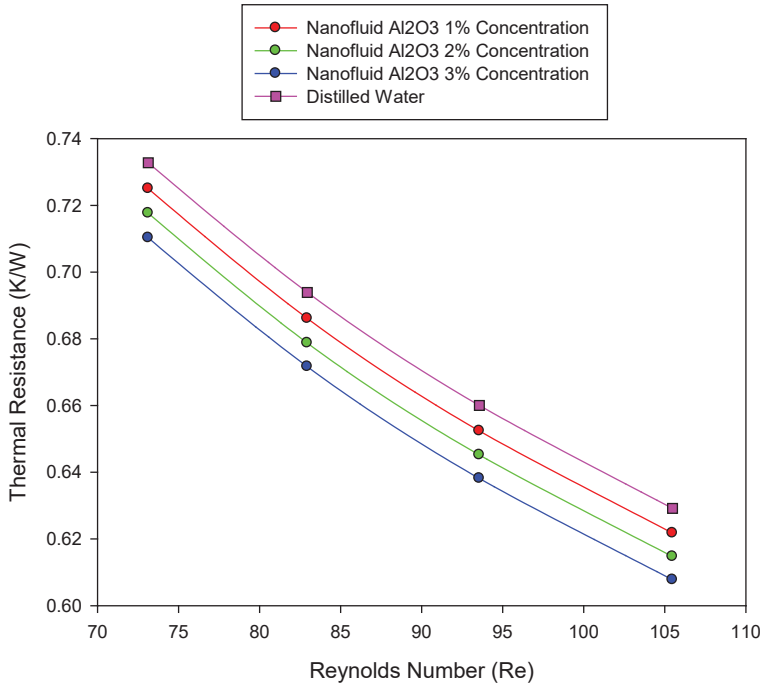

Figure 4.29: Thermal resistance for rectangular microchannel heat sink with alumina nanofluids with 1%, 2% and 3% concentrations, by simulation work.

4.6 Analysis of performance of microchannel by considering the effect of nanofluid types

Besides the analysis of the effect of nanoparticle concentration within base fluid, the type of nanoparticle within base fluid is also been analysed. For this analysis section, two types of nanoparticles are considered such as Al_2O_3 and SiO_2. The microchannel heat sink performance that using these nanoparticles within nanofluids (distilled water H_2O + 3% concentration of Al_2O_3 nanofluid and distilled water H_2O + 3% concentration of SiO_2 nanofluid) are analysed and compared with the case of base fluid.

a) Hydrodynamic performance

As shown in Figure 4.30, the pressure drop of silica and alumina nanofluids shows small difference as compared with the pressure drop of base fluid. It is shows that the

existence of various types of nanoparticles within base fluid will not much affect the pressure drop in small quantity. For the case of pumping power as in Figure 4.31, the pumping power for silica and alumina nanofluids also shows that they are close to the pumping power consumption by base fluid. As a result, it is found that the hydrodynamic performance of the microchannel heat sink is not much affect by the existence of nanoparticle type within base fluid in small quantity.

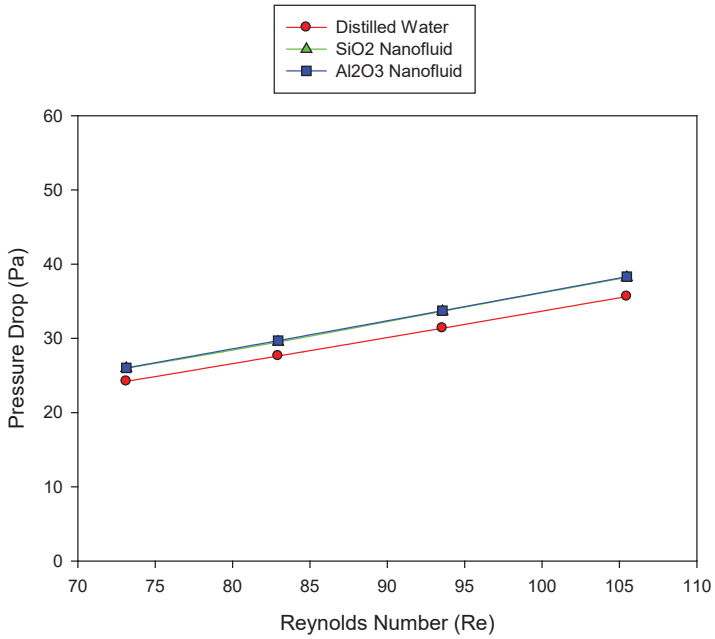

Figure 4.30: Comparison of pressure drop among various types of nanofluids within rectangular microchannel at 3% concentration of nanoparticles, by simulation work.

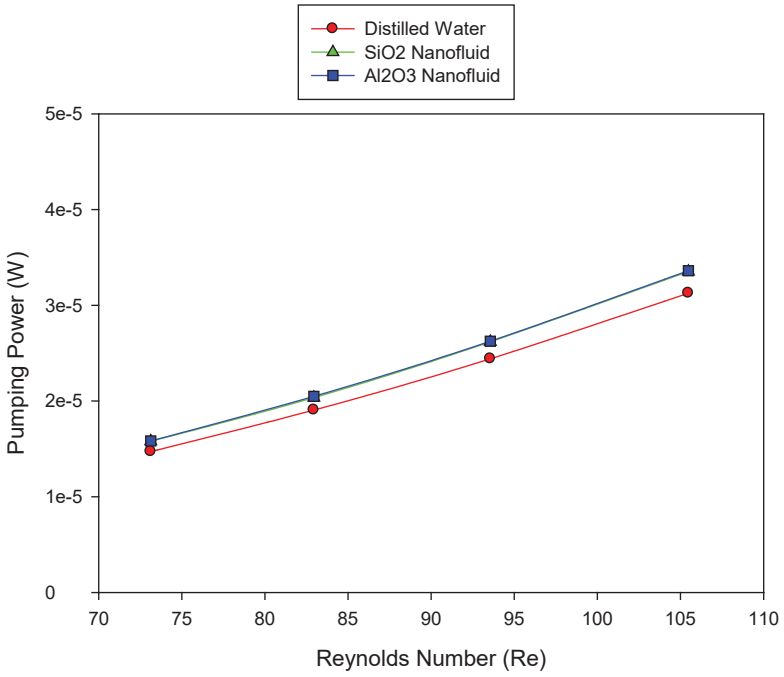

Figure 4.31: Comparison of pumping power among various types of nanofluids within rectangular microchannel at 3% concentration of nanoparticles, by simulation work.

b) Thermal performance

It is found that silica nanofluid shows slight reducing temperature of heat sink base temperature as shown in Figure 4.32. However, alumina nanofluid shows obvious reduction of heat sink base temperature. This is due to the effect of high thermal conductivity of alumina nanoparticles. Hence, the higher the thermal conductivity of nanoparticles within base fluid, the higher the thermal conductivity the nanofluid and higher heat can be transferred into the fluid flow.

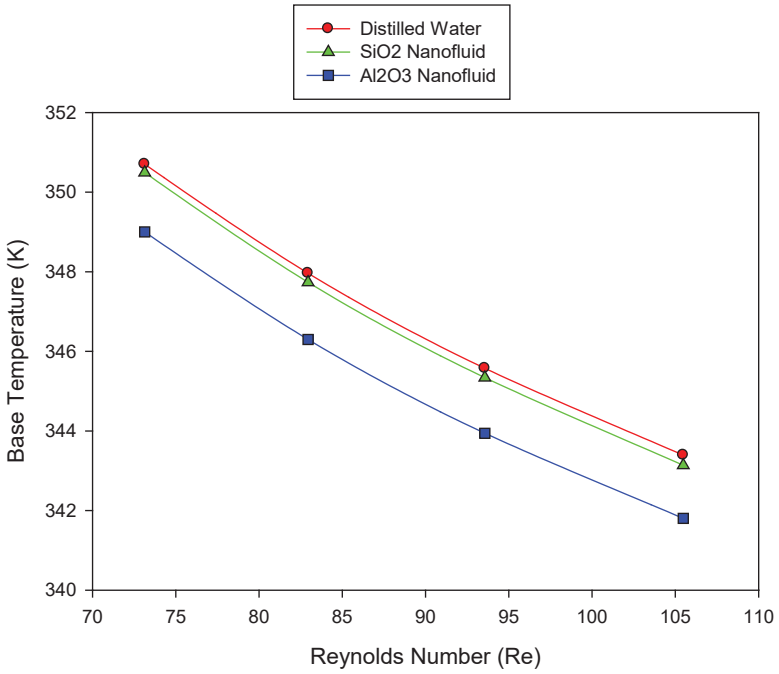

Figure 4.32: Comparison of heat sink base temperature among various types of nanofluids within rectangular microchannel at 3% concentration of nanoparticles, by simulation work.

Referring to Figure 4.33, alumina nanofluid provides the highest heat transfer coefficient in which it is indicating that high heat transfer between fluid flow and fin surface area. As compared with case of distilled water, it is about 11% improvement in heat transfer. For silica nanofluid, it is found that only 2% improvement in heat transfer. The silica nanofluid shows the intermediate thermal performance between alumina nanofluid and base fluid. Besides analysing the heat transfer coefficient, the thermal performance by considering the thermal resistance of microchannel heat sink is also been carried out and compiled in Figure 4.34.

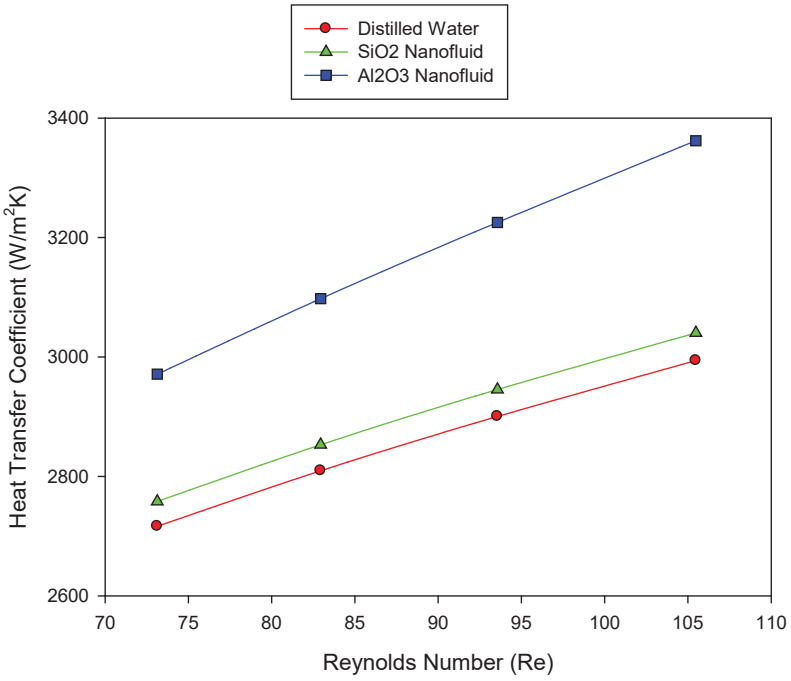

Figure 4.33: Comparison of heat transfer coefficient among various types of nanofluids within rectangular microchannel at 3% concentration of nanoparticles, by simulation work.

It is expected that alumina nanofluid will shows the lowest thermal resistance as shown in Figure 4.34. The silica nanofluid shows the intermediate thermal performance between alumina nanofluid and base fluid, which is consistent with the result that shown in Figure 4.33. Although the existence of type of nanoparticles within base fluid will not affect the hydrodynamic performance, but the type of nanoparticles for nanofluid is a vital parameter and need to be considered carefully for engineering cooling purpose.

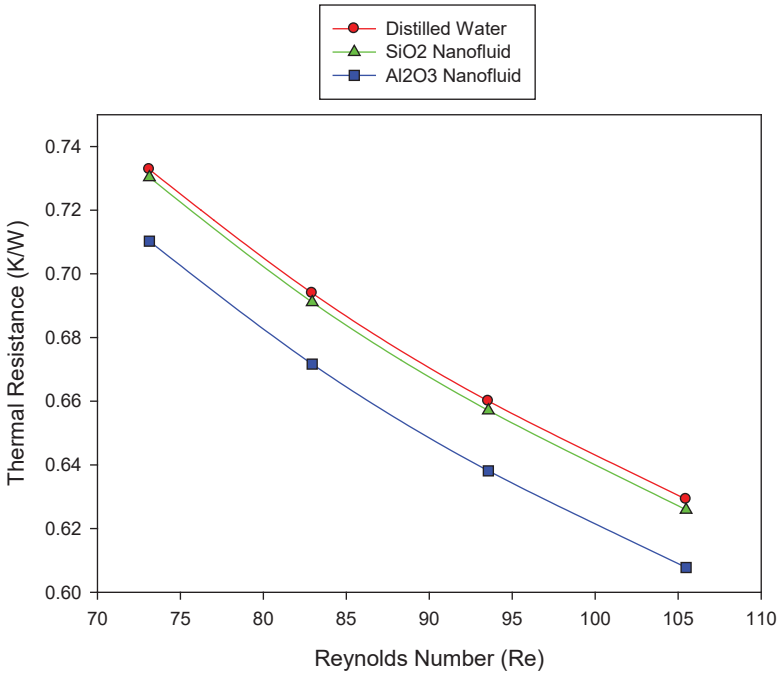

Figure 4.34: Comparison of thermal resistance among various types of nanofluids within rectangular microchannel at 3% concentration of nanoparticles, by simulation work.

To visualize the thermal performance of microchannel heat sink in temperature contour, Figures 4.35 shows the comparison of temperature contour of microchannel by using silica and alumina nanofluids. Comparatively, it is found that the application of alumina nanofluid can enhance the cooling rate by indicating wider cool area at the heat sink fin as well as the heat sink base.

Type of Nanofluid	Iso View	Bottom View
SiO_2 Nanofluid	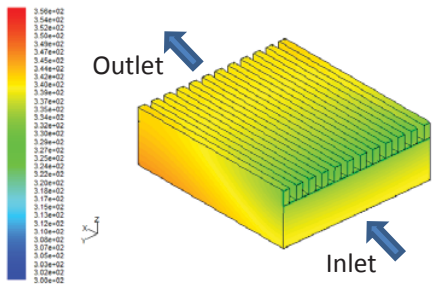	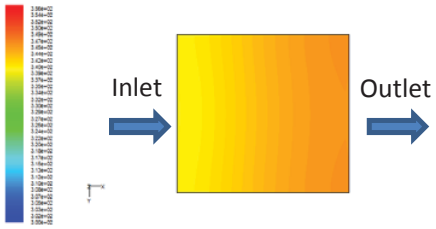
Al_2O_3 Nanofluid	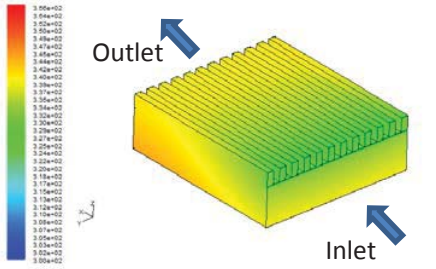	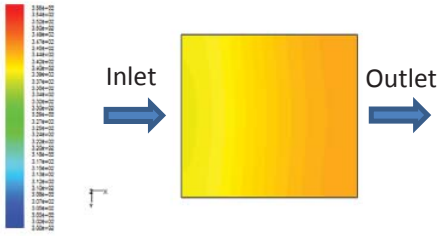

Figure 4.35: Comparison of temperature contour for microchannel heat sink with silica and alumina nanofluids (3% concentration) as cooling medium at fluid flow velocity of 0.0298 m/s.

4.7 Analysis of the effect of vertical and horizontal fin-tip gaps for the various geometrical configurations of microchannels

Referring to the previous sections for the analysis of the effect of nanofluid, nanoparticle concentration and type of nanoparticle within nanofluid on microchannel heat sink performance, it is known that the application of nanofluid able to improve performance of microchannel heat sink especially for thermal performance. Hence, it is practically proper way to further analyse the rectangular microchannel for the physical effect of vertical and horizontal fin-tip gaps by using base fluid as cooling medium within the microchannel.

4.7.1 Analysis of the effect of vertical fin-tip gap

In hydrodynamic performance of heat sink, Fig. 4.36 shows that the pressure drop in the microchannel heat sink decreases with the increasing vertical fin tip gap at constant volume flow rate. The reduction of the pressure drop is due to the lower flow resistance as the fin tip gap increases. In comparison among these various fin configurations, it is found that the triangular fin heat sink shows the lowest pressure drop. It is showing that lowest pumping power is required to drive the coolant flow through the microchannel. However, the rectangular fin heat sink shows the highest pressure drop. Hence, it is the highest pumping power that required as compared to the triangular and trapezoidal fin heat sinks. Hence, triangular fin heat sink shows the highest hydrodynamic performance in term of pressure drop.

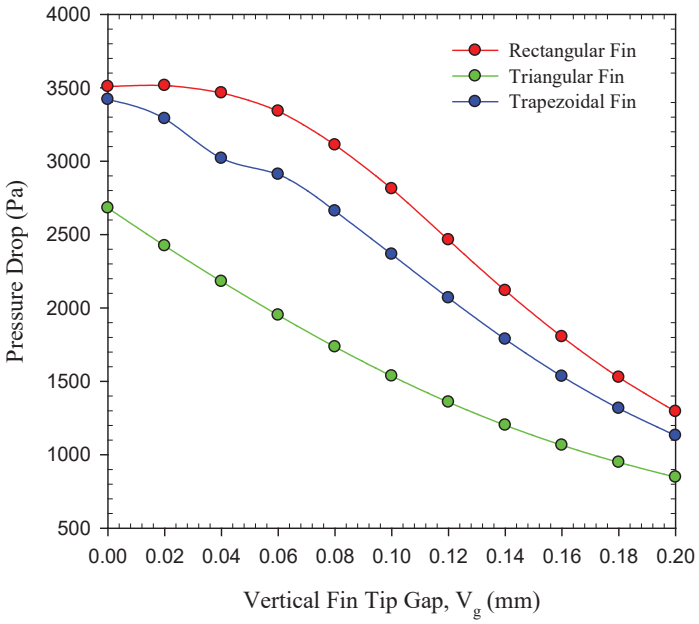

Figure 4.36: Pressure drop comparison as function of vertical fin tip gap, among various fin configurations of microchannel heat sink at volume flow rate of 6.8 x 10^{-7} m^3/s.

In thermal performance analysis, as shown in Fig. 4.37, the triangular fin heat sink has shown the highest total thermal resistance in which then followed by trapezoidal and rectangular fin cases subsequently. Comparatively, the triangular fin heat sink shows a continuous increment thermal resistance with the increment of vertical fin tip gap. The main reason behind this phemenon is due to the low convective area. As refer to Fig. 4.38, the convective area of triangular fin is the lowest as compared with the rectangular and trapezoidal fin cases. As the vertical fin tip gap increases, the triangular fin convective area decreases. As a result, the thermal resistance increases. Conversely, the rectangular fin shows the lowest total thermal resistance, and this condition is due to its highest convective area as shown in Fig. 4.38.

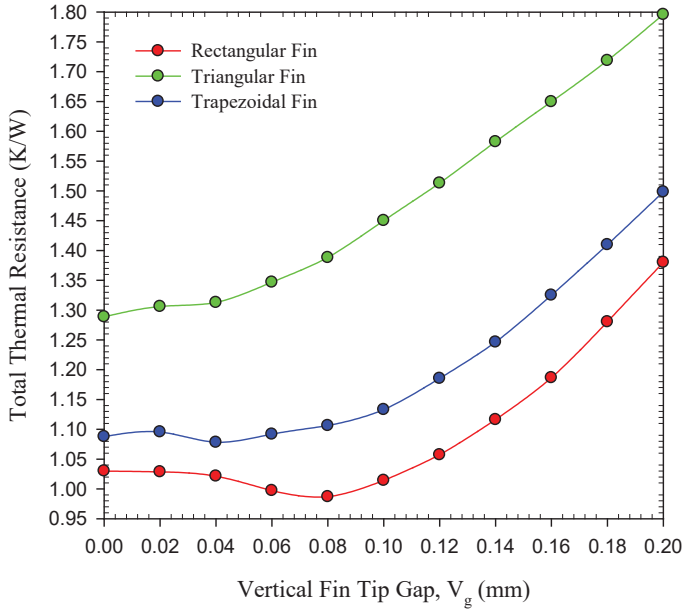

Figure 4.37: Total thermal resistance comparison as function of vertical fin tip gap, among various fin configurations of microchannel heat sink at volume flow rate of 6.8 x $10^{-7}m^3/s$ and heat flux of 300000 W/m^2.

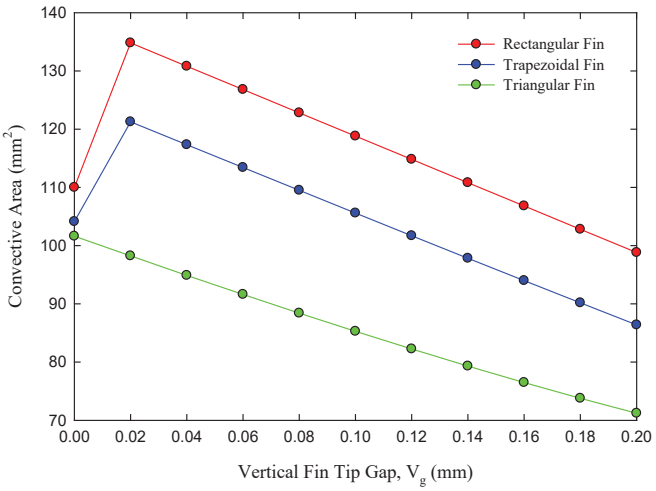

Figure 4.38: Convective area of various fin configurations of microchannel heat sink.

As vertical fin tip gap is introduced (i.e. at vertical fin tip gap of 0.02mm), the convective area increases which is due to the fin top surface as shown in Fig. 4.39, and then decreases as the fin tip gap increases.

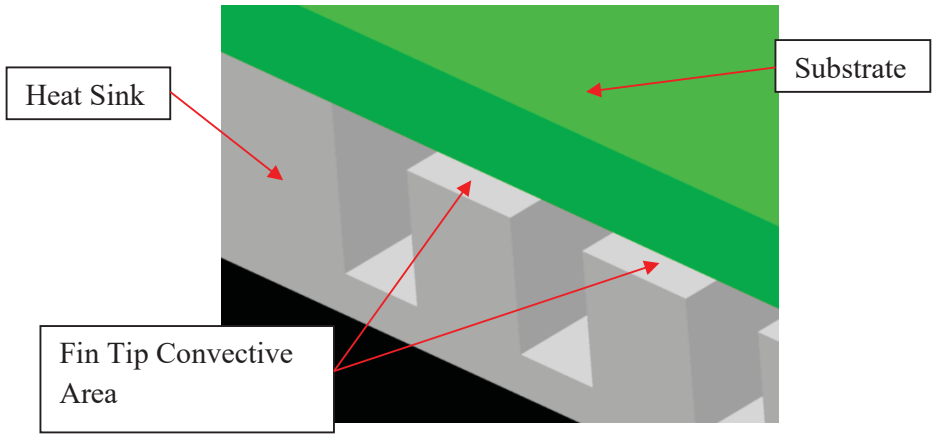

Figure 4.39: Introduction of new convective area as the vertical fin tip gap is introduced.

At $V_g \leq 0.04$mm, there is a very small reduction of total thermal resistance. Although the coolant flow at the fin tip gap is able to absorb the heat from the fin top surface, there is a limitation of heat absorption by the coolant along the fin tip gap. Due to the small fin

tip gap, the coolant flow velocity is low as shown in Fig. 4.40(a). As a result, the rate of heat absorption become lower as the coolant flow along the fin tip gap. At 0.04mm < V_g< 0.08mm, the coolant flow velocity increases and become easily to swept away the heat which has been absorbed from the fin top surface. Hence, the total thermal resistance obviously reduces in that range. At V_g = 0.08mm, the total thermal resistance has been minimized. In such condition, besides the absorbed heat along the fin tip gap is easily swept away by higher flow velocity (as shown in Fig. 4.40(b)), the high coolant velocity in the core channel has played a vital role of further swept away the heat from the fin tip gap convectively. At V_g> 0.08mm, even though the coolant flow velocity at the fin tip gap increases (as shown in Fig. 4.40(c)), but the convective area and coolant flow velocity in the core channel are further decreased in which become more influence to cause increment of thermal convective resistance. Therefore, the thermal convective resistance increases substantially during further increment of the fin tip gap. Similar trend has been observed by Jung et al. (2004), but their results are different in ratio value of the optimum vertical fin tip gap. This is because the present study has considered the whole heat sink structure and fluid flow domain that not being considered by Jung et al. For the trapezoidal fin case, the total thermal resistance is almost constant initially at Vg < 0.04mm in which then increases substantially after the range.

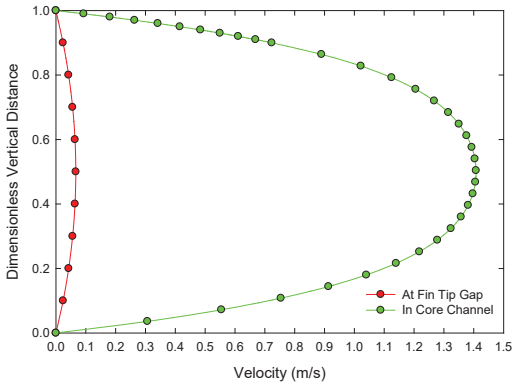

(a) At vertical fin tip gap 0.04mm

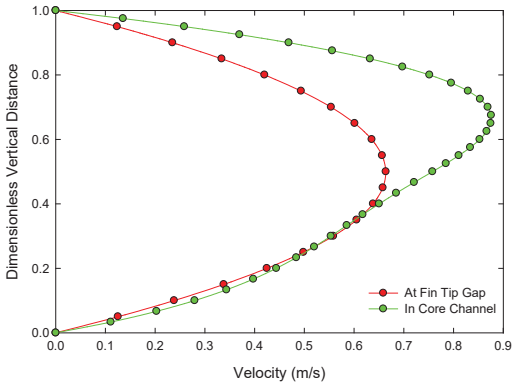

(c) At vertical fin tip gap 0.20mm

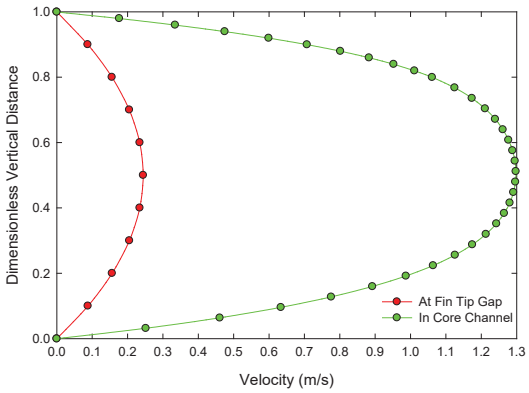

(b) At vertical fin tip gap 0.08mm

Figure 4.40: Velocity distribution in 6th rectangular channel and in the vertical fin tip gap above 5th rectangular fin at volume flow rate of 6.8 x 10^{-7}m^3/s.

Besides analysing heat sink thermal performance in term of total thermal resistance, it is also important to study the temperature distribution at the heat sink base during cooling process. The temperature distribution at the heat sink base is assumed as equivalent to the temperature distribution of microprocessor chip surface. As shown in Fig. 4.41, the triangular fins heat sink has shown the highest maximum base temperature. It is related to the high convective thermal resistance which resulted from the low convective area.

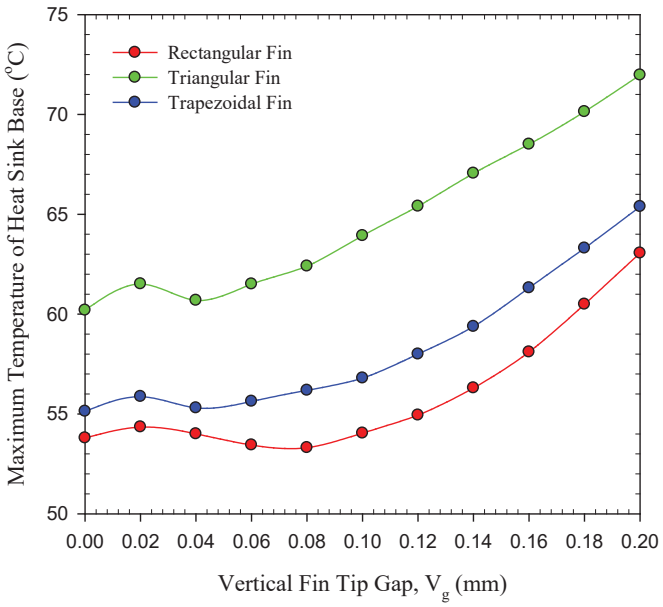

Figure 4.41: Maximum heat sink base temperature as function of vertical fin tip gap, among various fin configurations of microchannel heat sink at volume flow rate of 6.8 x 10^{-7} m^3/s and heat flux of 300000 W/m^2.

Since the thermal convective resistance is high, the heat at the triangular heat sink base is dissipated at low rate by the coolant in which causes high temperature as indicated by the temperature distribution contour in Fig. 4.42(a). Referring to the Fig. 4.42(b), trapezoidal fin heat sink shows a lower temperature and the fairly wider low temperature area as indicated by the temperature distribution contour. In the case of rectangular fin, the heat sink shows the lowest maximum heat sink base temperature as shown in Fig. 4.41, and it has shown the widest low temperature area as shown in Fig. 4.42(c). Generally, it is found that the heat sink base temperature distribution for every fin configurations is consistent with the total thermal resistance respectively in Fig. 4.37, i.e. the higher the thermal resistance the higher the temperature can be seen at the heat sink base as for the case of triangular fin configuration.

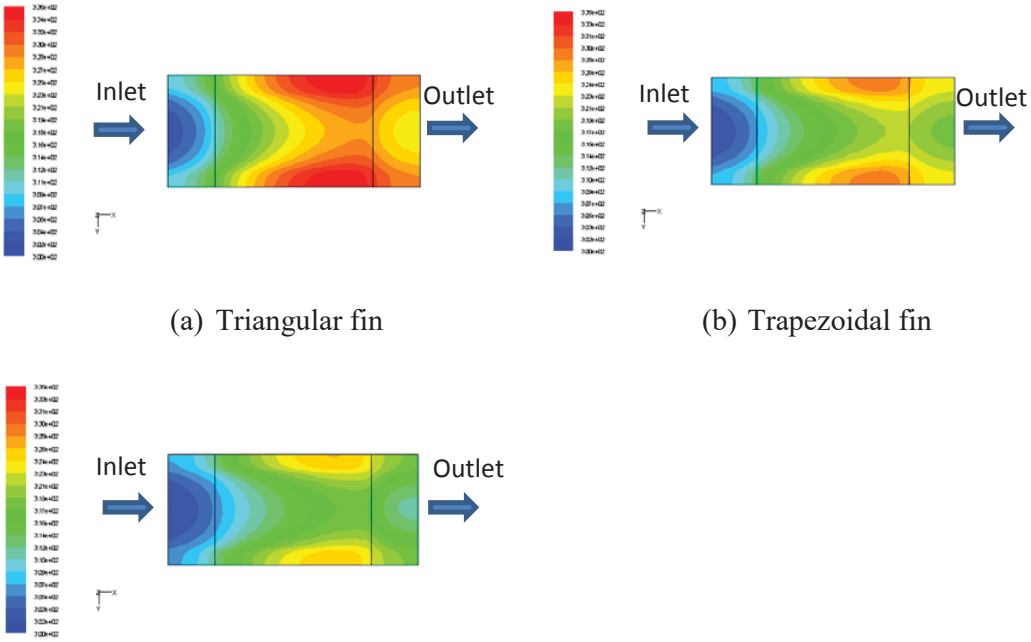

(a) Triangular fin

(b) Trapezoidal fin

(c) Rectangular fin

Figure 4.42: Temperature contour of heat sink base for various fin configurations of microchannel heat sink at vertical fin tip gap of 0.08mm, volume flow rate of 6.8 x 10^{-7} m^3/s and heat flux of 300000 W/m^2.

Since the main function of the heat sink is to remove heat from the computer microprocessor chip and ensure the microprocessor can function well without damage by overheating, the priority attention needs to be given to the thermal performance of the heat sink instead of hydrodynamic performance. Practically, the fabrication of rectangular fins is easier and lower in cost; furthermore, this fin configuration is common in use, as compared with the triangular and trapezoidal fins. However, there still can be an option in the market demand, whether priority is given to the thermal performance or hydrodynamic performance. For good thermal performance, higher price need to be paid for better cooling performance with high pumping power; whereas for good hydrodynamic performance, lower price for poorer cooling with low pumping power. In this study, the rectangular fin heat sink (with optimum vertical fin tip gap) becomes the good option in the cooling application, and it is chosen for further analysis in order to

study how far the thermal and hydrodynamic performances can be achieved by introducing the semi-hollow channels as follows.

4.7.2 Analysis of the effect of horizontal fin-tip gap

Referring to the analysis of the effect of vertical fin tip gap, it is found that the thermal resistance is minimum at the fin tip gap of 0.08mm for rectangular fin as compared with triangular and trapezoidal fins. Hence, the rectangular fin with vertical fin tip gap is further analysed by introducing horizontal sub-fin at the both sides of each rectangular fin as shown in Figure 4.43. As highlighted in Chapter 3, it is convenient to express the horizontal fin tip gap in terms of dimensionless parameter as ratio of the horizontal fin tip gap to channel width, G_c/W_c.

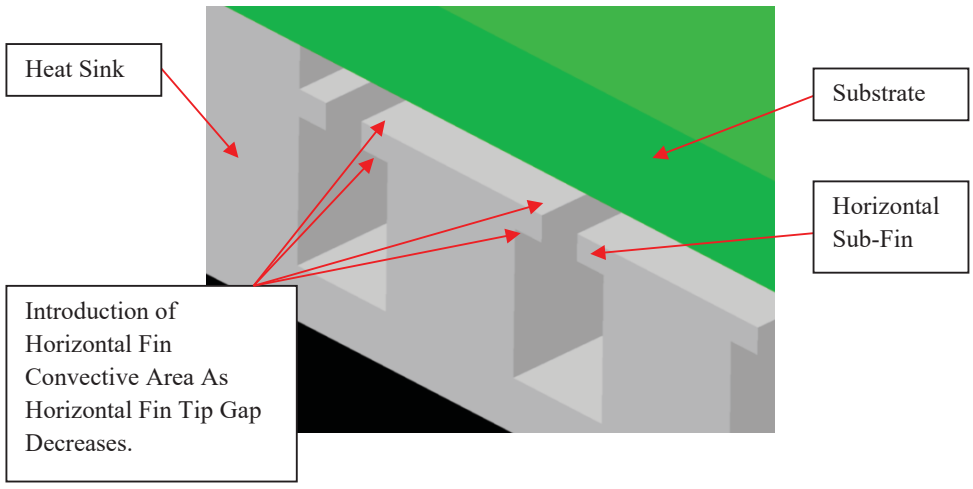

Figure 4.43: Introduction of horizontal fin convective area as the horizontal fin tip gap decreases.

As the horizontal fin tip gap decreases from ratio 1.0 to 0.1, the pressure drop increases but the total thermal resistance decreases as shown in Fig. 4.44 and Fig. 4.45 respectively. In the hydrodynamic field, it is expected that the fluid flow resistance

increases as the horizontal fin tip gap decreases. Hence, higher pumping power is required to overcome the increasing pressure drop.

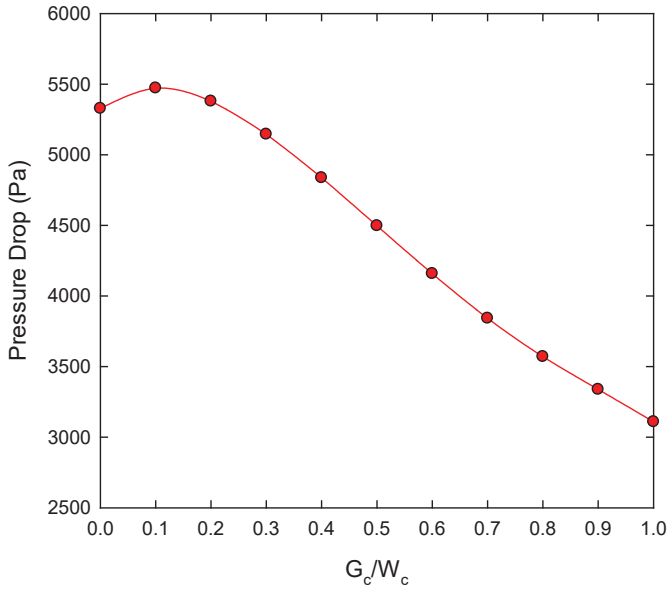

Figure 4.44: Pressure drop as function of different horizontal fin tip gap in microchannel heat sink with optimum vertical fin tip conditions at volume flow rate of 6.8 x 10^{-7} m^3/s.

In the thermal field, more heat can be dissipated by coolant as the horizontal fin tip gap decreases. The vital factors that contribute to this positive effect are due to the high convective heat transfer coefficient and higher fin convective area with the introduction of horizontal fin convective area as shown in Fig. 4.43. As a result, as the horizontal fin tip gap decreases, the fin convective area increases and more heat can be dissipated with the high convective heat transfer coefficient. At the horizontal fin tip ratio of 0.1 in Fig. 4.45, the total thermal resistance is the lowest which is 0.8035 K/W and is an optimum condition for the horizontal fin tip gap. As compared with the fin at the optimum vertical fin tip gap and without the horizontal sub-fin, the thermal performance of semi – hollow fin shows improvement of 14.35%. By further comparison with the original fin condition in which without any fin tip gap, the semi – hollow fin shows obvious improvement of thermal performance at 21.81%. As a result, the existence of vertical and horizontal fin

tip gaps can improve thermal performance of the microchannel heat sink significantly. After both ends of the horizontal sub-fin join to each other, wide single channel is formed at the upper portion and 11 units of smaller channels are formed at the lower portion of internal microchannel heat sink structure as shown in Fig. 3.13(b). In such physical heat sink structure, the total thermal resistance becomes higher, which is due to the lower convective heat transfer coefficient and lower fin convective area as compared with the opening horizontal fin tip gap with the ratio of 0.1.

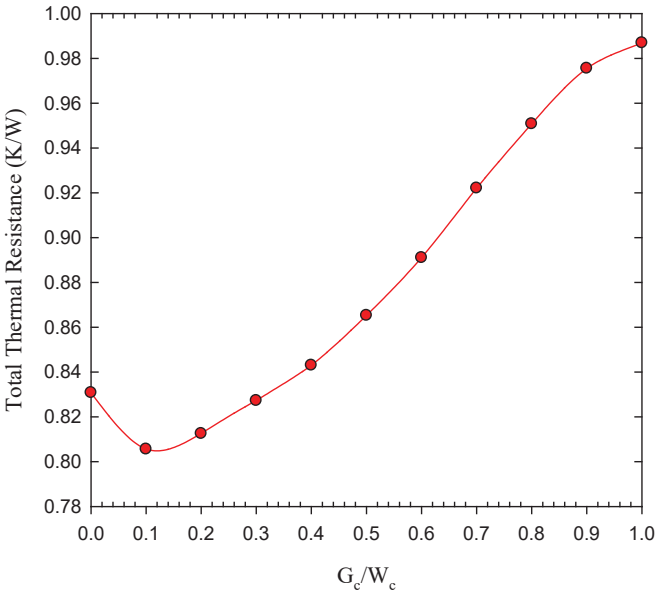

Figure 4.45: Total thermal resistance as function of different horizontal fin tip gap in microchannel heat sink with optimum vertical fin tip conditions at volume flow rate of 6.8 x 10^{-7} m^3/s and heat flux of 300000 W/m^2.

4.8 Analysis of the effects of geometry and number of hollow on the performance of microchannel heat sinks

Besides the analysis of the physical effect of vertical and horizontal fin-tip gap as been discussed in the previous section, the analysis of effect of geometry and number of hollow with het sink fin is analysed on rectangular microchannel heat sink by using base fluid of distilled water as cooling medium.

4.8.1 Effects of hollow and its geometry

Figure 4.46 shows the fluid velocity profiles within the channels and hollows for cases A, B1, C1 and D1, at volume flow rate of 1.3 $\times 10^{-5}$ m^3/s. As can be seen, velocity in the channel is higher than that in the hollow, owing to the difference in flow resistances. Generally, the fluid flow distributions in the channels and the hollows are almost uniform, ensuring uniform heat dissipation across the microchannel heat sink structure as also emphasized by Lu and Nnanna (2007). It is interesting to note that, unlike the channels, the flow inside hollows is found to be fully developed, as indicated clearly by Fig. 4.47. This is attributed to the fact that, the flow through small hydraulic diameters at low flow rates leads to low *Re* (laminar flow) and becomes fully developing at a fairly earlier stage compared to the flow through the channels. The effect of hollow on the pressure drop across the heat sink is also analysed, and the result is shown in Fig.4.48. It is observed that there is slight improvement in pressure drop by providing hollow, and the hollow geometry exhibited no significant influence.

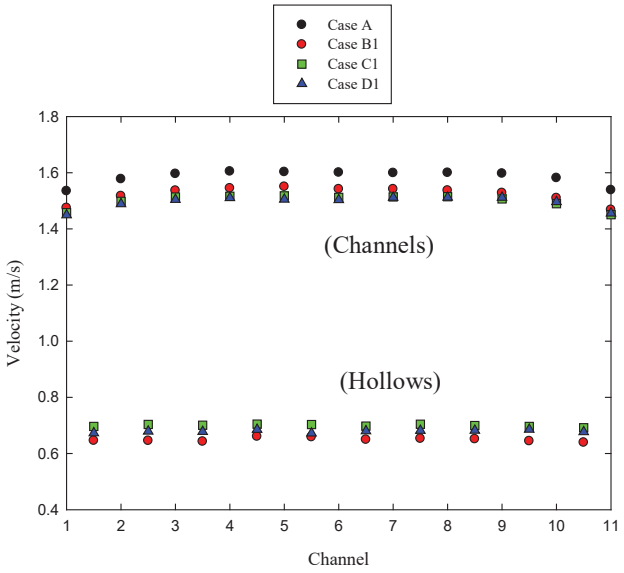

Figure 4.46: Comparison of velocity distributions of fluid flow across the channels and hollows among cases A, B1, C1 and D1.

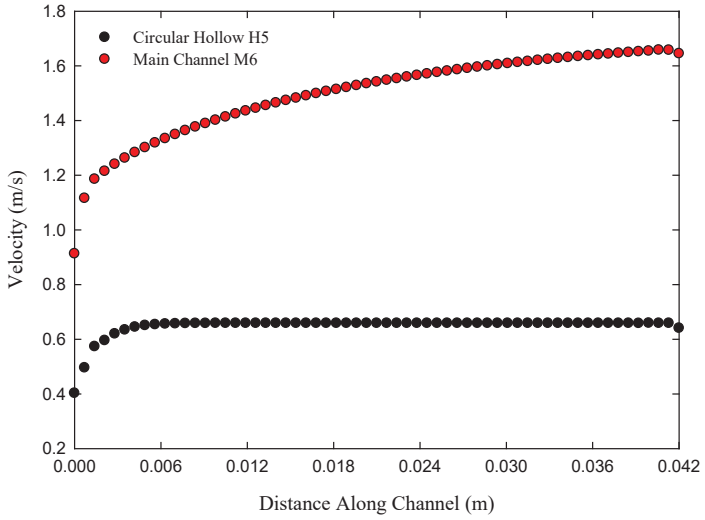

Figure 4.47: Comparison of velocity distributions between channel (M6) and hollow (H5).

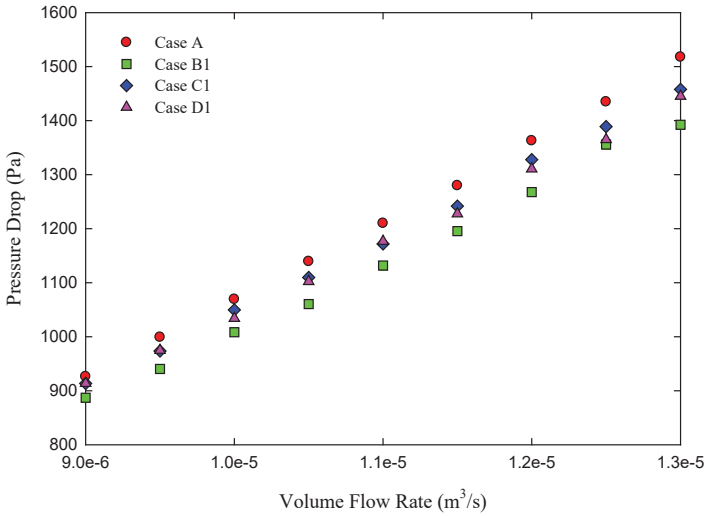

Figure 4.48: Comparison of pressure drop across the heat sink for cases with solid fin and single-hollow fins.

Figure 4.49 shows the temperature contours near the top surface of the heat sink structure (section A-A in Fig. 3.15) with solid fins and single-hollow fins. In general, the initial section of the fins in each case is obviously showing low temperature, owing to the high convective heat transfer rate resulted by the large temperature gradient between the cool entering fluid and hot fin surface. This phenomenon was also reported by Chein

and Chen (2009), and Chen et al. (2009). However, when hollow is introduced, the initial cool zone is significantly grown, presumably due to the enhanced heat transfer. Moreover, the presence of hollow could help cooling the hot spots at the heat sink edges, as well as the downstream regions of the fins, compared to the case A.

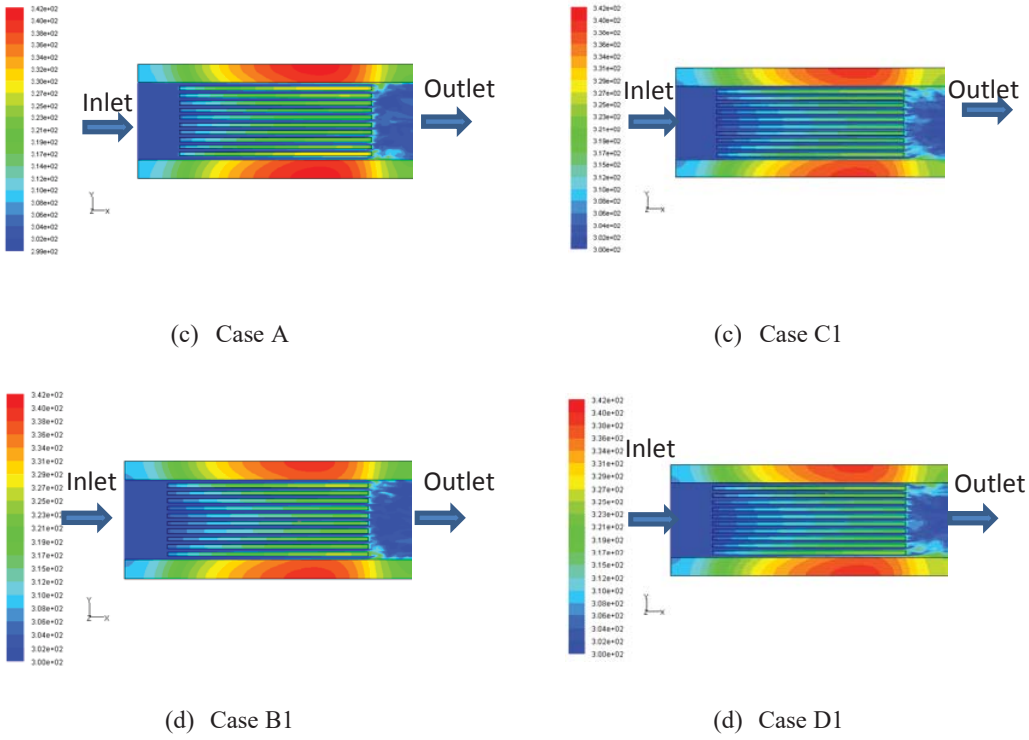

(c) Case A (c) Case C1

(d) Case B1 (d) Case D1

Figure 4.49: Temperature contour of heat sink structure with solid and single-hollow fins at volume flow rate of 1.3×10^{-5} m^3/s.

In order to further elucidate the benefit of hollowed fins, it is interesting to analyze the temperature of the heat sink base (section B-B in Fig. 3.15) which is directly exposed to the heat source. It is worth noting from Figures 4.50 and 4.51 that when hollow is introduced to the fins, the average base temperature is considerably reduced, which proves enhanced heat dissipation from the heat source. This is attributed to the additional exposed area of the fin for convection, causing the total thermal resistance to decrease.

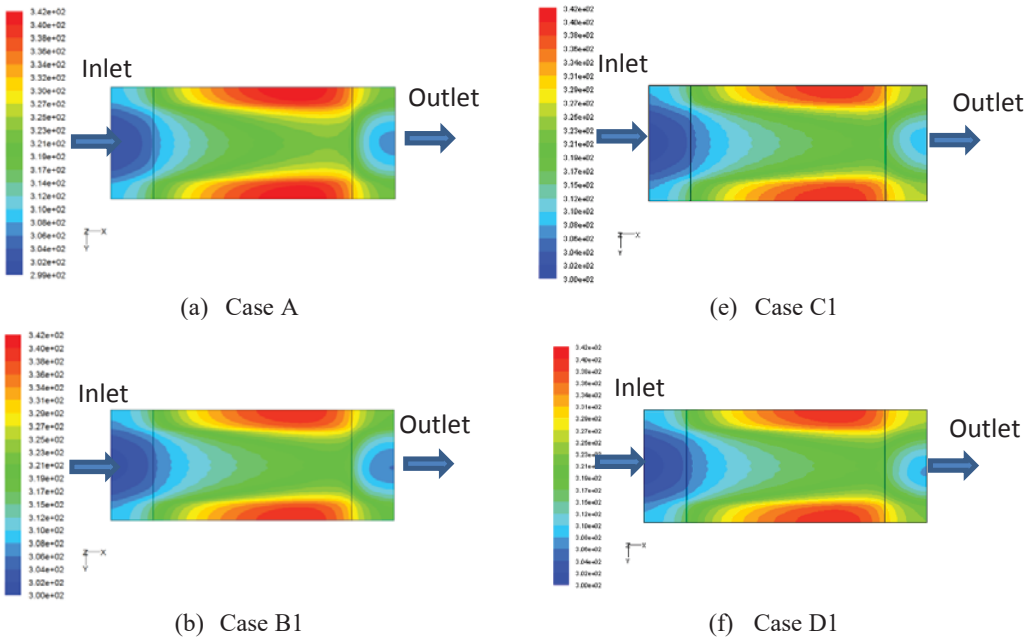

Figure 4.50: Temperature contour of heat sink base with solid and single-hollow fins at volume flow rate of 1.3 $\times 10^{-5}$ m^3/s.

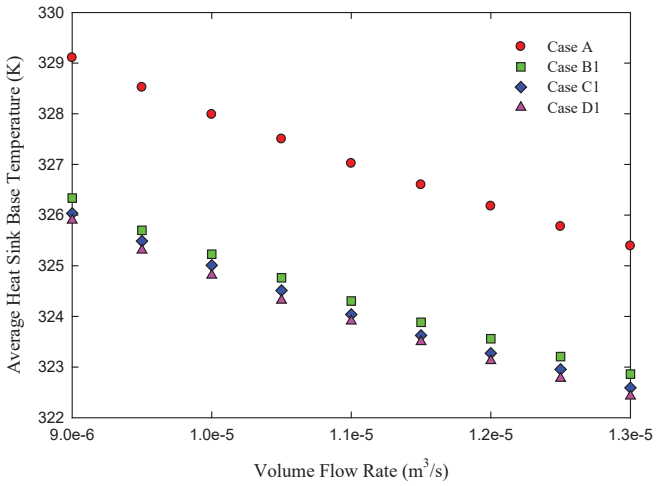

Figure 4.51: Average temperature of heat sink base with solid and single-hollow fins as function of volume flow rate.

As indicated in Fig. 4.52, thermal resistance decreases as the coolant volume flow rate increases. As expected, thermal resistance for Case A is the highest and significantly less for Cases B1, C1 and D1, in line with the low average heat sink base temperature as already seen in Fig. 4.51. Thus it is obvious that the presence of hollow can effectively

improve the heat sink thermal performance. It is also observed that the hollow geometry has no remarkable influence on the thermal performance.

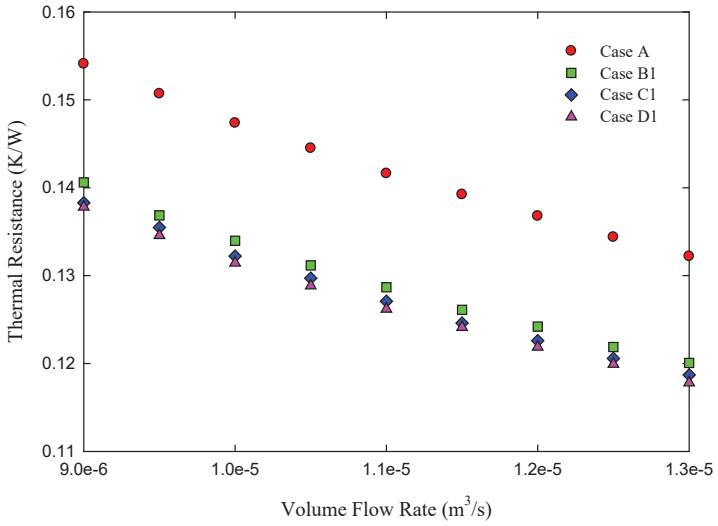

Figure 4.52: Comparison of total thermal resistance of heat sink with solid and single-hollow fins, as function of volume flow rate.

4.8.2 Effect of number of hollows

Having convinced by the excellent impact of hollowed fins on the hydrodynamic and thermal performances of heat sinks, further simulations are performed to study the effect of number of hollows in a given fin. Referring to Figure 4.53, it is worth noting that heat sink with the double- hollowed fins (cases B2, C2 and D2) shows slightly improved hydrodynamic performance (characterized by the decreased pressure drop) compared to the single-hollow case; this is attributed to the lower flow resistance.

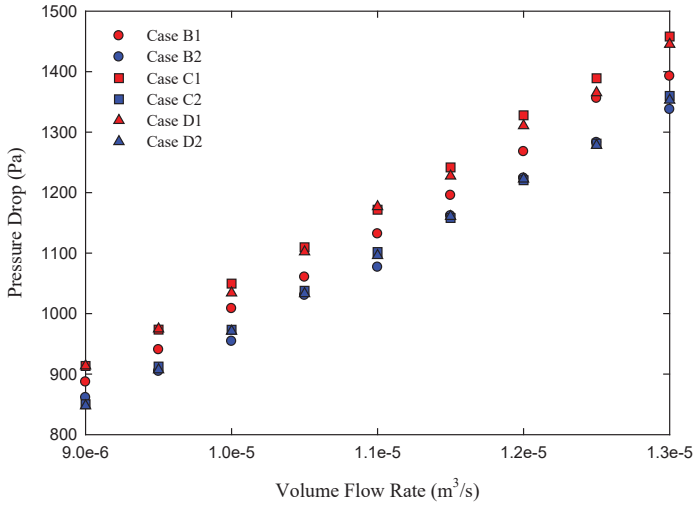

Figure 4.53: Pressure drop across the heat sink with single and double hollow fins as function of volume flow rate.

The average heat sink base temperature is further reduced with the increment of hollow, as observed in Figure 4.54. This is elucidated further by the temperature contours shown in Figure 4.55, the cool zone is spread wider in cases B2, C2 and D2, compared to the cases B1, C1 and D1.

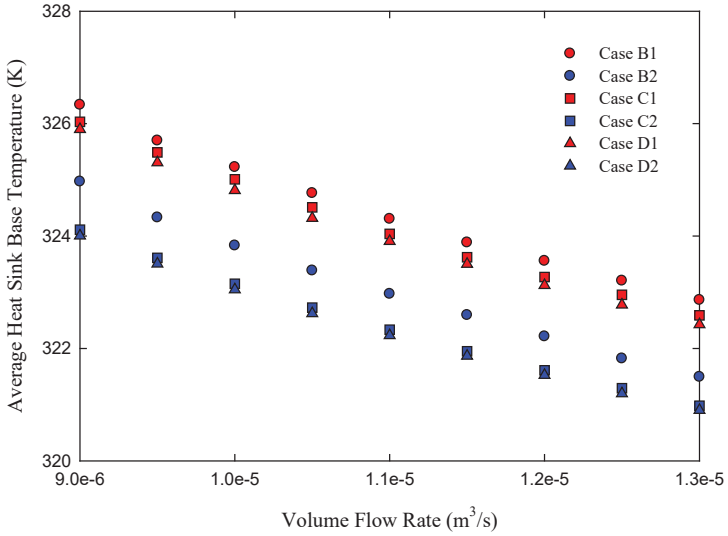

Figure 4.54: Average heat sink base temperature with single and double hollow fins as function of volume flow rate.

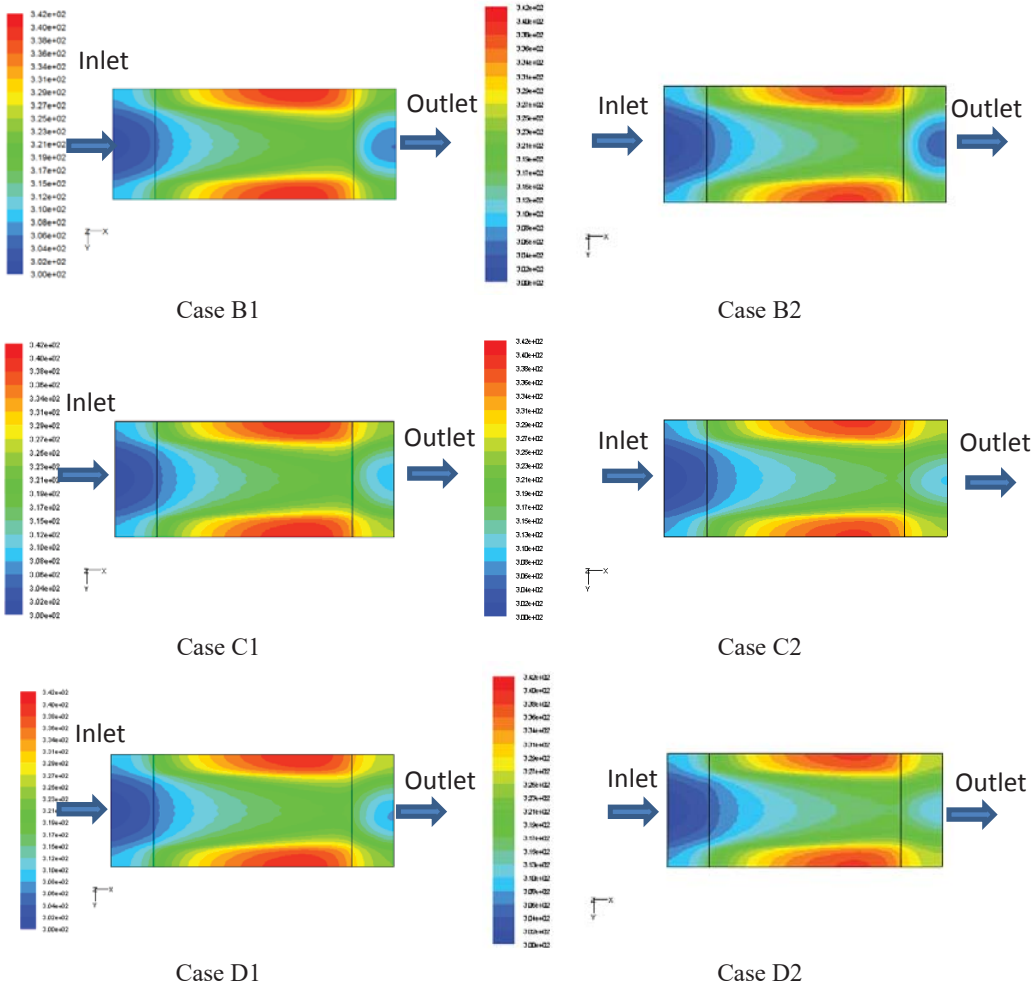

Figure 4.55: Temperature contours of heat sink base with single and double hollow fins at volume flow rate of 1.3×10^{-5} m^3/s.

Furthermore, as indicated by Figure 4.56, thermal resistance is reduced by increasing the number of hollow; reductions of 5.15%, 6.42%, and 6.21% are obtained for cases B2, C2 and D2 respectively, compared with B1, C1 and D1. It is also observed that, thermal resistance is not significantly affected by the hollow geometries. In general, by comparing thermal resistance of heat sink with double-hollowed fins with that of Case A, improvements of 13.84%, 16.04% and 16.34% are achieved for cases B2, C2 and D2 respectively. Thus, it can be concluded that the introduction of hollows inside the fins could remarkably enhance the thermal performance of heat sinks.

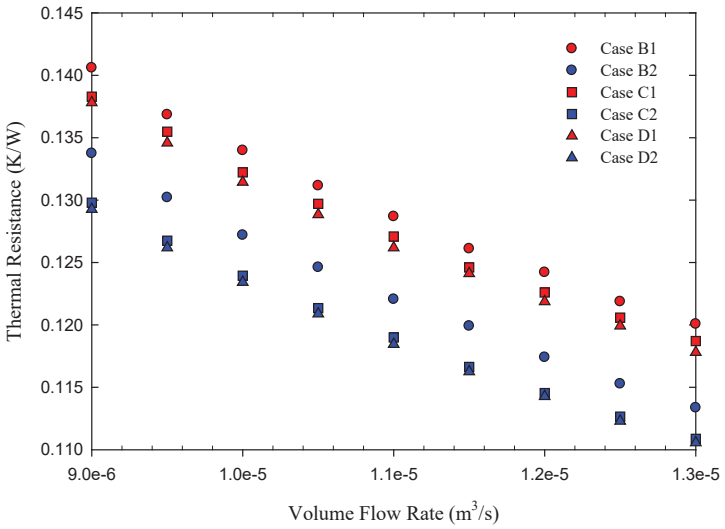

Figure 4.56: Total thermal resistance of heat sink with single and double hollow fins as function of volume flow rate.

As for discussion of this Chapter 4, it is found that difference geometrical configurations of microchannels can affect hydrodynamic and thermal performances of microchannel heat sink. Besides this, the existence of types of nanoparticles within base fluid and with different nanoparticle concentration also plays an important role for thermal performance without obviously affecting hydrodynamic performance. Although there are various types of nanoparticles can be found in market, further analysis need to be carried out to determine the best types of nanoparticles for cooling purpose. The analysis of fin tip gap has shown that the existence of within acceptable range can even improve thermal performance. Lastly, the analysis of hollow within heat fin also has shown that the hydrodynamic and thermal performances of microchannel heat sink can be improved with existence of hollow, and further improved with the increment of hollow quantity.

CHAPTER FIVE
CONCLUSION

5.1 Conclusion

In the current research work, experimental and simulation have been carried out to investigate the performance of microchannel heat sinks among various fin configurations. Comparatively, it has been proved by validation that the simulation results are not much deviation with the experimental results. Hence, it is showing that the simulation work is able to simulate the performance of microchannel heat sink in which detail information can be explored and discussed as already being shown in chapter 4. Various parameters have been analyzed such as pressure drop and pumping power for hydrodynamic performance, whereas heat sink base temperature, heat transfer coefficient and thermal resistance for thermal performance. All of the objectives as being mentioned in chapter 1 have been met, and the conclusion of each work scope is described as follow.

5.2 The effects of various geometrical configurations of microchannel on heat sink performance

The study has shown that the rectangular microchannel provides the highest thermal performance as compared with triangular and trapezoidal microchannels. In thermal performance, rectangular microchannel shows low heat sink temperature, low thermal resistance and high heat transfer coefficient. However, the rectangular microchannel shows poorer hydrodynamic performance with high pressure drop and pumping power. Comparatively, triangular microchannel shows the highest hydrodynamic performance with the lowest pressure drop and pumping power. Since the main function of heat sink is to remove the high heat that generated from electronic component, it is recommended rectangular microchannel instead of triangular

microchannel even though it is poor in hydrodynamic performance comparatively. Furthermore, the cost of fabrication for rectangular configuration is lower.

5.3 The effect of nanofluid on the performance of microchannel heat sink

The effect of nanofluid has shown improvement in thermal performance of microchannel heat sink with higher heat transfer coefficient, and lower heat sink base temperature and thermal resistance as compared with the base fluid. However, the existence of small amount of nanoparticle within nanofluid will not affect the hydrodynamic performance of microchannel heat sink. This is the advantage of using nanofluid as cooling medium to remove heat in microchannel heat sink.

5.4 The effect of nanoparticle concentration of nanofluid on the performance of microchannel heat sink

With the increment of nanoparticle concentration in nanofluid, the higher heat can be absorbed into nanofluid. It is found that the generated heat is not only absorbed into cooling fluid medium, more heat can be absorbed by the increment quantity of nanoparticle that exists in the base fluid medium. Although the quantity of nanoparticle is increased in small quantity, the effect of increment quantity of nanoparticle is still not much increase the pressure drop. Hence, the hydrodynamic performance is not affected; instead, the thermal performance of the microchannel heat sink has been improved further with the increment of nanoparticle within base fluid by indicating low thermal resistance and high heat transfer coefficient.

5.5 The effect of nanoparticles types of nanofluid on the performance of microchannelheat sink

The existence of the types of nanoparticle within nanofluid also play important role in the thermal performance of microchannel heat sink. As shown in the current research work, the use of alumina Al_2O_3 nanofluid in microchannel heat sink has shown the highest heat transfer coefficient and lowest thermal performance as compared with silica SiO_2nanofluid and base fluid. Hence, careful study needs to be given to this factor in order to select proper type of nanoparticle for nanofluid to meet various engineering requirement for removal of high generated heat.

5.6 The effect of vertical and horizontal fin tip gaps on the performance of microchannel heat sinks

In the analysis of vertical fin tip gap, it is found that the existence of small vertical gap above fin tip does not affect thermal performance of microchannel heat sink especially for the rectangular and trapezoidal microchannel heat sink fin. Comparatively, the rectangular fin shows improvement of thermal performance within the limitation of vertical fin tip gap, whereas the trapezoidal fin shows almost constant of thermal performance. Instead, the triangular fin shows a continuous increment of thermal resistance which is showing the thermal performance of the fin configuration is decreasing as the vertical fin tip gap increases. In the analysis of horizontal fin tip gap by further analyzing the case of rectangular fin, the thermal resistance can be further reduced by the existence of small horizontal fin tip gap.

As a result, it is concluded that the existence of small fin tip gap is not an obvious concern onto the thermal performance of rectangular and trapezoidal fins after fabrication and assembly process within acceptable tolerance. Furthermore, it is become advantage for the case of rectangular fin. Hence, the rectangular fin has shown the best

thermal performance even though with the existence of fin tip gap and it is recommended as the choice of selection among triangular and trapezoidal fins.

5.7 The effect of geometry and number of hollow on the performance of microchannel heat sinks

For further improvement of thermal performance of microchannel heat sink, the existence of hollow within heat sink fin enable more coolant to flow around the hollow fin and more heat can be absorbed by the coolant for removal. By the way, the pressure drop within the microchannel heat sink decreases. By further increase the number of hollow within heat sink fin, more contact surface area between fluid flow and heat sink surface is created. As a result, the rate of heat removal from the heat sink increases and improved. Besides this, the pressure drop within the microchannel heat sink also further decreases.

As comparison among existence of various configurations of hollow within fin, it is concluded that the effect of hollow geometry and number of hollow within fin has potential to improve thermal and hydrodynamic performances of microchannel heat sink. As a result, the effect of geometry and number of hollow need to be given consideration as factors for thermal and hydrodynamic performances improvement for microchannel heat sink.

5.8 Recommendation for future works

The following are the recommended future works for further analysis as for development of microchannel heat sink:

1. Improvement of settlement issue of various types of nanoparticle within base fluid.

2. Analysis of the effect of nanofluid in two-phase (boiling) flow within microchannel.
3. Numerical study of nanofluid in two-phase (boiling) flow that enable to predict the hydrodynamic and thermal performances of microchannel heat sink.

REFERENCES

Akyol, U., Bilen, K. (2006) Heat transfer and thermal performance analysis of a surface with hollow rectangular fins. Applied Thermal Engineering 2006, Vol. 26, p.209 – 216.

Anoop, K.B., Sundararajan, T., Das, S.K. (2009) Effect of particle size on the convective heat transfer in nanofluid in the developing region. International Journal of Heat and Mass Transfer, Vol. 52, p.2189 – 2195.

Bahram, R.F., Shahabeddin, K.M., Sanjeev, K.K., Zhang Y. (2015) Effects of pin tip-clearance on the performance of an enhanced microchannel heat sink with oblique fins and phase change material slurry. International Journal of Heat and Mass Transfer, Vol. 83, p.136 – 145.

Barlay E.O., O. Sara, O.N., Yapici, S., Arzutug, M.E.. (2009) Pressure drop and point mass transfer in a rectangular microchannel. International Communications in Heat and Mass Transfer, Vol. 36, p.618 – 623.

Behzad, F., Abbas, A., Mohammad, K. (2013) Effect of nanoparticles size on thermal performance of nanofluid in a trapezoidal microchannel-heat-sink. International Communication in Heat and Mass Transfer, Vol. 45, p.155 – 161.

Chai, L., Xia, G., Wang L., Zhou, M., Cui, Z. (2013) Heat transfer enhancement in microchannel heat sinks with periodic expansion-constriction cross-sections. International Journal of Heat and Mass Transfer, Vol. 62, p.741 – 751.ccccccc

Chein, R., Huang, G. (2005) Analysis of microchannel heat sink performance using nanofluids. Applied Thermal Engineering, Vol. 25, p.3104 – 3114.

Chein, R., Chen, J. (2009) Numerical study of the inlet/outlet arrangement effect on microchannel heat sink performance. International Journal of Thermal Sciences, Vol. 48, p.1627 – 1638.

Chein R., Jason C. (2007) Experimental microchannel heat sink performance studies using nanofluids. International Journal of Thermal Sciences, Vol. 46, p.57 – 66.

Chen, Y., Zhang, C., Shi, M., Wu, J. (2009) Three-dimensional numerical simulation of heat and fluid flow in noncircular microchannel heat sinks. International Communications in Heat and Mass Transfer, Vol. 36, p.917 – 920.

Chuan, L., Wang, X.D., Wang T.H. (2015) An improved design of double-layered microchannel heat sink with truncated top channels. Applied Thermal Engineering, Vol. 79, p.54 – 62.

Coetzer, C.B., Visser. J.A. (2003) Compact modeling of forced flow in longitudinal fin heat sinks with tip bypass. Journal of Electronic Packaging, Copyright © 2003 by ASME; DOI: 10.1115/1.1533803, Vol. 125, p.319 – 324.

Copeland, D., Behnia, M., Nakayama, W. (1997) Manifold microchannel heat sinks: isothermal analysis. IEEE Transactions on Components, Packaging and Manufacturing – Part A, Vol. 20, N0. 2, June 1997.

Dogruoz, M.B., Ortega, A., Westphal, R.V. (2006) A model for flow bypass and tip leakage in pin fin heat sinks. Journal of Electronic Packaging, Copyright © 2006 by ASME; DOI: 10.1115/1.2159009, Vol. 128, p.53 – 60.

Elshafei, E.A.M. (2007) Effect of flow bypass on the performance of a shrouded longitudinal fin array. Applied Thermal Engineering, Vol. 27, p.2233 – 2242.

Garcia-Hernando, N., Acosta-Iborra, A., Ruiz-Rivas, U., Izquierdo, M. (2009) Experimental investigation of fluid flow and heat transfer in a single-phase liquid flow micro-heat exchanger. International Journal of Heat and Mass Transfer, Vol. 52, p.5433 – 5446.

Garimella, S.V., Singhal, V. (2004) Single-phase flow and heat transport and pumping considerations in microchannel heat sinks. Heat Transfer Engineering, Vol. 25(1), p.15 – 25, Copyright © Taylor & Francis Inc., ISSN: 0145 – 7632 print/1521 – 0537 online, DOI: 10.1080/01457630490248241.

Harms, T.M., Kazmierzak, M.J., Gerner, F.M. (1999) Developing convective heat transfer in deep rectangular microchannels. International Journal of Heat and Fluid Flow, Vol. 20, p.149 – 157.

Harshit, K.G., Santosh, K. R., Tanuja, S, (2015) IHMT2015-60 Boiling Flow Heat Transfer In Microchannel: Experimental And Numerical Investigation, Conference Proceeding of the 23rd National Heat and Mass Transfer Conference and 1st International ISHMT-ASTFE Heat and Mass Transfer Conference IHMTC 2015, Vol. 23.

Ho, C.J., Wei, L.C., Li, Z.W. (2010) An experimental investigation of forced convective cooling performance of a microchannel heat sink with Al_2O_3 nanofluid. Applied Thermal Engineering, Vol. 30, p.96 – 103.

Hung, T.C., Yan, W.M., Wang, X.D., Chang, C.Y. (2012) Heat transfer enhancement in microchannel heat sinks using nanofluids. International Journal of Heat and Mass Transfer, Vol. 55, p.2559 – 2570.

Jang, S.P., Stephen Choi, U.S. (2006) Cooling performance of a microchannel heat sink with nanofluids. Applied Thermal Engineering, Vol. 26, p.2457 – 2463.

Jeng, T.M. (2008) A porous model for the square pin-fin heat sink situated in a rectangular channel with laminar side-bypass flow. International Journal of Heat and Mass Transfer, Vol. 51, p.2214 – 2226.

Jung, J.Y., Kwak, H.Y. (2008) Fluid flow and heat transfer in microchannels with rectangular cross section. Heat Mass Transfer, Vol. 44, p.1041 – 1049, DOI: 10.1007/s00231-007-0338-4.

Jung, Y.M., Seok, P.J., Sung, J.K. (2004) Effect of tip clearance on the cooling performance of a microchannel heat sink. International Journal of Heat and Mass Transfer, Vol. 47, p.1099 – 1103.

Jung, J.Y., Oh, H.S., Kwak, H.Y. (2009) Forced convective heat transfer of nanofluids in microchannels. International Journal of Heat and Mass Transfer, Vol. 52, p.466 – 472.

Kandlikar, S.G. (2006) Single-phase liquid flow in minichannels and microchannels, Heat Transfer and Fluid Flow in Minichannels and Microchannels, p.87 – 136.

Kandlikar, S.G., Steinke, M.E. (2003) Predicting heat transfer during flow boiling in minichannels and microchannels. ASHRAE Transactions, Vol. 109(1), p.1–9.

Khan, W.A., Yovanovich, M.M. (2007) Effect of bypass on overall performance of pin-fin heat sinks. Journal of Thermophysics and Heat Transfer, DOI: 10.2514/1.27544, Vol. 21, p.562 – 567.

Koo, J., Kleinstreuer, C. (2004) Viscous dissipation effects in microtubes and microchannels. International Journal of Heat and Mass Transfer, Vol. 47(14-16), p.3159-3169.

Lee, J., Mudawar, I. (2007) Assessment of the effectiveness of nanofluids for single-phase and two-phase heat transfer in micro-channels. International Journal of Heat and Mass Transfer, Vol. 50, p.452 – 463.

Lee, P.S., Garimella, S.V., Liu, D. (2005) Investigation of heat transfer in rectangular microchannels. International Journal of Heat and Mass Transfer, Vol. 48, p.1688 – 1704.

Li, H.Y., Tsai, G.L., Chiang, M.H., Lin, J.Y. (2009) Effect of a shield on the hydraulic and thermal performance of a plate-fin heat sink. International Communications in Heat and Mass Transfer, Vol. 36, p.233 – 240.

Li, J., Kleinstreuer, C. (2008) Thermal performance of nanofluid flow in microchannels. International Journal of Heat and Fluid Flow, Vol. 29, p.1221 – 1232.

Li, J., Peterson, G.P., Cheng, P. (2004) Three – dimensional analysis of heat transfer in a micro-heat sink with single phase flow. International Journal of Heat and Mass Transfer, Vol. 47, p.4215 – 4231.

Li, Z., He, Y.L., Tang, G.H., Tao, W.Q. (2007) Experimental and numerical studies of liquid flow and heat transfer in microtubes. International Journal of Heat and Mass Transfer, Vol. 50, p.3447 – 3460.

Liu, D., Yu, L. (2011) Single – phase thermal transport of nanofluids in a minichannel. Journal of Heat Transfer, Vol. 133 / 031009 – 1, Copyright © 2011 by ASME.

Min, J.Y., Jang, S.P., Kim, S.J. (2004) Effect of tip clearance on the cooling performance of a microchannel heat sink. International Journal of Heat and Mass Transfer, Vol. 47, p.1099 – 1103.

Mohammed, H.A., Gunnasegaran, P., Shuaib, N.H. (2010) Heat transfer in rectangular microchannels heat sink using nanofluids. International Communication in Heat and Mass Transfer, Vol. 37, p.1496 – 1503.

Mohammed, H.A., Gunnasegaran, P., Shuaib, N.H. (2011) Influence of various base nanofluids and substrate materials on heat transfer in trapezoidal microchannel heat sinks. International Communication in Heat and Mass Transfer, Vol. 38, p.194 – 201.

Mohammed, H.A., Bhaskaran, G., Shuaib, N.H., Abu-Mulaweh, H.I. (2011) Influence of nanofluids on parallel flow square microchannel heat exchanger performance. International Communications in Heat and Mass Transfer, Vol. 38, p.1 – 9.

Moores, K.A., Kim, J., Joshi, Y.K. (2009) Heat transfer and fluid flow in shrouded pin fin arrays with and without tip clearance. International Journal of Heat and Mass Transfer, Vol. 52, p.5978 – 5989.

Mostafa, M., Maziar, D. (2013) Investigation of flow and heat transfer of nanofluid in microchannel with variable property approach. Heat Mass Transfer, Vol. 49, p.1803 – 1811, DOI 10.1007/s00231-013-1217-9.

Mudawar, I. (2001) Assessment of high-heat-flux thermal management schemes. IEEE Transactions On Components and Packaging Technologies, Vol. 24, No. 2, June 2001.

Mushtaq I.H, Rageb, A.A., Yaghoubi, M., Homayon H. (2009) Influence of channel geometry on the performance of a counter flow microchannel heat exchanger. International Journal of Thermal Sciences, Vol. 48, p.1607 – 1618.

Naphon, P., Sookkasem, A. (2007) Investigation on heat transfer characteristics of tapered cylinder pin fin heat sinks. Energy Conversion and Management, Vol. 48, p.2671 – 2679.

Naphon, P., Khonseur, O. (2009) Study on the convective heat transfer and pressure drop in the micro-channel heat sink. International Communications in Heat and Mass Transfer, Vol. 36, p.39 – 44.

Pan, M., Tang, Y., Pan, L., Lu, L. (2008) Optimal design of complex manifold geometries for uniform flow distribution between microchannels. Chemical Engineering Journal, Vol. 137, p.339 – 346.

Park, H.S., Punch, J. (2008) Friction factor and heat transfer in multiple microchannels with uniform flow distribution. International Journal of Heat and Mass Transfer, Vol.51, p.4535 – 4543.

Pemachandran, B., Balaji, C. (2006) A correlation for mixed convection heat transfer from converging, parallel and diverging channels with uniform volumetric heat generating plates. International Communications in Heat and Mass Transfer, Vol. 33, p.350 – 356.

Qu, W., Mudawar, I. (2002) Experimental and numerical study of pressure drop and heat transfer in a single-phase micro-channel heat sink. International Journal of Heat and Mass Transfer, Vol. 45, p.2549 – 2565.

Ryu, J.H., Choi, D.H., Kim, S.J. (2003) Three-dimensional numerical optimization of a manifold microchannel heat sink.International Journal of Heat and Mass Transfer, Vol. 46, p.1553 – 1562.

Sara, O.N., Barlay E.O., Arzutug, M.E., Yapici, S. (2009) Experimental study of laminar forced convective mass transfer and pressure drop in microtubes. International Journal of Thermal Sciences, p.1 – 7.

Sata, Y., Iwasaki, H., Ishizuka, M. (1997) Development of prediction technique for cooling performance of finned heat sink in uniform flow. IEEE Transactions On Components, Packaging, And Manufacturing Technology, Publisher item identifier: S 1070-9886(97)03852-3, Part A, Vol. 20, p.160 – 166.

Steinke, M.E., Kandlikar, S.G. (2006) Single-phase liquid friction factors in microchannels. International Journal of Thermal Sciences, Vol. 45, p.1073 – 1083.

Tiew, W.T., Yew, M.H., Guo, N. (2014) Effects of steamwise conduction on thermal performance of nanofluid flow in microchannel heat sinks. Energy Conversion and Management, Vol. 78, p.14 – 23.

Tokit, E.M., Mohammed, H.A., Yusoff, M.Z. (2012) Thermal performance of optimized interrupted microchannel heat sink (IMCHS) using nanofluids. International Communications in Heat and Mass Transfer, Vol. 39, p.1595 – 1604.

Tonomura, O., Tanaka, S., Noda, M., Kano, M., Hasebe, S., Hashimoto, I. (2004) CFD-based optimal design of manifold in plate-fin microdevices. Chemical Engineering Journal, Vol. 101, p.397 – 402.

Tuckerman, D.B., Pease. R.F.W. (1981) High performance heat sinking for VLSI. IEEE Electron Device Lett. ELD-2 (5), p.126-129.

Wang, Y., Ding, G.F., Fu, S. (2007) Highly efficient manifold microchannel heat sink, Electronic Letters. 31st August 2007, Vol. 43, No. 18.

Wang, Y., Ding, G.F. (2008) Numerical analysis of heat transfer in a manifold microchannel heat sink with high efficient copper heat spreader. Microsyst Technol 14:389 – 395, DOI: 10.1007/s00542-007-0455-5.

Wang, X.D., Bin, A., Lin, L., Lee, D.J. (2013) Inverse geometric optimization for geometry of nanofluid-cooled microchannel heat sink. Applied Thermal Engineering, Vol. 55, p.87 – 94.

Wen, D., Ding, Y. (2004) Experimental investigation into convective heat transfer of nanofluids at the entrance region under laminar flow conditions. International Journal of Heat and Mass Transfer, Vol. 47, p.5181 – 5188.

Wong, K.C., Fashli, N.A.M. (2013) Heat transfer of a parallel flow two-layered microchannel heat sink. International Communications in Heat and Mass Transfer, Vol. 49, p.136 – 140.

Xia, G., Liu, Q., Qi, J., Xu, J. (2008) Influence of surfactant friction drop in a manifold microchannel. International Journal of Thermal Sciences, Vol. 47, p.1658 – 1664.

Xie, X.L., Liu, Z.J., He, Y.L., Tao, W.Q. (2009) Numerical study of laminar heat transfer and pressure drop characteristics in a water – cooled minichannel heat sink. Applied Thermal Engineering, Vol. 29, p.64 – 74.

Yun, Y., Shahabeddin, K.M., Zhang, Y. (2015) Analysis of performances of a manifold microchannel heat sink with nanofluids. International Journal of Thermal Science, Vol. 89, p.305 – 313.

Zhang, H.Y., Pinjala, D., Wong, T.N., Toh, K.C., Joshi, Y.K. (2004) Single – phase liquid cooled microchannel heat sink for electronic packages. Applied Thermal Engineering, Vol. 25, p.1472 – 1487.

Agarwal, G., Moharana, M.K., Khandekar, S. (2010) Thermo-hydrodynamics of developing flow in a rectangular mini-channel array. 20th National and 9th International ISHMT – ASME Heat and Mass Transfer Conference 2010, Research Publishing Services, ISBN: 978 – 981 – 08 – 3813 – 3, DOI: 10.3850/9789810838133_351.

Lei, N., Skandakumaran, P., Ortega, A. (2006) Experiments and modeling of multilayer copper minichannel heat sinks in single-phase flow. The Tenth Intersociety Conference on Thermal and Thermomechanical Phenomena in Electronics Systems, May 30 2006-June 2 2006.ITHERM '06. San Diego, California, p.9 – 18.

Lee, P.S., Ho, J.C., Xue, H. (2002) Experimental study on laminar heat transfer in microchannel heat sink. Inter Society Conference on Thermal Performance.

Pan, M., Tang, Y., Zhou, W., Lu, L. (2007) Flow distribution among microchannels with asymmetrical manifolds. IEEE International Conference on Control and Automation, Guangzhou (China) – May 30 to June 1, 2007.

Senta, M., Nnanna, A.G.A. (2007) Design of manifold for nanofluid flow in microchannels. Proceedings of the ASME Int. Mechanical Engineering Congress and Exposition, No.IMECE 2007-42720, November 11 – 15, 2007, Seattle, Washington, p.1-8.

Holman, J.P. (2010) Heat Transfer, 10th Edition, McGraw-Hill Series in Mechanical Engineering, ISBN: 978-0-07-352936-3.

Kandlikar, S.G., Garimella, S., Li, D., Colin, S., King, M.R. (2006) Heat Transfer and Fluid Flow in Minichannels and Microchannels, Elsevier Ltd., ISBN: 0-0804-4527-6.

Munson, B.R., Young, D.F., Okiishi, T.H., Huebsch, W.W. (2009) Fundamentals of Fluid Mechanics, 6th Edition, John Wiley & Sons Inc., ISBN: 978-0470-26284-9.

Ohadi, M., Choo, K., Serguei, D., Edvin, C. (2013) Next Generation Microchannel Heat Exchanger, Springer Briefs in Applied Sciences and Technology, Thermal Engineering and Applied Science, ISBN: 978-1-4614-0779-9.

White, F.M. (1998) Fluid Mechanics, 4th Edition, McGraw-Hill Series in Mechanical Engineering.

LIST OF PUBLICATIONS

H. J. Tony Tan, M. Z. Abdullah and M. Abdul Mujeebu, (2011) Effects of Geometry and Number of Hollow on the Performance of Rectangular Fins in Microchannel Heat Sinks, Journal of Thermal Science and Technology, June 2011, p. 01 – 09, ISSN 1300-3615.

H. J. Tony Tan and M. Z. Abdullah, (2012) Effects of Horizontal / Vertical Fin Tip Gaps on Microchannel Heat Sinks Performance in Electronic Cooling, Journal of Thermal Science and Technology, March 2012, p. 23 – 34, ISSN 1300-3615.